[redacted]

Copy 184
RM L56F05

NACA

RESEARCH MEMORANDUM

SUMMARY OF SUBSONIC-DIFFUSER DATA

By John R. Henry, Charles C. Wood,
and Stafford W. Wilbur

Langley Aeronautical Laboratory
Langley Field, Va.

NATIONAL ADVISORY COMMITTEE
FOR AERONAUTICS

WASHINGTON
October 12, 1956

[redacted]

TABLE OF CONTENTS

NATIONAL ADVISORY COMMITTEE FOR AERONAUTICS

RESEARCH MEMORANDUM

SUMMARY OF SUBSONIC-DIFFUSER DATA

By John R. Henry, Charles C. Wood,
and Stafford W. Wilbur

SUMMARY

The subsonic-diffuser data available in the literature are reviewed, reduced to certain appropriate performance coefficients, and presented as functions of the significant geometric and flow variables. The presentation is divided into the following parts: performance at low speeds (inlet Mach numbers of approximately 0.20), the effects of increasing the inlet speed up to choking Mach numbers, illustrations of the effectiveness of boundary-layer controls, and illustrations of the effects of distorted inlet velocity distributions as obtained at subsonic speeds with spoilers upstream from the inlet and as obtained from compression shocks in supersonic inlets. An analysis based on typical supersonic-inlet data indicates total-pressure losses chargeable to shock—boundary-layer interaction, and original data on a 5° converging-diverging conical diffuser illustrates these effects on the flow development throughout the diffuser.

INTRODUCTION

In recent years, the successful design of aircraft ducting has become essential in order to realize the desired aircraft performance. This situation is the result of the transfer of the propulsion systems for military aircraft from the propeller to the air-breathing jet, which requires internal air flow measurable in tons per minute. The thrust and general operation of the jet propulsion system are directly dependent on the duct pressure recoveries and flow characteristics.

One critical component of aircraft duct systems is the subsonic diffuser. The adverse pressure gradient attendant on subsonic diffusion promotes a rapid growth of the boundary layer, leading to various degrees of flow distortion, pressure pulsation, total-pressure loss, and flow instability if flow separation takes place. Subsonic diffusers are required between the supersonic inlet and the engine face, between the compressor and the combustor, and between the turbine and the afterburner. Thus, satisfactory subsonic-diffuser performance becomes a necessity for suitable engine performance.

The state of the knowledge of boundary-layer growth in adverse pressure gradients does not approach that required to derive diffuser design information; therefore, designers must rely on empirical data. The purpose of this paper is to summarize in a concise and useful form the best subsonic-diffuser data available with a view toward its use by duct designers and analysts of duct-system performance. Data at low inlet speeds (essentially incompressible) will be reviewed and summarized. Although several such reviews are available in the literature (see refs. 1 to 3), the data have never been fully exploited with a view toward current needs. In addition, the effects on diffuser performance of increasing the inlet Mach number up to the choking condition, the effectiveness of boundary-layer controls, and the effects on performance of shock—boundary-layer interaction will be covered as extensively as available data permit.

As is the case for any presentation of knowledge which uses empirical correlations as a basis, a given set of duct design conditions generally will not coincide exactly with any set of data presented herein. This situation will prevent the accurate prediction of performance and the accurate choice of an optimum configuration. The object of the presentation necessarily is limited to illustrating the effects of the principal variables for the less complex configurations. The designer must use the illustrations as a guide in designing specific configurations for specific conditions and in estimating the performance of the resulting design. Refined designs and performance figures still must be obtained by experiment in many cases.

SYMBOLS

a	rectangular-duct cross-sectional width (see fig. 22(c))
b	rectangular-duct cross-sectional height (see fig. 22(c))
b	vortex-generator span
c	vortex-generator chord
f	friction factor, $\frac{\Delta H/q}{4(L/D)}$ (see ref. 1)
n	exponent in boundary-layer equation, $(y/\delta)^{1/n} = u/U$
p	absolute static pressure
p_w	absolute static pressure from wall static-orifice measurements

q	dynamic pressure, $\frac{1}{2}\rho u^2$
q_c	compressible dynamic pressure, $H - p$
$\bar{q}$, $\overline{q_c}$	mass-weighted dynamic pressures corresponding to q and q_c, respectively
r	radial distance to a point in a duct cross section
s	spacing between adjacent vortex generators, measured on the duct inner surface at the 1/4-chord point
u	local velocity
$\bar{u}$	average velocity over a duct cross section
x, y	horizontal and vertical distances from duct wall, respectively
A	duct cross-sectional area
A_R	ratio of diffuser exit area to inlet area
D	duct diameter
H	absolute stagnation pressure
H_e	effective total pressure, defined as mass-momentum total pressure in reference 4
H_{Ref}	absolute stagnation pressure at reference station
$\bar{H}$	mass-weighted stagnation pressure
K	diffuser loss factor, $\frac{\Delta H/q}{\left(1 - \frac{1}{A_R}\right)^2}$
L	duct length along axis
M	Mach number
M^*	Mach number at inlet reference station for the choked flow condition
P_g	one-dimensional, compressible pressure gradient (fig. 16(a))

R radial distance to duct wall at a given station

R one-half the inlet gap for an annular-diffuser inlet

R ratio of suction or injection quantity to total flow, percent

R_N Reynolds number based on hydraulic diameter

U maximum velocity in a velocity profile at a given duct station

α angle of attack of a vortex generator measured with respect to the duct center line

γ ratio of specific heat at constant pressure to specific heat at constant volume

δ boundary-layer thickness to the point of maximum velocity

δ^* two-dimensional, incompressible displacement thickness of boundary layer, $\frac{\delta^*}{R} = \int_{1-(\delta/R)}^{1} \left(1 - \frac{u}{U}\right) d\frac{r}{R}$

η diffuser effectiveness

Δ difference between values of a given parameter at two different duct stations or at two points at a given station, used as a prefix for another symbol

Δ^* three-dimensional, imcompressible displacement area, $\frac{\Delta^*}{A} = \int_{\left[1-(\delta/R)\right]^2}^{1} \left(1 - \frac{u}{U}\right) d\left(\frac{r}{R}\right)^2$

Δ^*_c three-dimensional, compressible displacement area, $\frac{\Delta^*_c}{A} = \int_{\left[1-(\delta/R)\right]^2}^{1} \left(1 - \frac{\rho u}{\rho_l U}\right) d\left(\frac{r}{R}\right)^2$

2θ total diffuser expansion angle

$2\theta_c$ equivalent conical-diffuser expansion angle (included wall angle of a cone of the same length and inlet and exit areas)

$2\theta_w$ diffuser expansion angle (included angle between walls)

$2\theta_{cc}$ diffuser expansion angle (included wall angle of a cone circumscribed about a rectangular diffuser)

θ two-dimensional, incompressible momentum thickness of the boundary layer; $\frac{\theta}{R} = \int_{1-(\delta/R)}^{1} \frac{u}{U}\left(1 - \frac{u}{U}\right) d\,\frac{r}{R}$

θ_3 three-dimensional, incompressible momentum area; $\frac{\theta_3}{A} = \int_{[1-(\delta/R)]^2}^{1} \frac{u}{U}\left(1 - \frac{u}{U}\right) d\left(\frac{r}{R}\right)^2$

θ_{c3} three-dimensional, compressible momentum area; $\frac{\theta_{c3}}{A} = \int_{[1-(\delta/R)]^2}^{1} \frac{\rho u}{\rho_l U}\left(1 - \frac{u}{U}\right) d\left(\frac{r}{R}\right)^2$

ρ mass density

ρ_l mass density at the edge of the boundary layer

A primed quantity indicates a one-dimensional value consistent with continuity, the existing static pressure, and stagnation temperature.

Subscripts:

d diffuser

f friction

i inner wall

I injection boundary-layer control

o outer wall

s shock location or suction boundary-layer control

s+v suction boundary-layer control with a vane installation

tp tailpipe

sb shock—boundary-layer interaction

Subscripts for subsonic-diffuser stations (see fig. 21(d)):

1	inlet
2	exit
2a	slightly downstream of exit (also see fig. 30)
3	1.07 tailpipe diameters downstream of inlet, annular diffuser
4	2.09 tailpipe diameters downstream of inlet, annular diffuser (also see fig. 30(d))

Subscripts for supersonic-inlet configuration (see fig. 35):

0	free-stream conditions
1	upstream of cowl lip
1a	upstream of normal shock
2	downstream of normal shock or subsonic-diffuser inlet
3	subsonic-diffuser exit
w	oblique shock-wave angle
l	cowl lip angle
s	spike angle

SELECTION OF SIGNIFICANT VARIABLES

In order to prepare a summary of diffuser performance data, the geometric and flow variables which are most appropriate for use as independent variables in presenting the performance had to be determined and defined. In addition, the most desirable diffuser performance parameters had to be selected from the many variations available in the literature. In both cases, the quantities had to be determinable from the information available in the majority of reports.

Independent variables may be broken down into two general groups, geometric and flow. With regard to the former, the general configuration of the diffuser is significant; however, no parameter has been devised which represents an expression of the many possible diffuser shapes. Each general class of configurations is considered individually herein. Area

ratio and expansion angle are the other geometric variables used. In the case of a straight-walled conical diffuser, the expansion angle 2θ is defined as the included wall angle, and as such is a prime factor governing the diffuser pressure gradient. The application of the concept of expansion angle to other configurations will be discussed in later sections.

Independent flow parameters used to define inlet conditions include boundary-layer displacement thickness and shape factor, Reynolds number, and Mach number. Displacement thickness is used as an index to the proportion of total flow occupied by the boundary layer at the inlet station and is defined as follows:

$$\frac{\delta^*_1}{R_1} = \int_{1-(\delta/R)}^{1} \left(1 - \frac{u}{U}\right) d\,\frac{r_1}{R_1}$$

The two-dimensional definition is used because of its prevalence in the literature and because it is as satisfactory as a three-dimensional definition for the purposes intended. In the case of an annular cross section, the average displacement thickness of the inner and outer walls is referenced to one-half the gap width. For diffusers in which only two walls diverge the average inlet displacement thickness is referenced to one-half the distance between the two diverging walls at the inlet. For simplicity in all cases the inlet boundary-layer displacement thickness is identified by the same notation, δ^*_1/R_1, even though the definition varies according to the configuration. The inlet boundary-layer shape factor is defined as

$$\delta^*_1/\theta_1$$

where

$$\frac{\theta_1}{R_1} = \int_{1-(\delta/R_1)}^{1} \frac{u}{U}\left(1 - \frac{u}{U}\right) d\,\frac{r_1}{R_1}$$

The value of shape factor is indicative of the amount of pressure gradient which the boundary layer may experience prior to reaching a condition where separation is imminent. (See ref. 5.) Reynolds number is based on the duct diameter; however, a Reynolds number based on boundary-layer thickness may be obtained through use of the values for the inlet boundary-layer parameters. Mach number at the inlet is used as an index to speed

effects on diffuser performance. In most available data the true compressibility or Mach number effects on performance cannot be separated from Reynolds number effects because increasing inlet speeds produce both higher Reynolds and higher Mach numbers.

The independent parameters selected cover roughly all significant parameters used in boundary-layer theory, (See refs. 6 and 7.) The parameters 2θ, A_R, δ^*_1/R_1, and δ^*_1/θ_1 may be combined to produce the ideal one-dimensional value of

$$\frac{\theta_1}{q_1}\frac{q_1 - q_2}{L}$$

which is indicative of the average pressure gradient throughout the diffuser and, therefore, is the counterpart of the local pressure gradient $\frac{\theta}{q}\frac{dq}{dx}$ used in boundary-layer theory. The foregoing comparison is not intended to imply that the average pressure gradient is necessarily a correlating or governing parameter.

There are many significant variables which are not covered in detail because of the lack of suitable data. Such variables are flow obstructions, surface roughness, configuration of downstream ducting, flow asymmetry at the inlet, turbulence, and so forth. In addition, some data available in the literature were not included herein either because sufficient data were not available to illustrate a trend over a range of values for some parameters, or because all pertinent test conditions were not defined. For instance, the former reason applies to certain odd configurations for which only one or two data points were available.

The performance quantities or dependent variables of most interest to designers and analysts are total-pressure loss and exit flow distribution. The total-pressure loss is directly related to the drag of the system, and the exit flow distribution affects critically the operation of duct units or power-plant components located downstream of the diffuser. A third performance quantity of interest because of its ease of measurement and because of its relation to the former two quantities is the static-pressure rise. The static-pressure rise reflects the ability of the diffuser to accomplish its purpose, which is to convert kinetic energy into pressure energy.

Previous investigators (see refs. 8 to 10) have shown that for a given expansion angle and fixed inlet conditions the total-pressure loss of a diffuser is proportional to the theoretical, incompressible value of total-pressure loss for a sudden expansion of the same area ratio. The corresponding proportionality constant, referred to herein as the loss

factor, is defined as follows:

$$K \equiv \frac{\left(H_1 - H_2\right)/\overline{q_{c_1}}}{\left[\left(A_R - 1\right)/A_R\right]^2}$$

where the denominator is the sudden-expansion loss and the total pressures are average values. When other variables are fixed, the loss factor K is approximately constant over wide ranges of area ratio. Therefore, the loss factor K will be used as the total-pressure-loss parameter because it eliminates one variable.

Several methods of averaging or weighting total pressures for nonuniform flows are prevalent in the literature, and in many cases the differences between the results obtained by the several methods are not negligible. Wyatt (ref. 4) presents an analysis of errors introduced by several weighting methods. The analysis indicates that in order to evaluate various flow parameters by using one-dimensional relations the total pressures from surveys at a given duct station should be converted into an effective total pressure (referred to as mass-momentum method in ref. 4). The effective total pressure corresponds to a value which would be obtained by mixing the flow in a frictionless duct until the distribution becomes uniform. The calculation procedure inherently includes total-pressure losses due to mixing. Thus, the use of effective total pressure to determine loss values charges mixing losses to the ducting where the flow nonuniformity originates. This appears to be a more reasonable accounting procedure than that for mass- or volume-weighted total pressure, where the downstream ducting is charged with the mixing losses.

A large portion of the total-pressure-loss data presented herein is based on measurements made at the point of maximum static pressure in the tailpipe downstream of the diffuser. Thus, the total-pressure losses correspond to the effective total pressure previously discussed except that friction losses in the tailpipe are included. The friction losses are normally of less magnitude than the data scatter. Some of the loss data are based on mass-weighted total pressures and some on "mass-derived" total pressures. The latter is a calculated value which is consistent with continuity, the existing static pressure, and the stagnation temperature. Thus, a mass-derived total pressure charges the entire excess dynamic pressure associated with a nonuniform velocity distribution as a loss and is the most pessimistic value of the several common types in use.

In order to obtain some numerical values illustrating the differences between the various averaging procedures, the methods presented by Wyatt (ref. 4) were used to calculate mass-weighted, mass-derived, and effective

total pressures for a number of assumed velocity distributions and Mach numbers. The calculations were performed for the case of two-dimensional flow with power-profile boundary layers meeting on the duct center line. The results of the calculations are summarized in the following table in terms of the difference between the mass-weighted and mass-derived total pressures and the difference between the effective and mass-derived total pressures. The differences are nondimensionalized by dividing by the one-dimensional or mass-derived, compressible, dynamic pressure. The difference between the mass-weighted and effective values may be obtained by simple subtraction of corresponding values for the two coefficients given.

$\frac{\delta^*}{\theta}$	M' = 0.2		M' = 0.5		M' = 0.7	
	$\frac{\overline{H} - H'}{q_c'}$	$\frac{H_e - H'}{q_c'}$	$\frac{\overline{H} - H'}{q_c'}$	$\frac{H_e - H'}{q_c'}$	$\frac{\overline{H} - H'}{q_c'}$	$\frac{H_e - H'}{q_c'}$
1.29	0.04	0.03	0.05	0.03	0.05	0.03
1.40	.07	.05	.09	.06	.10	.06
1.67	.17	.12	.20	.13	.22	.12
1.80	.23	.16	.27	.17	.29	.16
2.60	.72	.48	.81	.46	----	----
3.00	1.03	.66	1.15	.61	----	----

The values in the table show that differences between the various weighting and averaging methods for boundary-layer shape factors corresponding to incipient separation ($\delta^*/\theta \geq 1.8$) are of the same order as diffuser loss coefficients. For this reason, the methods used in obtaining a mean total pressure become important. For cases where the boundary layer does not extend to the duct center line, the values given in the table would be reduced accordingly.

Three performance values related to the exit flow distribution will be presented because each has its own particular merits. The quantities are the exit dynamic-pressure distortion $\frac{\overline{q_{c_2}/q_{c_2}'}}{\overline{q_{c_1}/q_{c_1}'}}$, the exit displacement area $\frac{\Delta^*_2}{A_2}$, and the exit velocity distribution. The dynamic-pressure distortion is a quantity which may be measured or may be calculated from measurements of the static-pressure rise and total-pressure loss. The exit displacement area is of interest to designers because it indicates the relationship between geometric area and effective area. The actual

velocity distribution is the information required to give all the details of the flow distribution necessary for matching the diffuser performance to the requirements of a downstream unit.

The static-pressure-rise quantity will be given in terms of the diffuser effectiveness, which is defined as the actual rise in pressure energy divided by the ideal reduction in kinetic energy. The incompressible expression for the effectiveness is as follows:

$$\eta = \frac{\int_0^{A_2} p_2 u_2 \, dA - \int_0^{A_1} p_1 u_1 \, dA}{\int_0^{A_1} \frac{\rho}{2} u_1^3 dA - \frac{\rho}{2} \overline{u_2}^3 A_2 \frac{\int_0^{A_1} \frac{\rho}{2} u_1^3 dA}{\frac{\rho}{2} \overline{u_1}^3 A_1}} \tag{1}$$

In equation (1) the ideal reduction in kinetic energy is defined as the difference between what is available at the inlet and what would be available at the exit if the diffuser produced the same kinetic-energy distribution at the exit as that entering the inlet. The assumption regarding the type of ideal exit kinetic-energy distribution is based on the practical consideration that the diffuser should not be required to produce an exit velocity distribution which is superior to that entering the inlet. Using the definition of effectiveness of equation (1), it appears possible that in certain instances the effectiveness may reach values in excess of 100 percent, particularly for low-angle diffusers with separated flow entering the inlet.

If the dynamic-pressure quantities are defined as

$$\bar{q} = \frac{\int_{\rho/2}^{A} u^3 dA}{\bar{u}A}$$

and

$$q' = \frac{\rho}{2} \bar{u}^2$$

equation (1) becomes, for no radial gradient in static pressure,

$$\eta = \frac{p_2 - p_1}{\overline{q_1}\left(1 - \frac{q_2'}{q_1'}\right)} = \frac{p_2 - p_1}{\overline{q_1}\left(\frac{A_R^2 - 1}{A_R^2}\right)}$$

The latter expression is the ratio of the actual static-pressure rise to the ideal static-pressure rise as determined from the mean dynamic pressure at the inlet and the area ratio. For compressible flow, the ideal static-pressure rise can be determined from the mean compressible dynamic pressure at the inlet $\overline{q_{c_1}}$, the inlet static pressure p_1, and the area ratio, if the flow is assumed to be isentropic. The calculation can be performed by using any of the several published compressible-flow tables.

Three of the performance parameters previously discussed may be related through use of Bernoulli's equation, as follows:

$$\overline{\Delta H} = \left(\overline{q_{c_1}} - \overline{q_{c_2}}\right) - \left(p_2 - p_1\right)$$

which converts to

$$K = (1 - \eta)\frac{A_R + 1}{A_R - 1} - \frac{\dfrac{\overline{q_{c_2}}/q_{c_2}'}{\overline{q_{c_1}}/q_{c_1}'} - 1}{(A_R - 1)^2} \qquad (2)$$

Through use of equation (2) any one of the three parameters may be determined, provided the other two are known.

METHODS OF PERFORMANCE MEASUREMENT

The review of the literature and previous experience indicate that certain methods for making the performance measurements are most satisfactory. The inlet measurements required consist of the upstream static pressure p_1, a reference total pressure H_{Ref}, and total-pressure surveys at the inlet station. The inlet static pressure can be measured most accurately and efficiently by wall static-pressure orifices in a longitudinal location where negligible transverse static-pressure gradients exist. Stream static-pressure surveys are difficult to make, subject to

error in proximity to the wall, sensitive to tube misalinement, and unnecessary for irrotational flow. The longitudinal location of the wall static orifices, station 1, should be far enough upstream from the start of the geometric expansion to be free from regions of local acceleration in the vicinity of the change in wall slope at the inlet and should be close enough to the start of the geometric expansion to eliminate unnecessary penalties to static-pressure rise due to inlet ducting friction loss. (See fig. 1). The optimum location varies with the design, but it appears to range from a value of 1/4 to 1 hydraulic diameters upstream from the break in wall slope at the inlet.

Since total-pressure surveys should be made at only one station at a time, a correlating parameter, such as p_1/H_{Ref}, is required. The reference total-pressure tube should be fixed and located, if possible, in a plenum chamber or large duct upstream from the inlet. The effect of the reference total-pressure tube on the diffuser flow must be negligible. In addition to the reference total-pressure measurement, upstream total-pressure surveys are required at station 1 in order to determine the diffuser total-pressure loss and also the inlet boundary-layer parameters.

Downstream total-pressure surveys are required at two locations for satisfactory accuracy. Diffuser-exit velocity distributions are generally desired at the end of the geometric area expansion, and total-pressure-recovery measurements should be taken at a location which corresponds to a minimum of velocity distortion. The velocity surveys at the diffuser exit will be in error because of difficulties associated with measuring in a region of high velocity gradient (see refs. 11 to 15). However, the measurements are necessary to indicate the character of the exit velocity distribution. The total-pressure-recovery measurements should be located in a tailpipe at a downstream location where the velocity distribution has become reasonably uniform. This location may be as much as 6 diameters downstream from the diffuser exit, depending on the diffuser design and flow conditions. An alternative procedure is to locate a venturi about 3 hydraulic diameters downstream of the diffuser exit and to measure the total-pressure recovery in the throat. In most cases, the added friction loss of the tailpipe is negligible compared with errors introduced by attempting to measure recovery near the diffuser exit.

RESULTS

All the data presented in figures 1 to 32 correspond to favorable inlet boundary-layer distributions such as would be obtained in turbulent flow with negligible longitudinal pressure gradient unless otherwise noted.

Total-Pressure-Loss Factor

Conical diffusers.- Total-pressure-loss data in terms of the loss factor K for conical diffusers tested by Gibson (refs. 8 and 9) and Peters (ref. 10) are given in figure 2 as a function of expansion angle. A logarithmic scale was used for expansion angle in order to increase the spacing at the lower expansion angles, which are of most interest. The figure presents two types of loss factors: K, the total or measured quantity indicated by the curves faired through data symbols (which are identified in table I), and K_f, the calculated friction-loss factor which was determined by using the expression noted in the figure. The friction-loss-factor expression resulted from an integration of the differential form of the expression for friction loss in a straight pipe as given in reference 1. The expression noted in figure 2 assumes that friction losses in a differential length of the conical diffuser can be estimated by using the straight-pipe expression. This assumption is only approximate because as the flow proceeds through the diffuser the boundary layer becomes distorted, producing a reduction in the skin-friction coefficient (see ref. 7). However, approximate values are sufficient for this analysis.

As the expansion angle approaches zero, the total-loss factor approaches the value for the friction-loss factor because the rate of diffusion becomes negligible. At intermediate expansion angles, on the order of 5° to 10°, K_f may be about one-half of the total K. The variation of loss factor with changes in expansion angle, as described, results in the well-known fact that for conical diffusers an optimum expansion angle exists in the range of 5° to 8° which produces the least total-pressure loss for a given area ratio.

Peters' investigation covered a wide range of inlet boundary-layer thicknesses for an area ratio of 2.34 while Gibson's data cover a wide range of area ratios at one inlet boundary-layer thickness ($\delta^*_1/R_1 = 0.01$). For both sets of data, the total-pressure-loss factor is based on measurements in the tailpipe at the point of greatest static-pressure recovery, which corresponds to a velocity distribution approximating fully developed pipe flow. Therefore, the data should correspond to effective total pressures previously discussed and should be fully comparable. The left ends of all the data curves were faired in such a way that at very low angles the total K would become equal to K_f.

For expansion angles between 10° and 20°, a range of interest for practical application, the data curves for area ratios of 2.25, 4.00, and 9.00 for a δ^*_1/R_1 of 0.01 (Gibson) tend to coincide, illustrating the lack of dependence of the loss factor K on area ratio. For expansion angles less than 10° the friction component of the loss becomes substantial, as is indicated by the calculated friction curves. The friction-loss

factor is definitely a function of area ratio, as indicated by the expression noted in the figure. In order to estimate the loss factor for low-angle diffusers with area ratios other than those corresponding to the data, it is suggested that the value from the data curves be corrected for the difference in friction-loss factor due to the change in area ratio. For instance, for a 4° diffuser with an area ratio of 4.0 and a δ^*_1/R_1 of 0.029, the estimated loss factor is obtained as follows:

$$K = 0.27 - (0.14 - 0.09) = 0.22$$

In the range of expansion angles corresponding to the lowest loss factors the inlet boundary-layer thickness has a substantial effect on the value of loss factor. As the expansion angle is increased beyond 20° separation becomes the controlling factor and inlet boundary-layer thickness becomes irrelevant. Diffusers with expansion angles greater than 50° produce loss coefficients greater than that for a sudden expansion (K of 1.0).

Peters' data are compared with more recent data taken at higher inlet Reynolds numbers (refs. 13, 16, and 17; see table I) in figure 3. The loss factors for the diffusers with area ratio of 2.0, which were tested at the highest Reynolds numbers, all agree well with Peters' data except for two low points. This result may be circumstantial, however; the loss coefficients for the diffusers with area ratio of 2.0 are known to be low (see ref. 13) since the pressure recoveries were measured at the diffuser exits in large velocity gradients and since the total pressures are mass-weighted instead of effective values. Squire's data (ref. 16) for diffusers with A_R of 4.0, which appear to be higher than Peters' data and were taken at $2\frac{1}{2}$ times the Reynolds number, are probably more accurate than the data for diffusers with A_R of 2.0 because the measurements were taken 1 diameter downstream of the diffuser exit. It appears possible that the loss coefficient does increase with Reynolds number as indicated by boundary-layer theory (ref. 7); however, sufficient data are not available to substantiate this point.

Figures 2 and 3 show that Peters' data have a certain degree of uniform variation with respect to change in inlet boundary-layer thickness. The curves are very similar in shape, which suggests that the loss factor can be broken down into the product of two functions as follows:

$$K = \varphi(2\theta)\psi\left(\delta^*_1/R_1\right)$$

This process was accomplished, and the two functions are plotted in figure 4. The function of expansion angle, $\varphi(2\theta) = K_{Ref}$, was determined by assuming that K_{Ref} is approximately equal to the maximum value of K at any given expansion angle in figure 3. The empirical relation, which fits the data closely, shows that K_{Ref} is a function of $(2\theta)^{1.50}$. Above values of 2θ of 20° the relationship does not hold, probably because the extensive flow separation in such diffusers produces a radical change in flow pattern. For values of 2θ below about 8°, the data points diverge appreciably from the empirical relationship, indicating that the laws of friction loss are becoming predominant.

The boundary-layer function $\psi\left(\delta^*_1/R_1\right) = K\,K_{Ref}$ was evaluated directly from the measured values of K and the previously determined values of K_{Ref}. The results are plotted in figure 4 for values of expansion angle between approximately 8° and 20°. All the data of figure 3 within this angle range are included although, as previously noted, the data for the diffusers with an A_R of 2.0 are known to be low. The function of δ^*_1/R_1 appears to be linear with δ^*_1/R_1 and of high slope up to a value of δ^*_1/R_1 of 0.04. At this point, the curve breaks and assumes a much reduced slope. The sharp break in the curve can probably be associated with a change in flow pattern brought about by the filling of the diffuser cross section with boundary layer. The fact that K/K_{Ref} appears to be approaching a value of 1.0 at the maximum possible value of δ^*_1/R_1 suggests that K is equal to K_{Ref} for fully developed pipe flow at the inlet.

Rectangular and square diffusers.- Figures 5(a), (b), and (c) contain loss data on square and rectangular diffusers. In figure 5(a), equivalent conical expansion angle (defined as the included angle between the walls of a cone of the same length and inlet and exit areas) is used as the independent variable. The purpose of using the equivalent cone angle is to obtain an angle which is indicative of the same longitudinal pressure gradient that the conical diffuser has. It is apparent that the data do not correlate with the conical-diffuser curve and that other factors besides longitudinal pressure gradient must be significant.

Figure 5(b) contains the same data as figure 5(a) except that the included wall angle is used as the independent variable. The correlation with the conical-diffuser curve is satisfactory except for the square-diffuser data and Young and Green's data for rectangular diffusers with an A_R of 4.0 (ref. 18; see table I). The Young and Green data are higher than the other diffuser data because the exit total pressure was calculated from the static pressure and mass flow. This procedure charges the nonuniformity in the exit total-pressure distribution against

the loss coefficient, which is inconsistent with the other data. The degree of success obtained by using included wall angle as a correlating parameter suggests that the actual maximum change in flow direction from the mean direction is important in determining the loss factor.

Data for several designs of shaped diffusers developed by Gibson (refs. 8 and 9) are also included in figure 5(b) to show the advantage of special wall shapes in reducing losses, especially at expansion angles greater than about 18°. A crude statement of the apparent philosophy behind these designs is that for short diffusers the rate of area increase should be small at first in order to obtain the maximum pressure rise possible prior to boundary-layer separation. After separation, the area is increased at a high rate compatible with the shortness of the diffuser. Such a design undoubtedly produces highly distorted exit velocity distributions; however, the distributions may or may not be worse than those for any other wall shape.

The independent variable used in figure 5(c) is the included wall angle of a cone circumscribed about the diffuser. Use of the circumscribed-cone angle represents an extension of the thought that performance is a function of the angle of the maximum change in flow direction, which occurs in the corners of the diffuser. The circumscribed cone correlates the square-diffuser data well, further substantiating the conclusion relative to the importance of the change in flow direction.

Annular diffusers.- The measured loss factors for annular diffusers are compared with conical-diffuser data in figure 6(a). The data are plotted against included wall angle where possible. In the case of expanding inner and outer walls the included wall angle becomes converging; therefore, equivalent conical angles were used in this case. The annular diffuser data of figure 6(a) do not correlate with the conical-diffuser data, apparently because of the differences in friction losses between annular and conical diffusers. The calculated friction losses included in the figure show that for the annular diffusers with lower angles the losses are almost entirely friction.

In order to obtain a correlation, the calculated friction losses were subtracted from the measured losses to produce a loss factor K_d which is chargeable to diffusion only. The results given in figure 6(b) show good correlation with the conical data except for the A_R of 1.91 data, which are known to be low because the downstream total pressure was measured in a highly distorted velocity distribution. The correlation appears to be valid for engineering approximations.

Diffuser Effectiveness

Conical diffusers.- In accordance with equation 2 and in order to obtain values of the same order of magnitude as the loss factor, the data on diffuser effectiveness will be presented in terms of loss in effectiveness $1 - \eta$. Conical-diffuser data from several sources and corresponding to several area ratios are presented in figure 7. No data correlation is indicated by the presentation. The data for similar values of δ^*_1/R_1 and A_R agree well except for a few isolated points for an A_R of 2.0. The data indicate that $1 - \eta$ is not independent of area ratio.

The dependence of $1 - \eta$ on A_R is illustrated in figure 8 for both thin ($\delta^*_1/R_1 = 0.006$) and thick ($\delta^*_1/R_1 = 0.082$) inlet boundary layers. The curve for an area ratio of 2.34 and δ^*_1/R_1 of 0.006 is an extrapolation of Peters' data (ref. 10) based partially on the data for A_R of 2.0. The curves indicate that A_R has a large effect on $1 - \eta$ for thin boundary layers, corresponding to the following approximate proportion:

$$1 - \eta \approx A_R^{1.6}$$

The thick-boundary-layer curves were calculated by using the exit velocity-distribution data of reference 15 and the assumption that the data of reference 15 correspond to Peters' loss-factor results, which the loss-factor discussion indicates to be a valid assumption. The curve for an A_R of 2.3 is Peters' data. The thick-boundary-layer curves indicate that $1 - \eta$ is almost independent of A_R. The extreme difference in the dependence of $1 - \eta$ on A_R for the two boundary-layer conditions also may result from the flow phenomena produced by the fact that the boundary layer fills the diffuser in one case and does not fill it in the other case. The curves of figure 8 emphasize the need to consider all pertinent conditions in predicting or comparing diffuser performances.

Peters' data are presented as a product of two functions in figure 9 in a manner parallel to the loss-factor presentation of figure 4. The function of 2θ represents a curve of the maximum values of $1 - \eta$ occurring at any expansion angle as determined from cross plots of figure 7. Maximum values occur at an inlet boundary-layer thickness of approximately 0.056. The function of 2θ is linear with 2θ in contrast to the power function for the K factor. Owing to the nature of the 2θ function, the function of δ^*_1/R_1 reaches a value of 1.0 at

δ^*_1/R_1 of 0.056 and then decreases slightly with further thickening of the boundary layer. This result indicates that for a given diffuser expansion angle the exit velocity distribution must improve slightly with further thickening of the inlet boundary layer after the condition of complete filling of the diffuser with boundary layer is attained, because the loss factor continues to increase in this region. The correlations apply to expansion angles ranging from 5° to 20° for reasons discussed in connection with the K correlation. In addition, the correlations apply to an area ratio of 2.34 only, because of the dependence of $1 - \eta$ on A_R.

Rectangular diffusers.- Rectangular-diffuser data from several sources are presented in figure 10. Some of the data are plotted against both equivalent conical angle and included wall angle. It is apparent that the included wall angle is a better correlating parameter, which is in agreement with the analysis of the loss-factor data. The data indicate that area ratio has a substantial influence for rectangular diffusers also.

All the data of figure 10 are presented in figure 11 as a function of included wall angle, which considerably reduces the data spread due to the area-ratio variation at δ^*_1/R_1 of 0.008. The data spread was further reduced by dividing $1 - \eta$ by the arbitrary factor $A_R^{0.2}$, as indicated by figure 12. The correlating factor $A_R^{0.2}$ indicates much less dependence of $1 - \eta$ on A_R for rectangular diffusers than for conical diffusers at δ^*_1/R_1 of 0.006 (fig. 8). A power of 1.6 would have been required for the latter case. Judging from the variation in the dependence of $1 - \eta$ on A_R for conical diffusers, the correlation of figure 12 cannot be relied on to apply to thick boundary layers.

Annular diffusers.- Data on annular diffusers are summarized in figure 13, where included wall angle is the independent parameter used except for the one case noted. All the data plotted, except those at low expansion angles, fall below the conical-diffuser data for comparable boundary-layer thicknesses. Apparently, annular diffusers produce somewhat more static-pressure rise than conical diffusers under the same flow conditions.

The data for A_R of 1.75 (plotted in fig. 13 against equivalent cone angle) appear not to correlate well either in magnitude or trend. These two points, however, are the only ones which have friction components significantly different from the conical diffuser of the same angle, a situation resulting from the use of equivalent cone angle. If the friction component of $1 - \eta$ were subtracted from the measured

values, the data for these two diffusers would correlate; however, the correlation of the other data would not be improved.

Recovery of Diffuser Effectiveness in Tailpipe

Peters (ref. 10) measured static-pressure rise in the tailpipe; these measurements are summarized in figure 14. The left-hand plot presents the maximum gain in effectiveness in the tailpipe referenced to the loss in effectiveness in the diffuser proper as a function of expansion angle. Since the static-pressure rise in the tailpipe is entirely due to the velocity distribution becoming more uniform through natural mixing, the coefficient plotted is a measure of the amount of loss in diffuser effectiveness which is recoverable (as opposed to that irreversibly lost due to total-pressure losses). The curves have been faired to zero at expansion angles estimated from figures 7 and 13 to correspond to a minimum value of $1 - \eta$. This point has been interpreted as corresponding approximately to a fully developed pipe-flow distribution at the diffuser exit; such a distribution is stable and would recover no further static pressure. The data indicate that as much as 63 percent of the loss in diffuser effectiveness is recoverable in the tailpipe for δ^*_1/R_1 of 0.058.

The right-hand side of figure 14 gives the tailpipe lengths required to recover the maximum amount of effectiveness. Six diameters of tailpipe are required for δ^*_1/R_1 of 0.058 for conical diffusers.

The data of figure 14 have been converted into terms of overall loss in effectiveness for conical-diffuser—tailpipe combinations and are presented in figure 15. Since the optimum tailpipe length corresponds approximately to the point where fully developed pipe flow is obtained at the tailpipe exit (ref. 10), the net loss in effectiveness reaches a minimum at an expansion angle corresponding to the minimum loss coefficient. This fact may be substantiated by comparing figures 2 and 15. The table included in figure 15 shows that the overall expansion angles of the diffuser-tailpipe combinations $2\theta_{tp}$ fall within the range of 2° to 4° for all conditions, which corresponds to the angle range for diffusers alone for least loss in effectiveness (fig. 7). This result can be stated in other terms: for optimum tailpipe lengths and a given inlet boundary-layer thickness, the overall length of diffuser-tailpipe combinations remains approximately constant over wide ranges of values of diffuser angle $(2\theta)_d$.

Inlet Speed Effects

Inlet speed effects will be presented in terms of inlet Mach number M_1; however, the presentation should not be interpreted as implying

that the indicated effects are entirely due to Mach number or compressibility. Increasing the inlet Mach number also increases the inlet Reynolds number, which produces certain characteristic effects. For instance, increasing the Reynolds number decreases the friction coefficient and, therefore, the friction components of total-pressure loss and loss in effectiveness. In addition, reference 7 indicates that the loss in kinetic energy per unit length, normal to the direction of flow in the boundary layer, is a function of Reynolds number. The latter effect probably explains in part the phenomena in which the separation point in a diffuser travels upstream with increasing inlet speed.

Compressibility effect on ideal pressure gradient.- Boundary-layer theory (ref. 7) indicates that one of the prime factors which influence the rate of boundary-layer growth (and therefore diffuser performance) is the longitudinal pressure gradient. Mach number increases raise the longitudinal pressure gradient as a result of a compressibility effect predictable from one-dimensional relations. Naumann discussed this effect in 1942 in reference 19. Additional discussion of the same subject may be found in reference 20. The change in the isentropic one-dimensional compressible dynamic pressure per unit dynamic pressure for a given change in area increases as the Mach number increases and approaches infinity as the Mach number approaches 1.0 as follows:

$$P_g = \frac{dq_c}{q_c d(A/A_1)} = \frac{\gamma M^2}{A_R \frac{q_c}{p}(M^2 - 1)}$$

The preceding equation is plotted in figure 16(a) for several inlet Mach numbers over a range of area ratio from 1.0 to 3.0. The pressure gradient at the various Mach numbers used is referenced to the pressure gradient at a Mach number of 0.2. The curves show that the large effects are confined to small area ratios, indicating that the diffuser flow should be affected principally in a region near the inlet. The ideal pressure-gradient change may be only one of several important compressibility effects. Phenomena pertaining to the transverse pressure gradients and associated influences on the rate of boundary-layer growth may be an example. More research is needed to evaluate fully the importance of compressibility relative to diffuser performance and design.

The expression illustrated in figure 16(a) was used to modify the design of an 8° conical diffuser with 3 to 1 area ratio to obtain a design for an inlet Mach number of 0.8. It was assumed that the 8° conical diffuser operated satisfactorily at an inlet Mach number of 0.2. It was assumed further that a modified diffuser design which produced the same ideal pressure gradients at an inlet Mach number of 0.8 as those of the

conical diffuser at an inlet Mach number of 0.2 would operate satisfactorily. The latter assumption, as previously discussed, is somewhat questionable; however, it was desired to obtain an idea of the effects on configuration which are indicated by changes in the ideal pressure gradient.

The resulting design is compared with the original 8° diffuser in figure 16(b). The increase in pressure gradient obtained by raising the inlet Mach number from 0.2 to 0.8 was nullified by decreasing the expansion angles by amounts ranging from about 4.5° near the inlet to 0.08° near the exit. Thus, the diffuser length was increased about 15 percent. The resulting diffuser shape suggests that increasing the inlet Mach number requires making the wall shape such that the radius of curvature of the wall increases gradually from the inlet to the exit and also requires reducing the overall expansion angle.

Loss coefficient - conical diffusers.- Data on diffuser performance over a range of inlet Mach numbers are available in the literature from several sources. The total-pressure-recovery measurements for the conical and annular diffusers were made in regions where velocity-distribution distortions existed, which introduced some inaccuracies. In addition, the change in performance with increasing inlet Mach number or the slope of the data curves is the important factor, which requires data of higher than normal accuracy. Because of these circumstances, the data figures to be presented will be useful only in obtaining orders of magnitude.

Data on conical diffusers for inlet boundary-layer thicknesses δ^*_1/R_1 ranging between 0.003 to 0.006 are presented in figure 16(a) as the ratio of the loss coefficient at a particular Mach number to the loss coefficient for an inlet Mach number of 0.2. Values of choking Mach number, which are indicated in figures 17 to 19, are defined as the maximum value of average Mach number obtained at the inlet measuring station. The average Mach number is a value consistent with continuity and the existing static pressure and stagnation temperature. The 10° and 12° diffusers produced an average rate of increase in loss coefficient of 11 percent per unit change in Mach number up to Mach numbers of 0.73. Further increases in inlet speed produced various high rates of loss-coefficient increase which depended on local changes in flow pattern caused by local shock-wave formations. The data for the 23° diffuser indicate a rapid rate of increase in loss coefficient over the entire range of M_1. Considerable asymmetrical flow, flow separation, and flow unsteadiness existed in the diffuser.

Conical-diffuser data for thicker inlet boundary layers (δ^*_1/R_1 of 0.017 to 0.030) are presented in figure 17(b). Increasing the thickness of the inlet boundary layer by a factor of 5 or 6 produced higher rates of increase of loss coefficient for the 10° and 12° diffusers and lower choking Mach numbers. One of the 12° diffusers produced an average rate

of increase in loss coefficient as high as 56 percent up to a Mach number of 0.6. The 23° diffuser still produced the most severe performance losses although the rate of increase in $\Delta H/q$ was somewhat lower than for the thinner-boundary-layer case (fig. 17(a)).

Loss coefficient - rectangular diffusers.- Rectangular-diffuser data are presented in figure 17(c). Very little variation in the rate of loss-coefficient increase is indicated up to inlet Mach numbers of 0.6 for the several diffuser expansion angles tested. The three largest expansion angles produced various degrees of flow separation and unsteadiness. The average rate of increase in the loss coefficient was about 26 percent per unit Mach number up to inlet Mach numbers of 0.6. As noted previously, the rectangular-diffuser loss coefficient presented in reference 18 is not exactly comparable with other data presented herein because it includes a penalty due to the flow distortion at the exit.

Loss coefficient - annular diffusers.- The data of figure 17(d) emphasize the effect of Reynolds number on the friction component of the loss coefficient. For the two low-angle diffusers, the loss coefficient either remained constant or decreased very slightly with increasing inlet Mach number. This result could only be produced by a decreasing friction coefficient. The curve with the highest positive slope indicates an average rate of increase in loss coefficient of 48 percent per unit Mach number up to a Mach number of 0.8 even though this diffuser had a ratio of friction loss to total loss of about 70 percent. The rate of increase, however, could be drastically reduced by refairing the curve within the data scatter.

Effectiveness loss - conical diffusers.- Data for conical diffusers with very thin inlet boundary layers (δ^*_1/R_1 from 0.003 to 0.006) are given in figure 18(a). The diffusers with an area ratio of 2.0 produced a wide dispersion in the results, the two diffusers in which separation was prevalent corresponding to very high rates of increase in the effectiveness loss. The two diffusers with no separation produced decreases in the loss in effectiveness over most of the Mach number range. The diffusers with an area ratio of 4.0, all of which had low expansion angles, produced a uniform grouping of data corresponding to an average rate of increase in $1 - \eta$ of 20 percent per unit Mach number.

Figure 18(b) presents similar data for much thicker inlet boundary layers, δ^*_1/R_1 of 0.017 to 0.030. An average rate of increase of about 55 percent up to a Mach number of 0.7 was obtained. The data represent a wide variety of conditions relative to flow separation.

Figure 18(c) presents data from reference 20 comparing the characteristics of a straight-wall conical diffuser with those of a curved-wall diffuser. The expansion angle of the curved-wall diffuser increased

gradually from the inlet toward the middle and then decreased to a lower value toward the exit, resulting in an average expansion angle of 10.5°. The maximum local expansion angle was 13.5°. The straight-wall diffuser had an expansion angle of 8° over the entire length except for a faired region near the inlet, which resulted in an average angle of 7.25°. The data show that the curved-wall diffuser exhibited a definite superiority for all boundary-layer conditions. However, for the two thickest boundary layers, the advantage of the lower rate of increase of $1 - \eta$ of the curved-wall diffuser is eliminated by the higher value of $1 - \eta$ at a Mach number of 0.2 (see fig. 7). In general, the data show that the rate of increase in $1 - \eta$ becomes higher with increasing thickness of inlet boundary layer.

Effectiveness loss- rectangular diffusers.- The rectangular-diffuser data of figure 18(d) group closely for a wide range of expansion angles and indicate an average rate of increase in $1 - \eta$ of 27 percent per unit Mach number up to a Mach number of 0.6.

Effectiveness loss - annular diffusers.- The data of figure 18(e) show a favorable Reynolds number effect due to a decreasing friction loss for three of the diffusers, as in the case of the loss-coefficient data. A comparison of the data with figure 17(d) shows that the diffuser which indicated the high rate of increase in loss coefficient is not the same as the one with the high rate of increase in effectiveness loss. However, as in figure 17(d), the high rates of loss in performance could be reduced drastically by refairing the curve within the data scatter.

Choking Mach number.- Typical values of choking Mach number for diffuser flow are given in figure 19 as a function of the inlet boundary-layer displacement thickness. From such data maximum mass-flow capacities may be estimated. The mean choking Mach number plotted was in all cases measured at a reference station a short distance upstream of the diffuser inlet (0.4 to 1.0 diameters) where there was no transverse static-pressure gradient. Extensive pressure surveys near the inlet of a 12° conical diffuser by Little and Wilbur (unpublished) showed that when the diffuser reached the choking condition, the point of choke occurred near the end of the inlet ducting or near the start of the geometric expansion. The Mach number outside the boundary layer was slightly supersonic. These results indicate that the actual mean choking Mach number probably depends very little on the diffuser geometry but is primarily a function of inlet boundary-layer thickness. The exception to this statement is the case where the diffuser configuration includes a flow obstruction (such as a blunt inner body) which sets up a transverse static-pressure gradient at the inlet.

By using the concept of choking Mach number described in the last paragraph, an equation (noted in fig. 19) was derived expressing choking Mach number as a function of δ^*_1/R_1. The equation was derived on the

assumption that the Mach number outside the boundary layer is unity for the choking condition. Such an assumption would apply only to thin-boundary-layer cases because the stream Mach number would become appreciably supersonic for thick cases. The plot of this equation indicates that all the data correspond to somewhat lower Mach numbers, with one exception. The exception at δ^*_1/R_1 of 0.006 may be in error since no measurements of δ^*_1/R_1 were provided in reference 19 and therefore the value had to be estimated. The actual data should fall below the calculated curve by about the amount shown by the faired curve since the measuring stations were upstream from the actual point of choke.

Exit Flow Distributions

Currently, one of the most critical items with regard to diffuser performance is the exit velocity distribution delivered by the diffuser. This item has become critical because power-plant components, such as compressors and combustion chambers, cannot function properly without a relatively high degree of uniformity of flow distribution.

Acceptable limits on the velocity-distribution distortion are difficult to fix rigidly and vary with the application. For turbojet engines, the distortion at the compressor inlet is generally expressed in terms of total pressure, and limits have been quoted ranging anywhere from 2 to 20 percent variation in total pressure. In order to convert distortion limits in terms of total pressure into limits on the variation of velocity, the mean Mach number must be specified as indicated by figure 20.

The curves of figure 20 were calculated by assuming that the distortion was equally distributed above and below the mean total pressure and that the static pressure was uniform. Since the Mach number at the compressor inlet of turbojet engines is about 0.6, the maximum variation of the velocity would be about 5 percent for a 2-percent distortion in total pressure and about 13 percent for a 5-percent distortion. Assuming a Mach number of 1.0 at the subsonic-diffuser inlet, the theoretical area ratio for this condition is about 1.2. The same distortion limits for a Mach number of about 0.3 (ram-jet operation) would be 16 percent and 37 percent variation in u/U, with a maximum theoretical area ratio of about 2.0. From the preceding discussion, it is obvious that no general statement can be made as to what constitutes a satisfactory velocity distribution, and no attempt to do so will be made herein.

Conical diffusers.- The effects of diffuser expansion angle, inlet boundary-layer thickness, and area ratio on exit velocity distribution are illustrated in figure 21(a) for thin inlet boundary-layers corresponding to values of δ^*_1/R_1 of 0.003 to 0.026 and for M_1 values in

the range from 0.2 to 0.45. Increasing values of all three variables produced increased distortions within the ranges covered by the data. The curve for the 12° diffuser at δ^*_1/R_1 of 0.006 does not fit well with the other data because the inlet boundary layer was somewhat distorted in shape, which resulted in a lower than normal performance. For diffusers with an area ratio of 2.0, expansion angles in excess of 12° probably would produce separated flow. The net effects of expansion angle, inlet boundary-layer thickness, and area ratio on the velocity distribution are shown more directly by the plots of $\overline{u/U}$ at the top of figure 21(a). The mean velocity ratio $\overline{u/U}$ was obtained by integrating the velocity diagrams in the lower half of the figure. Effects which produce more distorted velocity distributions result in lower values of $\overline{u/U}$.

A similar type of data presentation for a thick inlet boundary layer (δ^*_1/R_1 of 0.082) is given in figure 21(b) for a value of M_1 of 0.45. The data were obtained by surveys at various positions in diffusers with an area ratio of 16; however, the results should be indicative of individual diffuser performances.

The data correspond to the condition where the boundary layer fills the duct at the inlet. For this case, increasing the area ratio produced progressively better velocity distributions within the range of the data, an effect which is directly opposite to that for thin inlet boundary layers. For values of expansion angle of 4°, 5°, and 6° essentially pipe-flow distributions were obtained at the higher values of area ratio. This result is indicated at the top of the figure by the curves which approach a mean velocity ratio value of 0.82, which corresponds to a pipe-flow distribution for a 1/7-power profile.

Rectangular diffusers.- Data for rectangular diffusers with a thin inlet boundary layer (δ^*_1/R_1 of 0.02) are given in figure 21(c)) in terms of velocity distributions along the horizontal center line (b) and along a vertical line (a) through the peak velocity point. Reference 18 states that a high degree of flow asymmetry and instability existed for the three higher expansion angles, while the two lowest ones produced stable flow. The distribution for 2θ of 15.8° does not show separated flow; however, separation may have existed intermittently at some location within the diffuser. In addition, the separation indicated for 2θ of 10.6° must have been minor in nature. For the type of diffuser illustrated, the data and observations of reference 18 show that expansion angles in excess of 10° may produce flow separation and instability.

Annular diffusers.- Data on annular diffusers with a cylindrical outer wall are given in figure 21(d) for a thick inlet boundary layer (δ^*_1/R_1 of 0.078). The velocity distributions at the diffuser exits (station 2) show separated flow for all but the 16.7° diffuser, which had highly distorted flow and also may have had local regions of separation. The measurements at the tailpipe station (station 3), which was located 1.07 outer diameters from the diffuser inlet, show greatly improved distributions obtained from natural mixing in the tailpipe, the 34° diffuser corresponding to the most uniform profile. The roughly elliptical shape of the inner bodies for the 26° and 34° diffusers may have influenced the performance beneficially. The data results furnish an example of the substantial advantage of a short length of constant-area duct at the diffuser exit.

Inlet speed effects.- As previously discussed, the effect on diffuser performance of increasing the inlet speed is adverse in all respects except for the cases where the expansion angle is so low that wall friction produces a substantial part of the total pressure loss. These general statements also apply to exit velocity distributions.

Data for conical diffusers with an area ratio of 2.0 and thin inlet boundary layers are given in figures 22(a) and 22(b). Adverse effects of increasing the inlet Mach number are shown to various degrees. In cases where the flow is separated the data may be expected to be optimistic and less accurate.

Data on rectangular diffusers with a thin inlet boundary layer are given in figures 22(c) and (d). The curves do not show a definitive effect due to inlet speed; however, reference 18 makes it clear that the effect is adverse.

Exit displacement area.- The character of the diffuser exit velocity distribution is not completely defined by limits on either the total pressure or the velocity distortion. Parameters which define a velocity distribution more accurately are displacement area and the boundary-layer shape parameter (the ratio of displacement area to momentum area). Both parameters are required to estimate the character of the distribution in the absence of actual data points. Since both quantities represent values integrated across the station, rather than point values in the flow, more uniform variation with changes in independent variables is to be expected. The following discussion will indicate that the behavior of these quantities can be mapped successfully for conical diffusers. Sufficient data do not exist for a map of other types of diffusers.

The three-dimensional exit displacement area Δ^*_2/A_2 is presented in figure 23 as a function of expansion angle. All measurements were made at the diffuser exit except those corresponding to an area ratio of 4.0 and δ^*_1/R_1 of 0.006, which were taken 1 diameter downstream in the tailpipe. The exit displacement area for this case would be higher than those shown. Figure 23 gives the immediate impression that thin and thick boundary layers produce two unrelated families of curves; however, close inspection indicates that extrapolation through use of cross plots of both sets of data to obtain curves for an area ratio of 2.0 and δ^*_1/R_1 of 0.082 might produce a curve common to both families. Increasing area ratio is noted again to produce opposite effects for thin and thick boundary layers. The exit displacement area is useful in estimating the area ratio required for a given diffuser application, since it can be added to a value determined from one-dimensional relations to determine the actual geometric exit area required to produce a given maximum velocity.

The same Δ^*_2/A_2 data are given in figure 24 as a function of the ratio of diffuser length to inlet diameter. Figure 25 shows that a single value of this independent parameter is determined by any combination of 2θ and A_R. The purpose of using the parameter was to determine whether A_R could be eliminated as a variable. The curves of figure 24 for the thick inlet boundary layer (Δ^*_1/A_1 of 0.136) show that there is a lack of dependence of Δ^*_2/A_2 on area ratio for values of L/D_1 in excess of about 17. Values of L/D_1 below 17 produce individual curves for each value of A_R which, at L/D_1 of zero, approach a value corresponding to a simple function of A_R and Δ^*_1/A_1. This function was derived on the assumption that for a diffuser of zero length the displacement area at station 2 is equal to that at station 1 plus the geometric area difference between stations 1 and 2. The values of Δ^*_2/A_2 for the thick-boundary-layer case become approximately constant for values of L/D_1 in excess of 28. The constant value corresponds approximately to a fully developed pipe-flow distribution. If sufficient data were available, it would probably show that a curve for any area ratio and inlet boundary-layer thickness would approach the same constant value of Δ^*_2/A_2 as L/D_1 increases, and the exit velocity distribution would approach that for pipe flow.

Exit mean dynamic pressure.- Since the loss factor K minus a term containing the loss in effectiveness $1 - \eta$ can be expressed as a function of the exit mean dynamic pressure (see eq. (2)), it is of interest to examine the behavior of the same conical-diffuser data in terms of this parameter. Figures 26(a) and 26(b) present the data as a function of 2θ

and L/D_1, respectively, in a fashion similar to that for the displacement area. Peters' data (ref. 10), which were calculated by using equation (2), are included for a thick and thin inlet boundary layer. Figures 26(a) and 26(b) show that the exit mean dynamic pressure behaves in much the same manner as the displacement area, and the same general comments may be applied to both.

Exit three-dimensional shape factor.- The conical-diffuser data are presented in terms of exit three-dimensional shape factor $\left(\Delta^*/\theta_3\right)_2$ in figure 26(c). The trends of the curves are the same as those for the exit displacement area and mean dynamic pressure. The table at the top of the figure notes two- and three-dimensional values of shape factor generally regarded as indicating limits on important ranges of values (ref. 5). The range of δ^*/θ between 1.286 and 1.80 is identified with attached flow, between 1.80 and 2.60 with either attached or separated flow, and beyond 2.60 with separated flow. The actual data points agree with this concept with two possible exceptions, the 10° diffusers for area ratios of 5.8 and 7.8. Although figure 21(b) shows these two profiles to be attached, the shape factors are in the range which should correspond to separated flow. It may be significant that reference 15 states that small regions of separated flow may have existed near the upstream end of the 10° diffuser. Of the data given in figure 26(c) no separated-flow profile produced a value for $\left(\Delta^*/\theta_3\right)_2$ of less than $2.5(\delta^*_2/\theta_2 = 2.1)$. The plot at the top of the figure was constructed from the flow-steadiness observations of reference 21 for a very thin boundary layer and a low inlet Mach number. Assuming that unsteady flow corresponds to separated flow, the plot is not in disagreement with the comparable data for conical diffusers. The relationship between maximum expansion angle for stable flow and area ratio probably would be altered by changes in inlet boundary-layer thickness or Mach number.

Boundary-Layer Control

The principal difficulty in almost all diffuser design requirements is that of obtaining the performance of a long, low-expansion-angle diffuser by using a short, high-angle diffuser since there is rarely sufficient space available for the optimum design. Boundary-layer-control devices are used frequently to improve the performance of short diffusers as well as to improve the performance of designs which do not operate satisfactorily for some reason not anticipated in the design stage. Because of the many additional variables introduced by boundary-layer control, few investigations are comprehensive enough to furnish design and performance data; therefore, the presentation will be in the nature of illustrations of improvements obtainable by use of boundary-layer controls.

The common forms of boundary-layer control may be grouped into three categories, as follows:

(a) Removal of low-energy air by suction, diverters, and so forth

(b) Reenergization of the boundary-layer air by injection of high-energy air, or by turbulence promoters or mixers such as vortex generators

(c) Reduction in energy dissipated in the boundary layer by alteration of the basic diffuser flow pattern through use of splitter or turning vanes, screens, and so forth

Each device has its own particular merits, and the proper choice is contingent on the individual requirements of each particular design.

Conical diffusers.- Examples of reductions in the loss in effectiveness obtainable with vortex generators and with suction are given in figure 27 for conical diffusers. For diffusers with expansion angles of 10°, 20°, and 30°, an area ratio of 5.2 and δ^*_1/R_1 of 0.007, curves with and without vortex-generator installations are given from reference 22. The generators were tapered airfoils designed to approximate constant circulation spanwise in the boundary layer and were NACA 64_1-812 airfoil sections. The table on the left-hand side of the figure furnishes information on the generator installations. Considerable improvement in the static-pressure rise was obtained for all three of the expansion angles tested, 10°, 20°, and 30°; however, in no case was separation eliminated. The separation point (as indicated by tufts) was moved downstream from the 8-percent length station to the 90-percent station by the use of the generators in the 10° diffuser. The installations were considered to be optimum. A series of points at 2θ of 23° is given (ref. 23) for several inlet boundary-layer thicknesses, with and without vortex-generator installations. The area ratio of the diffuser was 2.0 and the generators (see table on right side of figure) were rectangular NACA 0012 airfoils. Very large improvements were obtained for all boundary-layer conditions. The diffuser flow with no control exhibited separated and highly unsteady flow. The separation and unsteadiness were eliminated by the vortex-generator installations, which were considered to be approximately optimum.

Data curves with and without suction control for diffusers with A_R of 4.0 and δ^*_1/R_1 of 0.006 (ref. 24) are given, as well as points at 2θ of 30° for several values of δ^*_1/R_1. Suction slots were cut in the diffuser wall at optimum locations. The wall consisted of a cardboard cone supported by wire screen. Values of static-pressure rise were obtained by using wall static orifices in a fixed strut extending along the axis of the diffuser. The optimum suction-flow quantity (noted adjacent to each data point) was determined by using an arbitrary evaluation of the suction

power which was not related to diffuser inlet conditions. The optimum quantities are, therefore, subject to question. It was noted during the tests that optimum conditions reduced flow fluctuations satisfactorily. The data show very large improvements at high expansion angles and indicate that no improvement would have been obtained at an expansion angle of about 13°. The optimum suction quantities vary from 3 to 6 percent for δ^*_1/R_1 of 0.006 to 16 percent for δ^*_1/R_1 of 0.031.

Annular diffusers.- Data for annular diffusers with several types of boundary-layer control are given in figure 28. The curve showing $1 - \eta$ with vortex generators corresponds to one of the better installations with vortex generators mounted on the inner wall only. The isolated points at expansion angles of 26° and 34° with vortex generators correspond to two rows of generators in tandem mounted on the inner wall. Vortex generators which were mounted on the inner wall only allowed the boundary layer on the outer wall to become thicker as a result of the additional pressure rise produced by the vortex generators. The isolated point at 2θ of 16.7° corresponds to vortex generators mounted on both the inner and outer walls and indicates a considerable improvement due to the outer-wall installation. Separation on the inner body was eliminated for the 16.7° diffuser only.

The boundary-layer-control data corresponding to suction, suction with a vane installation, and injection indicate higher gains in performance than with vortex generators. This result is to be expected since the vortex-generator action is limited to mixing the energy available in the diffuser flow, whereas control using auxiliary flow is limited only by the auxiliary-flow-system design. Suction quantities on the order of 2 percent produced large improvements in contrast to the 16 percent used for the conical-diffuser investigation, which had less than one-half of the inlet boundary-layer thickness. The 2-percent quantity is close to an optimum quantity as determined from effectiveness values corrected for a suction power calculated by using the diffuser inlet conditions as a reference. The data for diffusers with an area ratio of 3.19 show essentially no gains produced by use of splitter vanes; however, the splitter-vane design was not made optimum. The use of the controls stabilized the flow for the diffusers which were unstable ($2\theta > 8.5°$).

Exit velocity distributions.- A number of examples showing the improvements in exit velocity distribution obtainable with several diffusers with cylindrical outer bodies and an area ratio of 1.91. Where vortex generators, suction, or injection were used, the improvements would be expected to be confined to the center of the duct since all controls were located on the inner wall. This situation necessarily caused the outer-wall distribution to depreciate with control. In most

cases, the distributions are presented for two stations, one at or near the end of the inner body, and one at a common tailpipe station (station 3) which was located 1.07 outer duct diameters from the diffuser inlet.

Figures 29(a) and (b) give results with vortex-generator control. For all diffusers at both stations the flow was shifted toward the center of the duct. All but the 16.7° diffuser produced separated flow off the inner body, with or without generators. At the tailpipe station, the vortex generators in the 34° diffuser produced the most uniform distribution near the center line.

Figures 30(a) to (d) indicate the effects of suction, injection, and vanes. The curves at the top of figure 30(a) show that suction through discrete holes distributed over an appreciable area of the surface of the inner body for a 34° diffuser eliminated separation on the inner body and more than doubled the velocity on the center line at the tailpipe station. This result was obtained with 3.5-percent-suction flow. Adequate control on the outer wall might have provided almost constant velocity across the duct. The curves at the bottom of figure 30(a) show that suction through a backward-facing slot was superior to injection because of flow separation off the cowl with injection.

The use of suction and injection in conjunction with a turning vane is illustrated at the top of figure 30(b). The vane increased the effectiveness of both suction and injection, resulting in better distributions at lower auxiliary flows. The single vane installation illustrated at the bottom of the figure resulted in no appreciable improvement because the design placed the vane wake near the center line of the inner body instead of in the center of the annular exit area.

Suction and injection control in conjunction with a vane in an abrupt-dump diffuser (fig. 30(c)) required high auxiliary flow quantities to obtain significant improvements with the short vane. The longer vane produced fairly uniform flow; however, the loss coefficient was high because of the abrupt dump. Suction and injection alone with an abrupt dump (fig. 30(d)) again required high auxiliary flows.

Exit displacement area.- The data of figures 21(d), 29, and 30 were converted into terms of exit displacement area Δ^*_2/A_2 in order to obtain a better comparison of the effects of various controls on the uniformity of the exit velocity distribution. The results are given in figure 31. The data for the diffusers with A_R of 1.91 show that the 1- and 2-percent-suction cases produced the biggest improvements at the station located at the end of the inner body. At the tailpipe station (identified by the sketch showing a tailpipe length), the 1-percent-suction case has less displacement area than the 2-percent-suction case because of the adverse effect of the increased pressure rise on the

distribution on the outer wall. At the tailpipe station the vortex generators produced the smallest values of displacement area. Values of Δ^*_2/A_2 below about 0.18 have less displacement area than a pipe-flow distribution.

Design of boundary-layer-control systems.- When reduced to a common basis, the data of references 23 and 25 on investigations of the performance of vortex generators installed in diffusers agree reasonably well with respect to optimum values of geometric variables. The generators used were of rectangular plan form with NACA 0012 sections. The agreement obtained between the two investigations would indicate that the resulting design numbers may be quite general since the diffuser configurations and inlet conditions differed widely. Values of span, chord, spacing, and location have been expressed in terms of the two-dimensional displacement thickness at the reference inlet station (fig. 32), which corresponded approximately to the vortex-generator location. For both sets of data an angle of attack of $\pm 15^\circ$ (counterrotating) was found to be optimum. In addition, figure 32 indicates the following values to be very close to optimum for all curves:

Span, b/δ_1^*	5
Chord, c/δ_1^*	20.8
Spacing, s/δ_1^*	15.4
Location, L/δ_1^*	-50

The curves show that increasing the inlet speed makes the performance more sensitive to the degree to which the installation differs from the optimum. The annular-diffuser data indicate no optimum chord within the range of the data, which is contrary to the conical-diffuser data. The optimum chord and span values chosen correspond to an aspect ratio of 0.24. The value of optimum location is mostly academic because if space were available to locate generators far upstream of the inlet, the diffuser could, in many cases, be lengthened, thus eliminating the need for vortex generators.

The table of reference values given in figure 32 corresponds to the basic installation used when each variable was changed. It is evident that the reference conditions were not optimum; therefore, it follows that the indicated optimums may not be exactly accurate. The biggest discrepancy between the indicated optimums for the three data curves and the reference values occurs for the chord ratio c/δ^*_1. The value of

20.8 is about $1\frac{1}{2}$ times that used for a reference and might correspond, for instance, to a larger optimum spacing than that indicated. Reference 26 presents data illustrating clearly the effects of vortex generators on turbulent boundary-layer flow. In the reference a parameter is discussed which is referred to as the "solidity" and is defined as $\frac{c \sin \alpha}{s}$. A maximum value of 0.35 is recommended for the parameter. Since it is considered to be proportional to the vortex strength, the maximum value is assumed to be optimum, and thus the value of 20.8 was selected for the ratio of chord to displacement thickness. Corresponding values of span and angle of attack recommended in the reference are approximately equal to those chosen herein.

In any diffuser with boundary-layer control, the principal object is to obtain a satisfactory performance from the standpoint of total-pressure loss or velocity distribution, or both. Since in systems which involve secondary flow (suction or injection) the auxiliary-flow power and quantities must be considered in evaluating the performance, the secondary objective is to minimize these quantities. References 14 and 27 indicate that the most satisfactory suction power coefficient is as follows:

$$P_s = \frac{R}{100} \frac{\overline{H_1} - H_s}{\overline{q_{c_1}}}$$

where, as shown in figure 33, $\overline{H_1} - H_s$ is the pressure rise across the auxiliary-flow pump. If the auxiliary-flow ducting losses are significant, they should also be included in the pump pressure rise. If desired, the coefficient may be divided by the pump efficiency. In an actual design, it is quite probable that the suction air would not be discharged into the diffuser inlet, and in addition it is possible that a pump would not be required if a suitable low-pressure region is available for discharge of the suction air. However, for research purposes as well as to evaluate the performance, it is necessary to reference the pump pressure rise to inlet total pressure to avoid the use of variables extraneous to the flow in the diffuser. In addition, it is clear that in an actual installation the pump pressure rise as indicated is equivalent to the pressure drop chargeable to the auxiliary-flow system, since the system can only be responsible for pressure deficiencies below the total pressure at the diffuser inlet. The diffuser performance may be corrected

for pumping power as follows:

$$\eta = \frac{\left(\Delta p / \overline{q_{c_1}}\right)_{actual}}{P_s + \left(\Delta p / \overline{q_{c_1}}\right)_{ideal}}$$

$$\frac{\overline{\Delta H}}{\overline{q_{c_1}}} = \left(\frac{\overline{\Delta H}}{\overline{q_{c_1}}}\right)_{measured} + P_s$$

The preceding discussion and a study of the investigations available in the literature and of unpublished data lead to the following general guiding principles applying to the design of suction boundary-layer-control systems:

(a) The basic diffuser design should be as aerodynamically efficient as the space and other restrictions will allow in order to reduce to a minimum the suction-flow quantities and pressure drops required.

(b) The final design, when used with control, should be free from flow separation in the diffuser because this drastically increases the suction-flow quantities and pressure drops required.

(c) The area of the diffuser wall covered by suction-flow openings (holes, slots, porous media, etc.) should extend to a position slightly upstream from the location of natural flow separation without control. This procedure locates the suction openings as near to the high-pressure end of the diffuser as possible, thus reducing the pump pressure rise. The use of suction control appreciably upstream from the natural separation point is not justified since there appears to be no particular merit to maintaining low boundary-layer shape factors except at the diffuser exit where uniform velocity distributions are desired.

(d) The diffuser wall area covered by suction-flow openings should extend a sufficient distance downstream to produce the quality of exit velocity distribution desired.

(e) The suction openings should be the maximum size consistent with structural integrity and the maintenance of an aerodynamically satisfactory surface. The size and distribution of the suction openings should also be such that H_s (fig. 33) does not exceed P_x at the upstream openings, a situation which would allow recirculation of the suction flow through the diffuser wall.

While the preceding principles will serve as a guide in laying out a design, they furnish no quantitative values. Quantitative values, in general, are not available in the literature. For instance, such basic quantities as the amount of suction flow required for a given design and set of conditions still have to be determined experimentally. The optimum quantity for a given configuration would be expected to be determined by the condition of the inlet boundary layer. The data of reference 24 for a conical diffuser with A_R of 4.0 and 2θ of 30° indicate that a suction quantity of 4 to 6 percent of the inlet total flow per increment of 0.01 in δ^*_1/R_1 is required. However, this result should be considered with reservations because of the method used in reference 24 for evaluating suction power, which was the prime factor in determining optimum performance. Unpublished data by Wilbur and Higginbotham on a 34° annular diffuser with a cylindrical outer body and A_R of 1.91 show that for this case, for δ^*_1/R_1 of 0.078, the optimum value of suction quantity varies between 0.13 percent and 0.32 percent per increment of 0.01 in δ^*_1/R_1 according to the value of total open area of the suction holes. An upper limit for the optimum value of 0.36 percent was indicated and was fixed by the deterioration of the boundary layer on the uncontrolled flow near the outer wall. The deterioration was caused by the increased pressure gradient produced by the suction control on the inner wall. In the case of a single-wall diffuser, such as a conical diffuser, a limitation of this type would not be imposed unless struts or a similar drag-producing object were installed in the diffuser. Another significant result derived from Wilbur and Higginbotham's investigation is that the principal advantage of suction from an appreciable area of the diffuser walls, as opposed to suction from a restricted sector such as a slot, appears to be that area suction produces better exit velocity distributions. Static-pressure rise and total-pressure loss were unaffected by varying the extent of area covered by the suction openings. These results necessarily are limited to the particular configuration tested since similar data for other types are not available.

Effects of Distorted Inlet Velocity Distribution

All data presented and discussed prior to this section of the paper have corresponded to favorably shaped inlet boundary-layer distributions such as would be obtained in flow along a surface in practically a zero pressure gradient. A few minor exceptions have been noted. In any practical diffuser installation the diffuser is preceded by some other duct element, such as a bend, air inlet, or turbine, which in many cases does not discharge a uniform or favorable velocity distribution. In such instances, the diffuser performance is generally adversely affected and is substantially below that predicted by most research data. Distorted velocity distributions may occur at the diffuser inlet in either

subsonic or supersonic flow systems; however, the most serious cases occur in the subsonic diffuser preceded by a supersonic compression inlet which has subjected the boundary layer to intense pressure gradients produced by compression shock waves.

Conical diffusers.- Reference 20 presents data on the effect of various degrees of inlet velocity distortion on the performance of curved-wall diffusers with different lengths of low-expansion-angle (2θ of 2°) ducting on the upstream end of the diffuser. These data are summarized in figure 34(a) in terms of loss in effectiveness[1] as a function of inlet boundary-layer thickness for an inlet Mach number of 0.2. Inlet velocity profiles and boundary-layer shape factors are given at the top of the figure. It will be noted that the two thickest boundary layers correspond to separated flow at the inlet. The variation in inlet velocity distribution was obtained by mounting spoilers on the wall of the inlet bell upstream of the diffuser. One curve of Peters' data (ref. 10) for a straight-wall, 10° diffuser and for a low inlet boundary-layer shape factor is given for comparison purposes.

For the two thinnest boundary layers, the longer diffusers suffered performance losses due to excessive friction losses. For the two thickest boundary layers with separated flow, the longer diffusers produced higher performance because the upstream low-expansion-angle ducting allowed the flow to become attached and more uniform before the high expansion rate started. At a boundary-layer thickness δ^*_1/R_1 of 0.06 the data of reference 20 are optimistic compared with Peters', especially since Peters' data correspond to the more favorable inlet conditions. The results show clearly that some length of low-expansion-angle ducting is advantageous for cases where the inlet flow distribution is distorted.

The effect of changes in inlet Mach number on the loss in effectiveness of the diffusers of reference 20 is illustrated in figure 34(b) for three cases of distorted inlet velocity distributions. The superiority of lengths of low-expansion-angle ducting upstream of the main diffuser is again apparent for cases where the inlet flow is distorted.

---

[1]For the data of reference 20 in figures 34(a) and 34(b), the previously discussed definition of effectiveness η does not apply. The assumption of quasi-one-dimensional flow inherent in the definition of ideal static-pressure rise used heretofore was violated by the existence of separated flow at the inlet to the point where it appeared advisable to modify the definition. In these instances (figs. 34(a) and 34(b)), the ideal static-pressure rise was defined as the sum of two quantities. One of the quantities was defined as the static-pressure rise obtainable ideally by mixing the inlet velocity distribution until it is uniform in a constant-area duct with no total-pressure loss. The other quantity was the isentropic, one-dimensional, static-pressure rise associated with the diffuser area ratio, M_1', and q_{c_1}'.

Annular diffusers.- Reference 28 presents data on the effect on $1 - \eta$ of various degrees of inlet velocity distortion, which were obtained by mounting spoiler screens in the ducting upstream of the diffusers. Figure 34(c) summarizes these data for two cases, with and without a splitter-vane installation. Since the several distributions tested represent no regular progression of a single variable defining the amount of distortion, the data have been presented as a principal function of expansion angle, and the values of inlet boundary-layer thickness and shape factor have been identified.

For sufficient distortion of the inlet flow for the lowest expansion angle, with or without splitter vanes, the loss in η approached the theoretical value for a sudden expansion, which is 0.48. The curve for the highest degree of distortion suggests that an expansion angle of about 4° would be required to obtain a performance approaching that for the undistorted flow at the optimum angle of about 7°. High performance could also have been obtained through use of boundary-layer controls or by smoothing out the distribution upstream of the diffuser through use of a constant-area straight section or some other device. Sufficient data do not exist to determine the most efficient procedure. The use of a splitter vane produced stable flow; however, high performance was not obtained in any case, apparently because of the friction losses associated with the splitter-vane surface. No attempt was made to obtain the optimum splitter-vane installation.

Analysis of shock—boundary-layer interaction effects.- The flow delivered by supersonic inlets to the subsonic diffuser has generally been subjected to a normal shock and in some cases also oblique shocks. The incidence of these shocks on the boundary layer upstream of the subsonic diffuser may produce seriously distorted boundary-layer velocity distributions at the subsonic diffuser inlet. The boundary layer in such a condition cannot negotiate high pressure gradients; therefore, unless boundary-layer control or its equivalent is used in the throat of the inlet, the rate of area expansion of the subsonic diffuser must be low, especially near the throat. An approximate analysis has been made by using typical supersonic-inlet recovery data in order to determine the magnitude of the losses chargeable to shock—boundary-layer interaction; where shock—boundary-layer interaction loss is defined as the loss experienced in the subsonic diffuser in excess of that which would have been obtained with a favorable inlet boundary-layer distribution.

The analysis was based on data from investigations of the general configuration shown in figure 35. Since the majority of the data in the literature is on conical spike inlets with no contraction and since this type of inlet appeared to have the broadest application, it was selected as the basis for the analysis. However, a limited amount of data is also included for the designs with internal contraction. Only test data corresponding to supersonic supercritical operation at 0° angle of attack were used in order to make possible the calculation of shock losses.

Comparisons of theoretical shock pressure recoveries with measured overall recoveries are given in figures 36 and 37. The symbols used are identified with regard to the reference source and configurations in tables II and III. Figure 36 contains data on inlets with no internal contraction and figure 37 on inlets with contraction. For simplicity of presentation, the curves of figures 36 and 37 were calculated by using cone surface values for the flow parameters required to calculate normal-shock losses. In addition, the curves of figure 37 are based on the maximum area contraction for starting the inlet. The difference between the recovery values for each symbol and the appropriate calculated shock recovery curve represents losses occurring in the subsonic diffuser. This difference varies between 4 and 20 percent of free-stream total pressure H_0 with the majority of the data corresponding to about 8 percent. The data scatter is not surprising in view of the wide variety of configurations included. For all cases given in table II except the highest expansion angles and area ratios, a loss of $0.08H_0$ in the subsonic diffuser is far in excess of what would be predicted from data such as those given in figures 3 and 6. The conclusion is that large losses may be obtained in the subsonic diffuser as a result of shock—boundary-layer interaction effects.

The data of figures 36 and 37 were used to estimate the subsonic-diffuser loss chargeable to shock—boundary-layer interaction. The calculation consisted of subtracting from the overall measured loss the sum of the calculated shock losses and the estimated subsonic-diffuser loss for favorable inlet boundary-layer conditions (based on figs. 3 and 6). Since only supersonic supercritical operation with the normal shock at approximately the minimum-area section was considered, the shock losses and conditions upstream of the normal shock at the subsonic-diffuser inlet could be accurately computed. Flow conditions at and upstream of the cowl inlet were determined from conical-flow theory. The total pressure and Mach number in the plane of the inlet were determined by averaging the values at the cone surface and cowl lip. This procedure was not used in calculating the curves of figures 36 and 37 because it would have introduced another variable, the ratio of cowl diameter to cone diameter. The small increase in accuracy did not justify the added complication in presentation. The total pressure and Mach number based on average values are used as independent variables in presenting shock—boundary-layer induced losses for cases with no internal contraction or straight section. The quantities differ from weighted averages by less than 1 percent. With internal contraction and/or a straight section, average values in the plane of the inlet were used in calculating supersonic flows downstream of the inlet by one-dimensional relations and also in calculating total-pressure losses and Mach number changes due to friction effects in ducting between the inlet and the minimum-area section. Passage areas involved in the calculations corresponded to planes through the average normal to the annular surfaces. The basic subsonic-diffuser loss corresponding to a favorable inlet velocity distribution was estimated by using figures 3

and 6. The extra friction loss of annular diffusers, as compared with that for conical ones, was accounted for. Since the expansion angles of all the diffusers were low, no correction for increased loss coefficient due to high inlet Mach numbers was used.

The shock—boundary-layer interaction losses calculated according to the preceding procedure are given in figure 38 for configurations with no internal contraction and in figure 39 for the cases with internal contraction. The data are presented as a function of the Mach number just upstream of the normal shock since the Mach number determines the normal-shock strength, which should govern the interaction losses. The total-pressure loss was referenced to the total pressure upstream of the normal shock for the same reasons. Since the normal-shock strength is the only independent variable accounted for in figures 38 and 39, differences in loss values at any given Mach number M_{1a} are probably due to differences in geometry and/or differences in the condition of the boundary layer prior to the normal shock.

The data of figure 38 form two distinct groups. One group produces an approximately constant loss coefficient ($\Delta H/H$ of 0.028) with changes in Mach number and includes the majority of the data. The other group, which originated from a single source, produces a loss-coefficient variation which increases rapidly with Mach number. The similarity of the models and test conditions (see table II for identification of symbols) indicates that differences in the condition of the boundary layer prior to the normal shock probably were not significant. The most probable reason for separation of the data into two groups is the differences in subsonic-diffuser expansion angles. The high curve corresponds to an expansion angle of 9.4° whereas the expansion angles for the data averaging a loss coefficient of 0.028 range from about 3° to 5°. The data scatter about the lower curve probably results from the secondary effects of the many differences in model configuration, such as cowl shape, inner-body angle and shape, length of constant-area passage, and so forth.

The data with internal contraction given in figure 39 cover the same expansion-angle range as the lower curve in figure 38; however, much higher losses are indicated. The data scatter is large, which produces low correlation accuracy. The higher losses indicated presumably could be due to thickening and distortion of the boundary layer in the contracting section.

From the standpoint of estimating performance, it is of interest to determine the relation of shock—boundary-layer interaction losses to the basic diffuser loss predictable from data for favorable inlet boundary-layer distribution. Figure 40 presents the data for no internal contraction in the form of the ratio of interaction loss to basic diffuser loss as a function of Mach number. The data for low expansion angles (3° to 5°) showed an average interaction loss equal to 75 percent of the

basic diffuser loss. The interaction loss for the expansion angle of 9.4° increased rapidly with Mach number, reaching a value of about 16 times the basic diffuser loss at a Mach number of 1.87.

The effect of thicker boundary layers on interaction losses may be obtained from the data of figure 41, which presents test results on half-conical inlets mounted either on a flat plate or a fuselage shape. Such configurations would produce an initial boundary-layer thickness at the cone apex. The subsonic-diffuser expansion angles were 3° and 5°. The presence of the thicker boundary layer increased the loss substantially in each case. The use of boundary-layer control reduced the losses substantially.

Shock—boundary-layer measurements in a 5° diffuser.- Data were obtained on a 5° converging-diverging conical diffuser run at a Mach number of 1.4 to provide additional information on shock—boundary-layer interaction effects on diffuser performance. The configuration, tests, and measurements are described in the appendix. Total- and static-pressure surveys were made at several stations in the diffuser for a series of normal-shock locations. This procedure resulted in Mach numbers before the normal shock ranging from about 1.27 to 1.57. Thus, the test conditions differ from those pertaining to the prior analysis of the spike-type inlets where the performance applies only to the case with the shock near the minimum section.

The values of shock—boundary-layer interaction loss coefficient obtained in the investigation are given in figure 42 as a function of the Mach number before the normal shock. The total-pressure loss is referenced to the compressible dynamic pressure after the normal shock. The loss coefficient increased rapidly with increasing Mach number even though the expansion angle was small and no separation was measured in the diffuser. The loss curve of figure 39 for spike-type inlets with contraction was converted into terms of $\Delta H/q$ and is also presented in figure 42. There is a marked similarity between the two curves, with the conical diffuser producing appreciably higher losses at the higher Mach numbers. This result is probably due to the appreciable run of supersonic flow between the throat and the downstream shock positions. This segment of the flow was subjected to alternate compression and expansion waves which may have impaired the boundary-layer shape.

The growth of the boundary-layer parameters Δ^*_c, θ_{c_3}, and Δ^*_c/θ_{c_3} along the length of the diffuser for several different shock positions is shown in figures 43, 44, and 45, respectively. The boundary-layer parameters correspond to three-dimensional, compressible values. The ratio of the area at a local station to the area at the shock position is the independent variable. The displacement and momentum areas increased in a systematic fashion with diffuser length for the two weaker shocks. The

two stronger shocks produced abrupt increases at first, followed by lesser rates of increase. In general, the overall rate of increase became higher as the normal-shock strength increased.

The behavior of the shape factor Δ^*_c/θ_{c_3} resulting from the changes in Δ^*_c and θ_{c_3} (fig. 45) indicates that after the initial increase in shape factor caused by the shock, the 5° expansion angle produced a general reduction in the value of Δ^*_c/θ_{c_3} as the flow proceeded along the length. This is an important result since it indicates that an expansion angle of 5° is low enough to produce an improvement in the boundary-layer distribution under adverse inlet conditions. The range of two-dimensional, incompressible δ^*/θ generally associated with flow separation is 1.8 to 2.6. Since some of the higher values indicated in figure 45 fall within this range when converted to two-dimensional quantities, separated flow could be expected. The measurements indicated no separation; however, some flow asymmetry could have existed with small local regions of separation.

The change in Mach number distribution at the several survey stations with changes in shock position is illustrated in figure 46. As the shock was moved downstream, the subsonic distributions became more distorted and exhibited higher peak Mach numbers. For instance, the peak Mach numbers at station 5 were 0.52, 0.58, 0.71, and 0.93 for shock positions 1, 2, 3, and 4, respectively, which illustrates the magnitude of the adverse effects of shock—boundary-layer interaction obtainable even though flow separation was not present to any measureable extent.

The velocity distributions at the exit of the subsonic diffuser are given in figure 47 for several Mach numbers before the normal shock. Although the curves do not show an exactly progressive change with increasing Mach number, a definite trend towards less uniform velocity distributions with increasing normal-shock strength (increasing Mach number before shock) is apparent in general. In each case the depression in velocity near the center line of the duct was caused by the total-pressure loss due to the combination of the normal shocks on the throat center line and in the diffuser proper. As the diffuser normal-shock losses increased, the total-pressure losses at the walls due to shock—boundary-layer interaction increased at a higher rate, which produced a trend towards smaller deficits in u/U on the center line and a thicker boundary layer as the normal-shock strength increased. While the 5° diffuser produced better boundary-layer velocity distributions at the exit than those at the inlet and thus produced low values of boundary-layer shape factor at the exit, figure 47 clearly shows that the resultant exit velocity distributions for the higher shock strengths were quite nonuniform when considered on an area basis. Smaller expansion angles or boundary-layer controls would be required to obtain more uniform distributions.

CONCLUDING REMARKS

The subsonic-diffuser data available in the literature have been reviewed, reduced to certain appropriate performance coefficients based on the total-pressure loss, static-pressure rise, and exit velocity distribution, and presented as functions of the significant geometric and flow variables. The presentation has been divided into the following parts: performance at low speeds (inlet Mach numbers of approximately 0.20), effects of increasing the inlet speed up to choking Mach numbers, illustrations of the effectiveness of boundary-layer controls, and illustrations of the effects of distorted inlet velocity distributions as obtained at subsonic speeds with spoilers upstream of the inlet and as obtained from compression shocks in supersonic inlets.

At low inlet speeds the construction of several fairly extensive performance maps for conical, rectangular, square, and annular diffusers was accomplished from the large amount of data available in the literature. Orders of magnitude were determined for the effect on performance parameters of increasing the inlet speed. The compressibility effect on optimum diffuser design was found to be largely unknown. Illustrations of the effectiveness of boundary-layer controls, in particular vortex generators and suction, were drawn from the available data, and some engineering approximations for optimum configurations of vortex-generator installations were made. From an approximate analysis of typical supersonic-inlet data, estimates of shock—boundary-layer interaction effects on total-pressure losses were made for a variety of shock conditions and diffuser configurations. Original data presented herein illustrate the effects of shock—boundary-layer interaction on the flow development in a 5° conical diffuser.

Certain aspects of diffuser design and performance were found to be in particular need of more research effort, including the effect of compressibility on optimum diffuser design, design information on boundary-layer-control systems for short diffusers with favorable inlet conditions, and optimum diffuser and boundary-layer-control designs with unfavorable inlet conditions (for example, with shock—boundary-layer interaction).

Langley Aeronautical Laboratory,
National Advisory Committee for Aeronautics,
Langley Field, Va., May 18, 1956.

APPENDIX

DETAILS OF AN INVESTIGATION OF A 5° CONVERGING-DIVERGING DIFFUSER AT A MACH NUMBER OF 1.41

Additional information relative to the data presented in figures 42 to 47 is given in the following paragraphs.

Apparatus and Instrumentation

The setup, which is diagramed in figure 48, consisted of an inlet bell of 20:1 contraction ratio, a supersonic nozzle with an 8- by $9\frac{1}{8}$-inch test section, and the converging-diverging diffuser mounted in the supersonic nozzle. The nozzle produced a Mach number of 1.41 with a maximum variation in Mach number of 0.006 in the vicinity of the diffuser inlet. The cross-sectional area of the nozzle test section was increased somewhat near the diffuser inlet in order to prevent the duct from choking in this section. The disturbances originating from the point where the contour changed intersected the model downstream of the diffuser inlet and did not affect the entering flow. The converging-diverging diffuser was started by momentarily increasing the test-section Mach number through use of a retractable conical body inserted in the throat of the inlet bell.

The line drawing of the diffuser (fig. 49) includes the apparent shock locations and the survey stations. The convergent section had an inlet diameter of 4.491 inches, a contraction ratio of 1.066, an included wall angle of 5°, and an external lip angle of 8°. The diverging section had a ratio of exit area to throat area of 2.0. The break in contour at the junction of the converging and diverging sections was rounded slightly. A straight section 1.13 diameters in length was located downstream of the diffuser exit. Butterfly-type doors at the end of the straight section were used to vary the diffuser back pressure and thus the shock location. The duct surface was chromium plated on machined steel.

Wall static orifices were installed along two generatrices 90° apart in a region extending from the inlet lip to $1\frac{1}{2}$ inches downstream of the throat. One of these rows was extended along the full length of the diffuser. Eight orifices were equally spaced circumferentially at the diffuser exit. Sting-supported total- and static-pressure tubes were used to make surveys at the several stations indicated in figure 49. A shielded total-pressure tube located upstream of the inlet bell was used

to obtain reference total-pressure readings. The ratio of the absolute static pressure immediately downstream of the normal shock to the reference total pressure was used as a correlating parameter in resetting a given shock condition.

Flow Distribution in the Throat

The pressure and Mach number distributions entering the diverging part of the diffuser were obtained by surveying the throat at station 1. The results of these surveys are presented in figure 50 for the case with the oblique shock attached. The total-pressure distribution indicates a boundary-layer growth on the wall and a high loss on the center line extending over a very small region. The maximum value of the loss on the center line is approximately equal to that for a normal shock at a Mach number of 1.41. The normal shock at the apex of the conical shock theoretically should have occurred slightly downstream of the throat for the 5° convergence angle; however, because of the boundary-layer growth the effective convergence angle was apparently somewhat higher. This result placed the normal shock slightly upstream of the throat.

The static-pressure distribution shows a peak static pressure in the center region due to the normal shock. The static pressure in the throat did not reach a value corresponding to the pressure rise through a normal shock at a Mach number of 1.41. Since the normal shock occurred upstream of the throat, the static pressure on the center line in the throat was determined partially by the ambient static pressure of the surrounding supersonic stream. The Mach number distribution resulting from the total- and static-pressure variations was nonuniform and varied from a value of 1.23 near the wall to about 0.93 on the center line. Surveys a short distance downstream of the diffuser throat indicated that the Mach number on the center line became supersonic again as a result of the lower static pressures produced by the increasing Mach number of the surrounding supersonic stream.

REFERENCES

1. Henry, John R.: Design of Power-Plant Installations. Pressure-Loss Characteristics of Duct Components. NACA WR L-208, 1944. (Formerly NACA ARR L4F26.)

2. Patterson, G. N.: The Design of Aeroplane Ducts. Rules to be Followed for the Reduction of Internal and External Drag. Aircraft Engineering, vol. XI, No. 125, July 1939, pp. 263-268.

3. Patterson, G. N.: Modern Diffuser Design. Aircraft Engineering, vol. X, No. 115, Sept. 1938, pp. 267-273.

4. Wyatt, DeMarquis D.: Analysis of Errors Introduced by Several Methods of Weighting Nonuniform Duct Flows. NACA TN 3400, 1955.

5. Von Doenhoff, Albert E., and Tetervin, Neal: Determination of General Relations for the Behavior of Turbulent Boundary Layers. NACA Rep. 772, 1943. (Supersedes NACA WR L-382.)

6. Tetervin, Neal, and Lin, Chia Chiao: A General Integral Form of the Boundary-Layer Equation for Incompressible Flow With an Application to the Calculation of the Separation Point of Turbulent Boundary Layers. NACA Rep. 1046, 1951. (Supersedes NACA TN 2158.)

7. Rubert, Kennedy F., and Persh, Jerome: A Procedure for Calculating the Development of Turbulent Boundary Layers Under the Influence of Adverse Pressure Gradients. NACA TN 2478, 1951.

8. Gibson, A. H.: On the Flow of Water Through Pipes and Passages Having Converging or Diverging Boundaries. Proc. Roy. Soc. (London), ser. A, vol. 83, no. 563, Mar. 2, 1910, pp. 366-378.

9. Gibson, A. H.: On the Resistance to Flow of Water Through Pipes or Passages Having Divergent Boundaries. Trans. Roy. Soc. Edinburgh, vol. 48, pt I, no. 5, 1911, pp. 97-113.

10. Peters, H.: Conversion of Energy in Cross-Sectional Divergences Under Different Conditions of Inflow. NACA TM 737, 1934.

11. Persh, Jerome, and Bailey, Bruce M.: A Method for Estimating the Effect of Turbulent Velocity Fluctuations in the Boundary Layer on Diffuser Total-Pressure-Loss Measurements. NACA TN 3124, 1954.

12. Wood, Charles C., and Higginbotham, James T.: Effects of Diffuser and Center-Body Length on Performance of Annular Diffusers With Constant-Diameter Outer Walls and With Vortex-Generator Flow Controls. NACA RM L54G21, 1954.

13. Little, B. H., Jr., and Wilbur, Stafford W.: Performance and Boundary-Layer Data From 12° and 23° Conical Diffusers of Area Ratio 2.0 at Mach Numbers up to Choking and Reynolds Numbers up to 7.5×10^6. NACA Rep. 1201, 1954. (Supersedes NACA RM L9H10 by Copp and Klevatt, RM L9K10 by Persh, and RM L50C02a by Little and Wilbur.)

14. Wilbur, Stafford W., and Higginbotham, James T.: Investigation of Two Short Annular Diffuser Configurations Utilizing Suction and Injection as a Means of Boundary-Layer Control. NACA RM L54K18, 1955.

15. Squire, H. B., and Carter, P.: Further Experiments on Conical Diffusers. Rep. No. T.P. 320, British N.P.L. (Rep. No. 13,499, A.R.C.), Nov. 6, 1950.

16. Squire, H. B.: Experiments on Conical Diffusers. Rep. No. Aero 2216, British R.A.E., Aug. 1947.

17. Copp, Martin R.: Effects of Inlet Wall Contour on the Pressure Recovery of a 10° 10-Inch-Inlet-Diameter Conical Diffuser. NACA RM L51E11a, 1951.

18. Young, A. D., and Green, G. L.: Tests of High-Speed Flow in Diffusers of Rectangular Cross-Section. R. & M. No. 2201, British A.R.C., 1944.

19. Naumann: Wirkungsgrad von Diffusoren bei hohen Unterschallgeschwindigkeiten. FB Nr. 1705, Deutsche Luftfahrtforschung (Berlin-Adlershof), 1942.

20. Scherrer, Richard, and Anderson, Warren E.: Preliminary Investigation of a Family of Diffusers Designed for Near Sonic Inlet Velocities. NACA TN 3668, 1956.

21. Reid, Elliott G.: Performance Characteristics of Plane-Wall Two-Dimensional Diffusers. NACA TN 2888, 1953.

22. Taylor, H. D.: Application of Vortex Generator Mixing Principle to Diffusers - Concluding Report. Air Force Contract W33-038 ac-21825. U.A.C. Rep. R-15064-5, United Aircraft Corp. Res. Dept., Dec. 31, 1948.

23. Valentine, E. Floyd, and Carroll, Raymond B.: Effects of Some Primary Variables of Rectangular Vortex Generators on the Static-Pressure Rise Through a Short Diffuser. NACA RM L52B13, 1952.

24. Gratzer, L. B., and Smith, R. H.: Boundary Layer Control for Wide Angle Diffusers. Rep. No. 300 (ONR Contract N6ori-217, Task Order No. I, Project No. NR-061-004), Univ. Washington Aero. Lab., Nov. 22, 1948.

25. Wood, Charles C.: Preliminary Investigation of the Effects of Rectangular Vortex Generators on the Performance of a Short 1.9:1 Straight-Wall Annular Diffuser. NACA RM L51G09, 1951.

26. Tanner, L. H., Pearcey, H. H., and Tracey, C. M.: Vortex Generators; Their Design and Their Effects on Turbulent Boundary Layers. Preliminary Report. Rep. No. F.M. 2015, British N.P.L. (Rep. No. 16,487, A.R.C.), Jan. 18, 1954.

27. Henry, John R., and Wilbur, Stafford W.: Preliminary Investigation of the Flow in an Annular-Diffuser—Tailpipe Combination With an Abrupt Area Expansion and Suction, Injection, and Vortex-Generator Flow Controls. NACA RM L53K30, 1954.

28. Johnston, I. H.: The Effect of Inlet Conditions on the Flow in Annular Diffusers. C.P. No. 178, British A.R.C., 1954.

29. Nelson, William J., and Popp, Eileen G.: Performance Characteristics of Two 6° and Two 12° Diffusers at High Flow Rates. NACA RM L9H09, 1949.

30. Persh, Jerome: The Effect of Surface Roughness on the Performance of a 23° Conical Diffuser at Subsonic Mach Numbers. NACA RM L51K09, 1952.

31. Nussdorfer, Theodore J., Obery, Leonard J., and Englert, Gerald W.: Pressure Recovery, Drag, and Subcritical Stability Characteristics of Three Conical Supersonic Diffusers at Stream Mach Numbers From 1.7 to 2.0. NACA RM E51H27, 1952.

32. Ferri, Antonio, and Nucci, Louis M.: Preliminary Investigation of a New Type of Supersonic Inlet. NACA Rep. 1104, 1952. (Supersedes NACA TN 2286.)

33. Moeckel, W. E., Connors, J. F., and Schroeder, A. H.: Investigation of Shock Diffusers at Mach Number 1.85. I - Projecting Single-Shock Cones. NACA RM E6K27, 1947.

34. Weinstein, Maynard I., and Davids, Joseph: Force and Pressure Characteristics for a Series of Nose Inlets at Mach Numbers From 1.59 to 1.99. III - Conical-Spike All-External-Compression Inlet With Supersonic Cowl Lip. NACA RM E50J30, 1951.

35. Leissler, L. Abbott, and Hearth, Donald P.: Preliminary Investigation of Effect of Angle of Attack on Pressure Recovery and Stability Characteristics for a Vertical-Wedge-Nose Inlet at Mach Number of 1.90. NACA RM E52E14, 1952.

36. Esenwein, Fred T., and Valerino, Alfred S.: Force and Pressure Characteristics for a Series of Nose Inlets at Mach Numbers From 1.59 to 1.99. I - Conical Spike All-External Compression Inlet With Subsonic Cowl Lip. NACA RM E50J26, 1951.

37. Brajnikoff, George B., and Rogers, Arthur W.: Characteristics of Four Nose Inlets As Measured at Mach Numbers Between 1.4 and 2.0. NACA RM A51C12, 1951.

38. Beke, Andrew, and Allen, J. L.: Force and Pressure-Recovery Characteristics of a Conical-Type Nose Inlet Operating at Mach Numbers of 1.6 to 2.0 and at Angles of Attack to 9°. NACA RM E52I30, 1952.

39. Nettles, J. C.: The Effect of Initial Rate of Subsonic Diffusion on the Stable Subcritical Mass-Flow Range of a Conical Shock Diffuser. NACA RM E53E26, 1953.

40. Gorton, Gerald C.: Investigation of Translating-Spike Supersonic Inlet as Means of Mass-Flow Control at Mach Numbers of 1.5, 1.8, and 2.0. NACA RM E53G10, 1953.

41. Goelzer, H. Fred, and Cortright, Edgar M., Jr.: Investigation at Mach Number 1.88 of Half of a Conical-Spike Diffuser Mounted as a Side Inlet With Boundary-Layer Control. NACA RM E51G06, 1951.

42. Piercy, Thomas G., and Johnson, Harry W.: Investigation at Mach Number 2.93 of Half of a Conical-Spike Diffuser Mounted as a Side Inlet With Boundary-Layer Control. NACA RM E52G23, 1952.

43. Allen, J. L., and Simon, Paul C.: Performance Characteristics at Mach Numbers to 2.0 of Various Types of Side Inlets Mounted on Fuselage of Proposed Supersonic Airplane. II - Inlets Utilizing Half of a Conical Spike. NACA RM E52G08, 1952.

44. Baughman, L. Eugene, and Gould, Lawrence I.: Investigation of Three Types of Supersonic Diffuser Over a Range of Mach Numbers From 1.75 to 2.74. NACA RM E50L08, 1951.

45. Wittliff, Charles E., and Byrne, Robert W.: Preliminary Investigation of a Supersonic Scoop Inlet Derived From a Conical-Spike Nose Inlet. NACA RM L51G11, 1951.

46. Ferri, Antonio, and Nucci, Louis M.: Theoretical and Experimental Analysis of Low-Drag Supersonic Inlets Having a Circular Cross Section and a Central Body at Mach Numbers of 3.30, 2.75, and 2.45. NACA Rep. 1189, 1954. (Supersedes NACA RM L8H13.)

47. Luidens, Roger W., and Hunczak, Henry: Preliminary Investigation of Cone-Type Diffusers Designed for Minimum Spillage at Inlet. NACA RM E7K19, 1948.

TABLE I.- SUBSONIC-DIFFUSER DATA

Reference	Symbol	Configuration	Control	2θ	A_R	$\frac{\delta^*_1}{R_1}$ (1)	$\frac{\delta^*_1}{\theta_1}$ (1)	M_1	R_{N_1} (1)
10	○	Conical	----------	Variable	2.33	Variable	1.2 to 1.3	0.13	0.2×10^6
13	□	Conical	----------	12°	2.00	Variable	1.26	Variable	2.1
13	◇	Conical	----------	23°	2.00	Variable	1.23	Variable	2.1
13	△	Conical	----------	12°	2.00	Variable	1.22 to 1.33	Variable	1.2
16	◺	Conical	----------	Variable	4.00	≈0.006	----------	< 0.45	0.5
17	◺	Conical	----------	10°	2.00	Variable	1.45	Variable	1.2
23	⌂	Conical	Vortex generators	23°	2.00	Variable	1.28	Variable	2.8
19	◇	Conical	----------	Variable	4.00	≈0.006	----------	Variable	1.0
21	◇	Rectangular	----------	Variable	Variable	≈0.006	----------	0.10	0.8
24	⌂	Conical	Suction	Variable	4.00	Variable	1.58 to 1.21	0.18	0.7
18	▷	Rectangular	----------	Variable	4.00	≈0.02	----------	Variable	0.3
12	▱	Annular	Vortex generators	Variable	1.91	0.078	1.20	< 0.40	0.7
14	▱	Annular	Suction, Injection	Variable	1.91	0.078	1.20	< 0.40	0.7
27	◇	Annular	Suction, Injection	78°	1.91	0.078	1.20	< 0.40	0.7
29	▱	Annular	----------	Variable	1.75	0.017	1.52	Variable	0.6
29	◁	Annular	----------	Variable	1.75	0.002	1.15	Variable	1.9
8, 9	◹	Conical	----------	Variable	Variable	≈0.01	----------	< 0.20	0.2
8, 9	◹	Rectangular	----------	Variable	Variable	≈0.01	----------	< 0.20	0.2
8, 9	◻	Square	----------	Variable	4.00	≈0.01	----------	< 0.20	0.2
8, 9	◇	Rectangular	----------	Variable	Variable	≈0.01	----------	< 0.20	0.2
8, 9	◹	Conical	----------	Variable	Variable	≈0.01	----------	< 0.20	0.2
15	▽	Conical	----------	Variable	Variable	0.082	1.34	0.45	0.45
Unpublished (Wilbur, Higginbotham, and Wood)	▱	Annular	Injection, Suction, Vane	34°	1.91	0.078	1.20	< 0.40	0.7
22	◇	Conical	Vortex generators	Variable	5.20	≈0.007	----------	0.50	2.4
Unpublished (Wilbur and Higginbotham)	▱	Annular	Suction	34°	1.91	0.078	1.20	< 0.40	0.7
28	◿	Annular	Vane	Variable	3.19	Variable	Variable	0.30	0.4
25	◿	Annular	Vortex generators	16.7°	1.91	0.078	1.20	< 0.40	0.7
31	◸	Conical	Surface roughness	23°	2.00	0.014	1.17	Variable	2.1
20	◺	Conical	----------	Variable	1.96	Variable	Variable	Variable	0.35
Unpublished (Wilbur and Higginbotham)	▱	Annular	Injection, Suction, Vane	70°	1.91	0.078	1.20	< 0.40	0.7

[1]Values taken at an inlet Mach number of 0.2 if possible.

TABLE II.- SUPERSONIC-INLET DATA FOR MODELS WITHOUT INTERNAL CONTRACTION

Reference	Symbol	Equivalent conical expansion angle of subsonic diffuser	Area ratio of subsonic diffuser	Length of minimum section preceding diffuser inlet (inlet hydraulic diameters)	θ_s	θ_l	M_0	Remarks
		3.08	3.02	0	25	43.1	1.7, 1.9, 2.0	Conical
31	○	3.12	2.82	0	20	27.4	1.7, 1.9, 2.0	Conical
		3.32	3.15	0	25	31.9	1.7, 1.9, 2.0	Conical
32	□	1.5	1.18	0	30	42	1.72	Conical
					15	31.2	1.65	Conical
					20	39.8	1.85	Conical
					20	30	1.85	Conical
33	◇	5	4.08	0	25	37.2	1.85	Conical
					30	44.2	1.85	Conical
					15	22.9	1.85	Conical
34	△	6.7	2.6	3.3	25	46.2	1.79	Conical
35	◿	6.7	2.6	0	17	----	1.9	Conical with wedge center body
36	◭	7	2.3	3.3	25	46.2	1.59, 1.79	Conical
37	⌂	5.3	1.73	0	30	46	1.7, 2.01	Conical
38	◇	4.3	2.58	0	25	43	2.0	Conical
				3.0	25	43	2.0	Conical
		4.3	2.58	0	25	43	2.0	Conical
		4.6	2.58	1	25	43	2.0	Conical
39	◊	4.9	2.58	2	25	43	2.0	Conical
		5.6	2.58	3.5	25	43	2.0	Conical
		4.3	2.58	0	30	48	2.0	Conical
40	⌂	4.3	2.58	0	25	43	1.8, 2.0	Conical with translating center body
41	▽	5	3.9	0	25	38	1.88	Half-conical on flat plate
42	◹	4.5	6.7	0	30	39.4	2.93	Half-conical on flat plate
43	◹	4.75	2.38	0	25	46	1.57, 1.74, 1.83	Half-conical on fuselage
44	◡	9.4	3.48	0	30	42.6	1.75, 2.10 2.30, 2.50, 2.74	Conical
45	◇	3.0	1.63	0	30	50	1.6, 1.9	Half-conical on flat plate

TABLE III.- SUPERSONIC-INLET DATA FOR MODELS

WITH INTERNAL CONTRACTION

Reference	Symbol	Equivalent conical expansion angle of subsonic diffuser	Area ratio of subsonic diffuser	θ_s	θ_l	Internal contraction ratio, A_1/A_2	M_0	Remarks
46	○	3.7 to 5.3	2.47 to 3.67	20	26 to 32	1.06 to 1.16	2.45	Conical
		4.5	2.54	25	37 to 39	1.12, 1.14	2.45	Cowl lip angle and ratio of inner body to cowl inlet diameter varied.
		4.5 to 5.5	2.54 to 3.67	20	27 to 30	1.09 to 1.26	2.75	
		4.5	2.56	25	37	1.12	2.75	
		4.5 to 5.5	2.5 to 3.5	20	27 to 30	1.09 to 1.32	3.30	
		5 to 6	3.87 to 4.62	25	31 to 33	1.22 to 1.25	3.30	
		5	3.12	30	38.8	1.10	3.30	
47	□	4.5	3.4	15	37.5	1.12	1.85	Conical
		4.7	3.73	20	40.5	1.08	1.85	Conical
33	◇	5	4.08	15	31.4	1.32	1.85	Conical
				20	36.2	1.13	1.85	Conical
				25	41.4	1.04	1.85	Conical
37	▱	2.48	1.55	25	46	1.05	1.5, 1.7	Conical

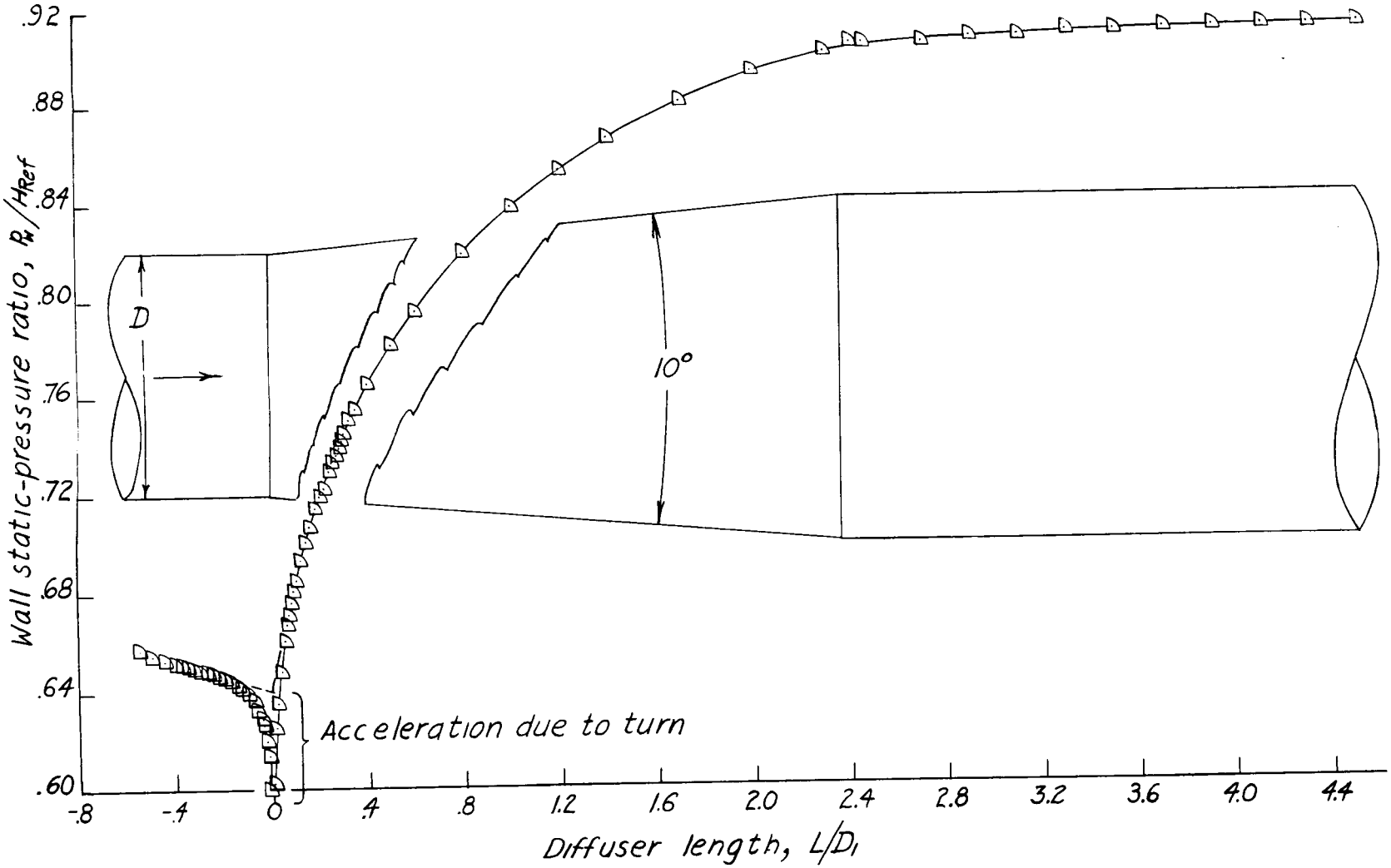

Figure 1.- Typical longitudinal static-pressure distribution. Conical diffuser; $\delta^*_1/R_1 = 0.006$; $M_1 = 0.82$; reference 17.

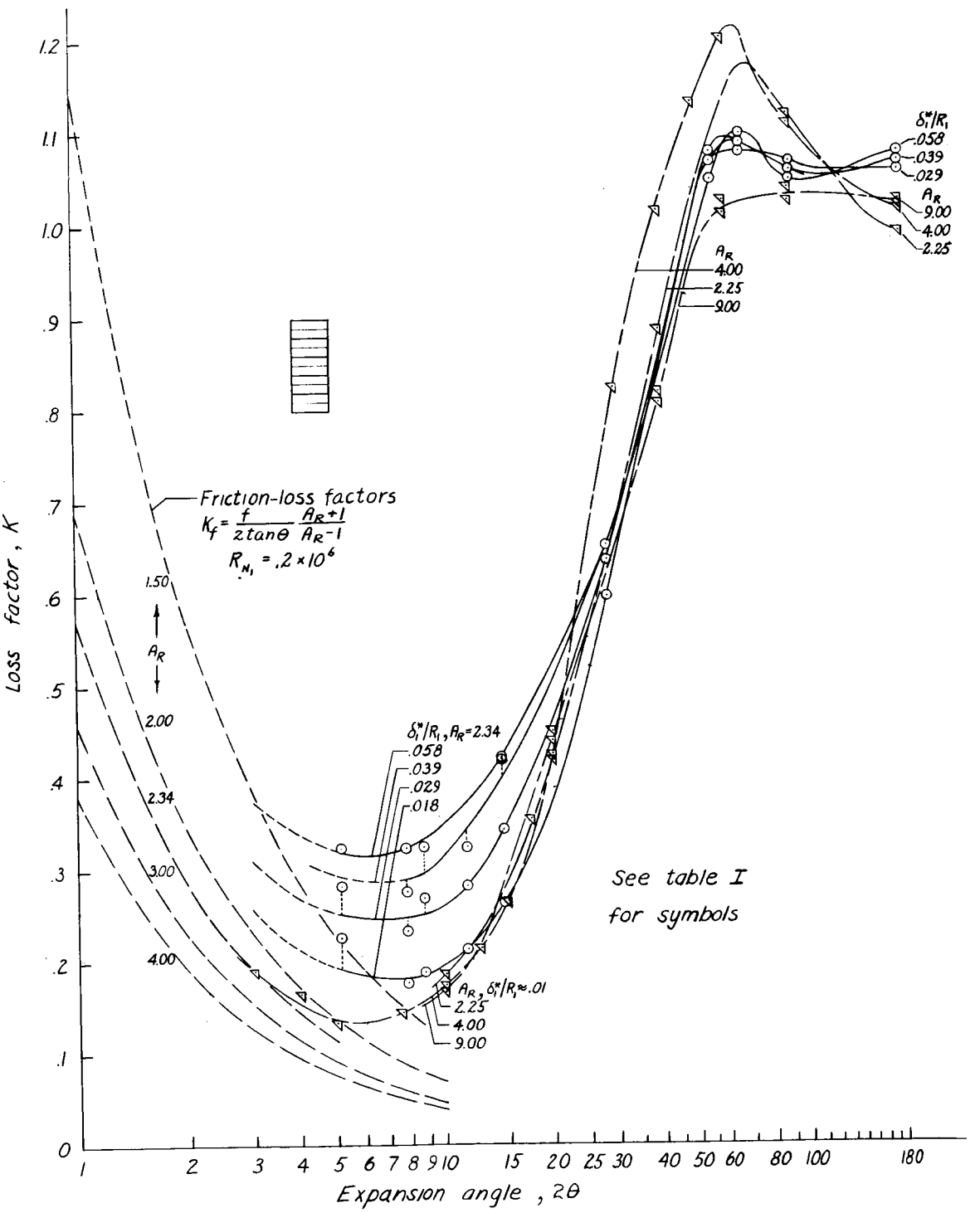

Figure 2.- Total-pressure-loss factor. Conical diffusers; $M_1 < 0.2$.

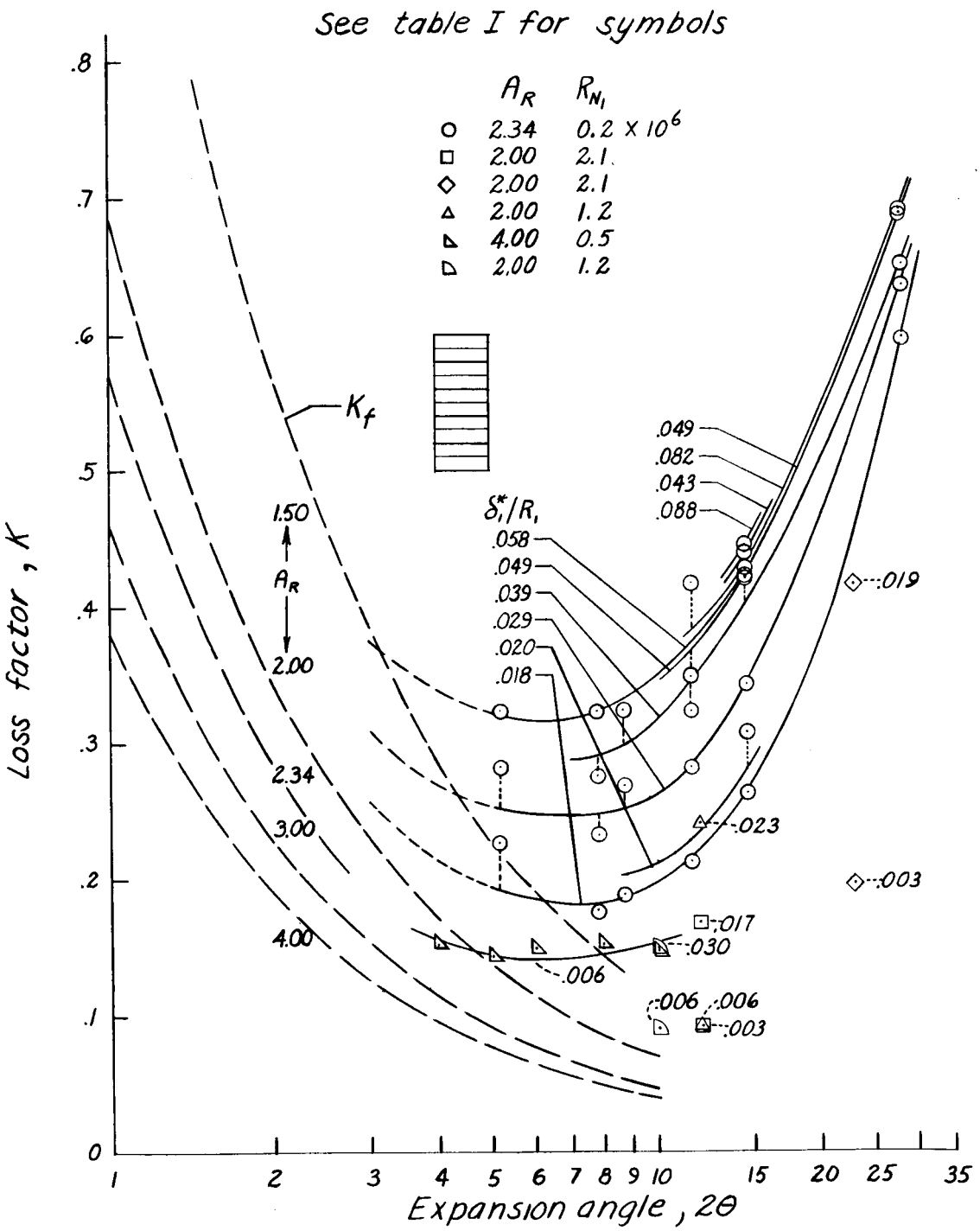

Figure 3.- Loss factor including high Reynolds number data. Conical diffusers; $M_1 \leq 0.2$.

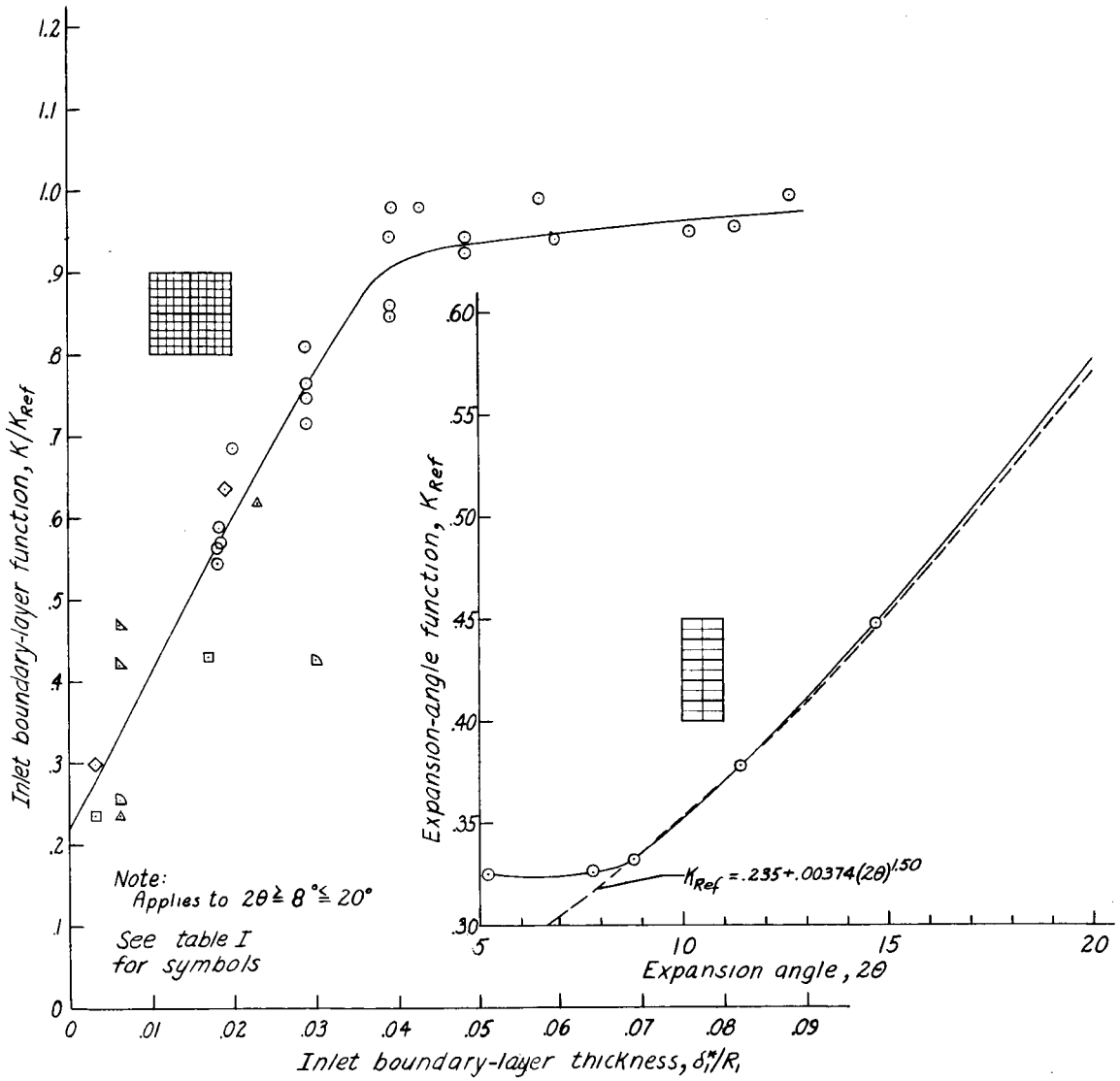

Figure 4.- Loss-factor correlation. Conical diffusers; $M_1 \leq 0.2$.

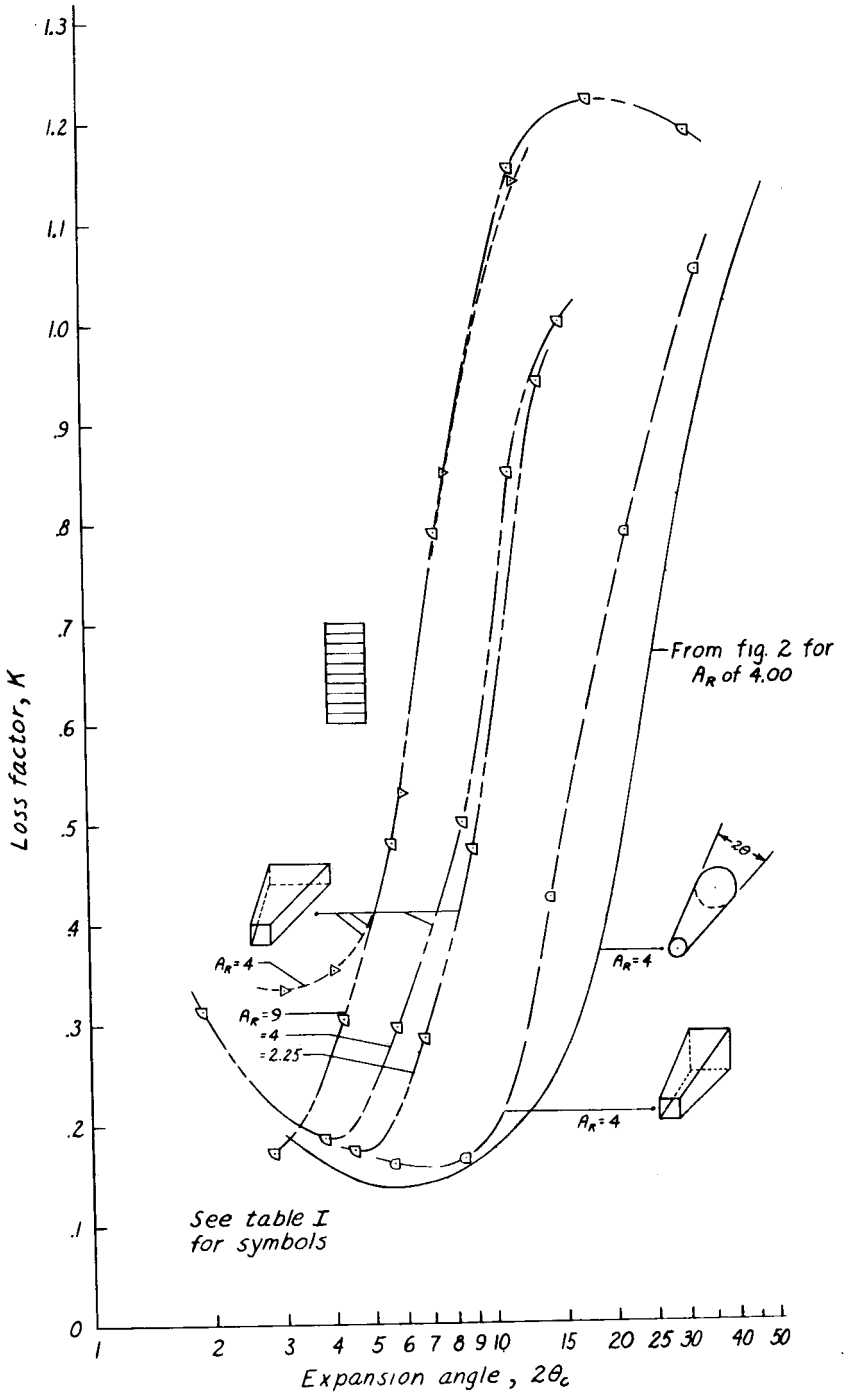

(a) Function of $2\theta_c$.

Figure 5.- Loss factor. Rectangular diffusers; $M_1 < 0.2$.

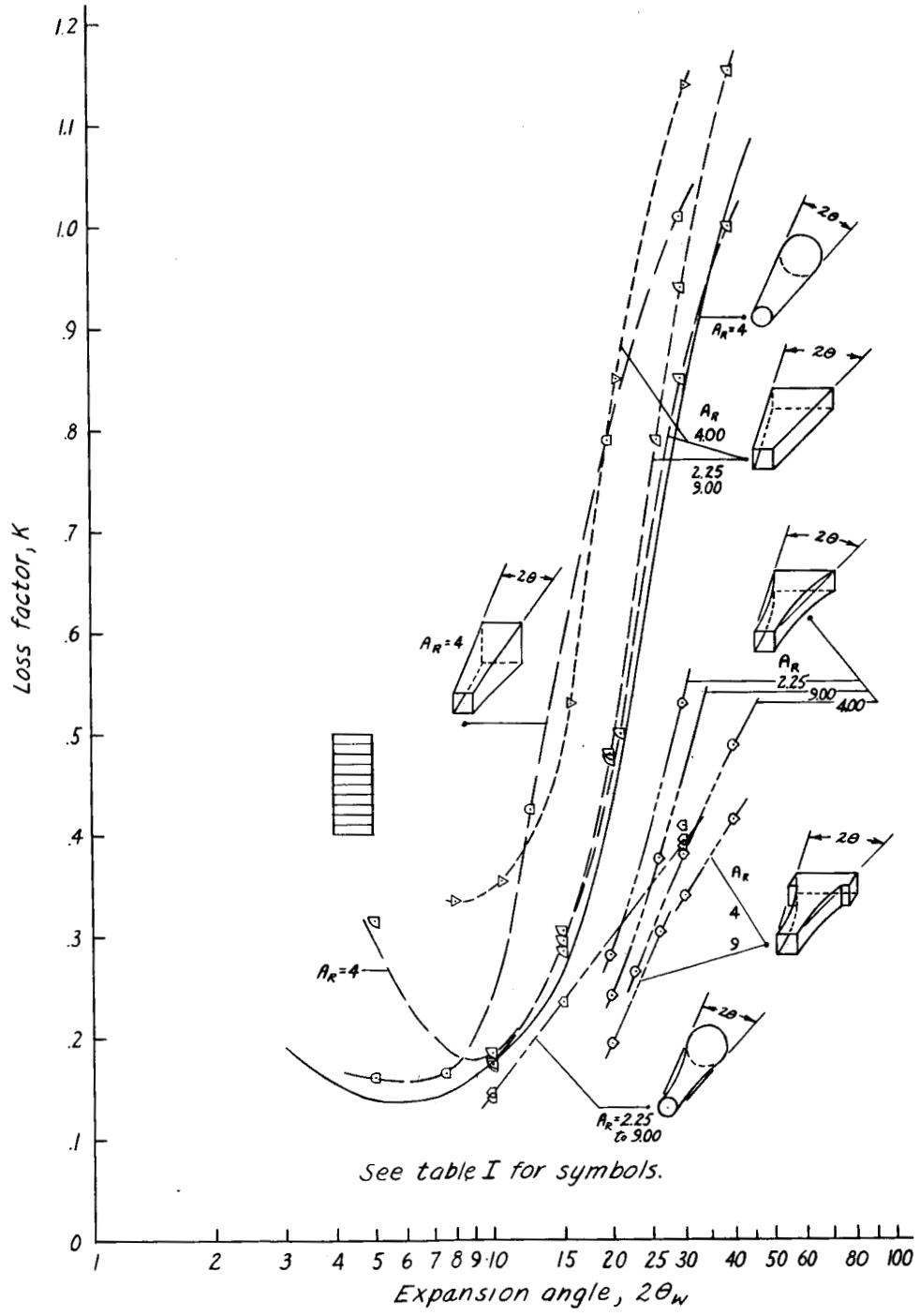

(b) Function of $2\theta_w$.

Figure 5.- Continued.

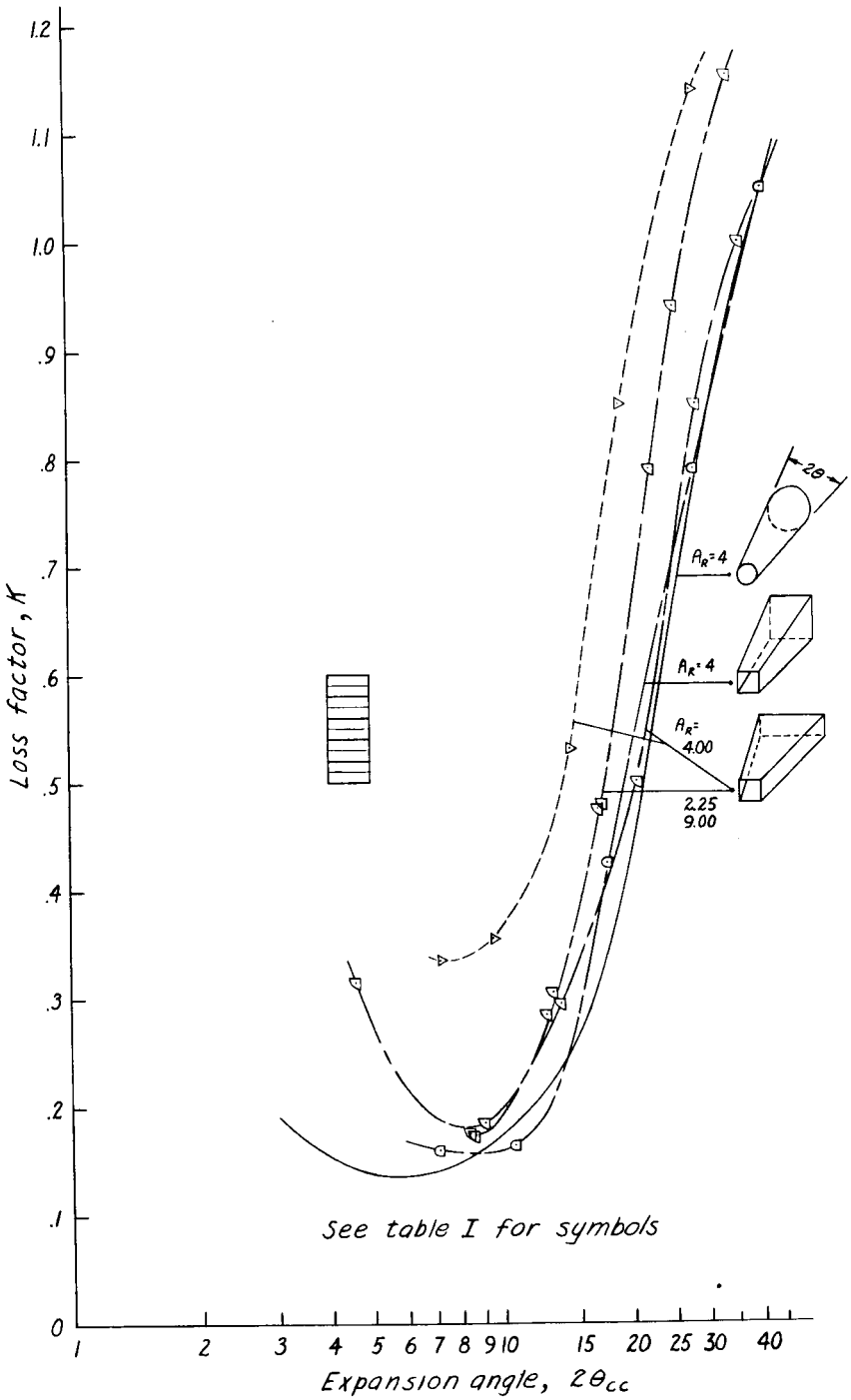

(c) Function of $2\theta_{cc}$.

Figure 5.- Concluded.

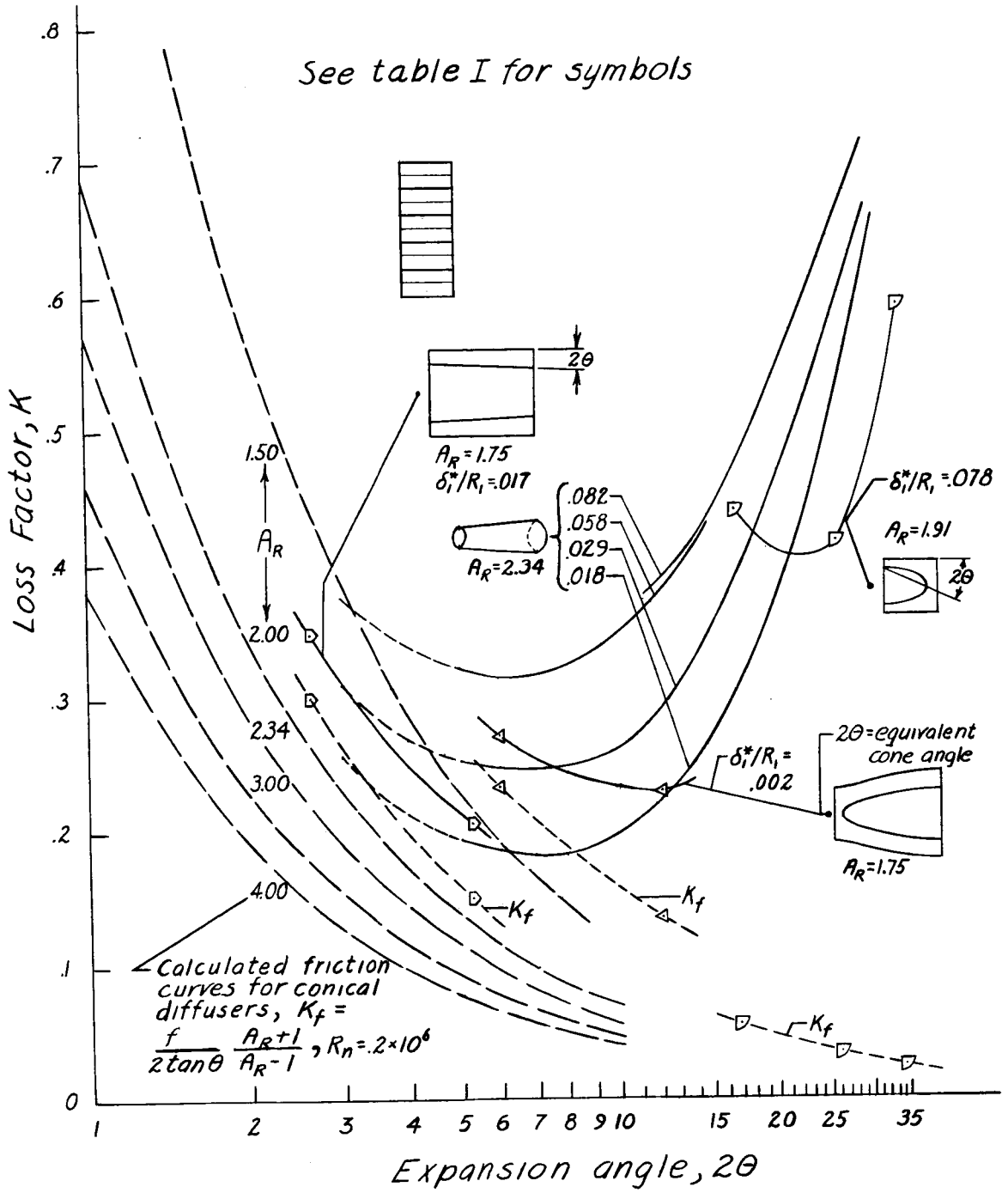

(a) Measured values.

Figure 6.- Loss factor. Annular diffusers; $M_1 \approx 0.2$.

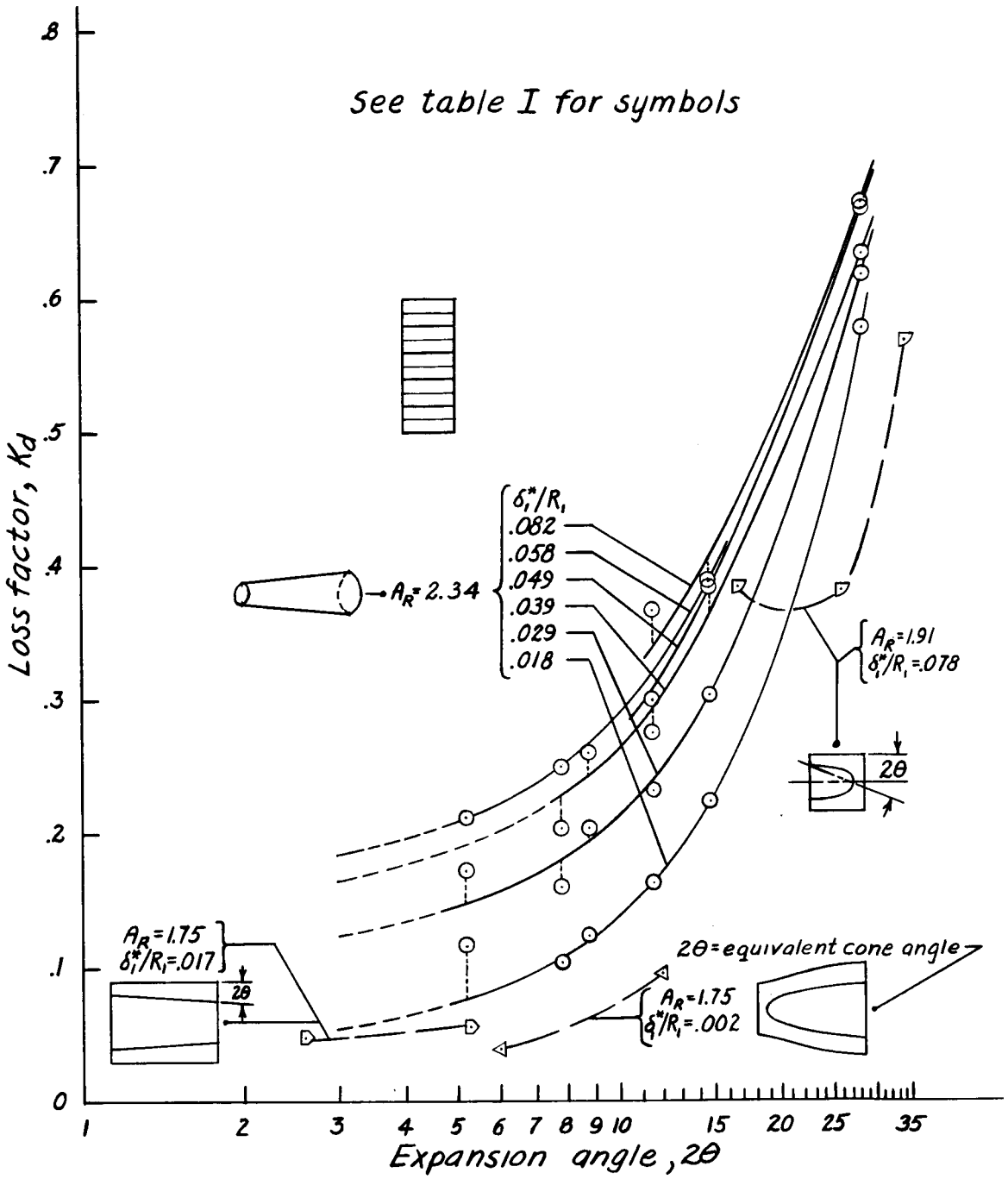

(b) Measured values minus friction; $K_d = K - K_f$.

Figure 6.- Concluded.

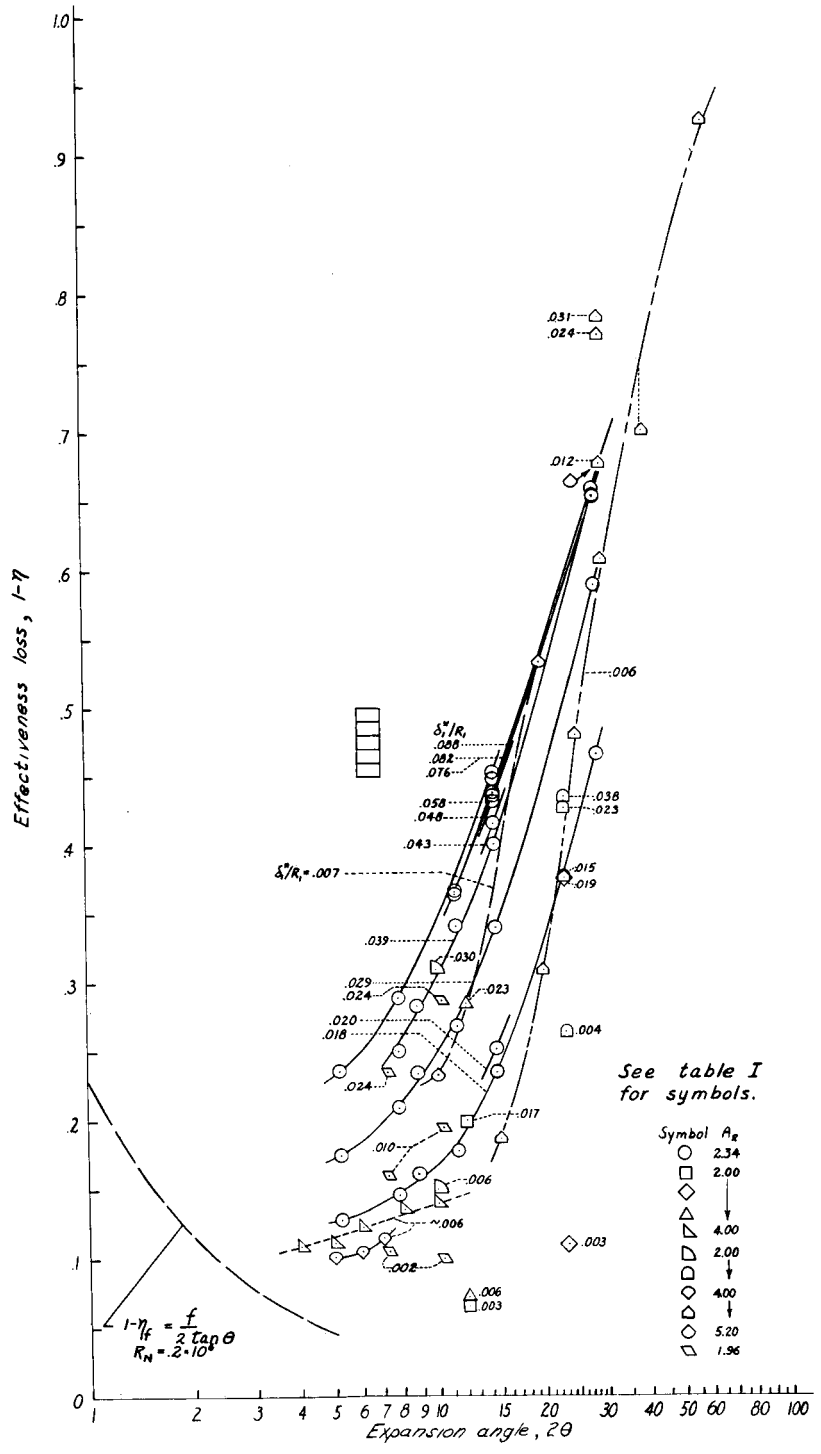

Figure 7.- Effectiveness loss. Conical diffusers; $M_1 \approx 0.2$.

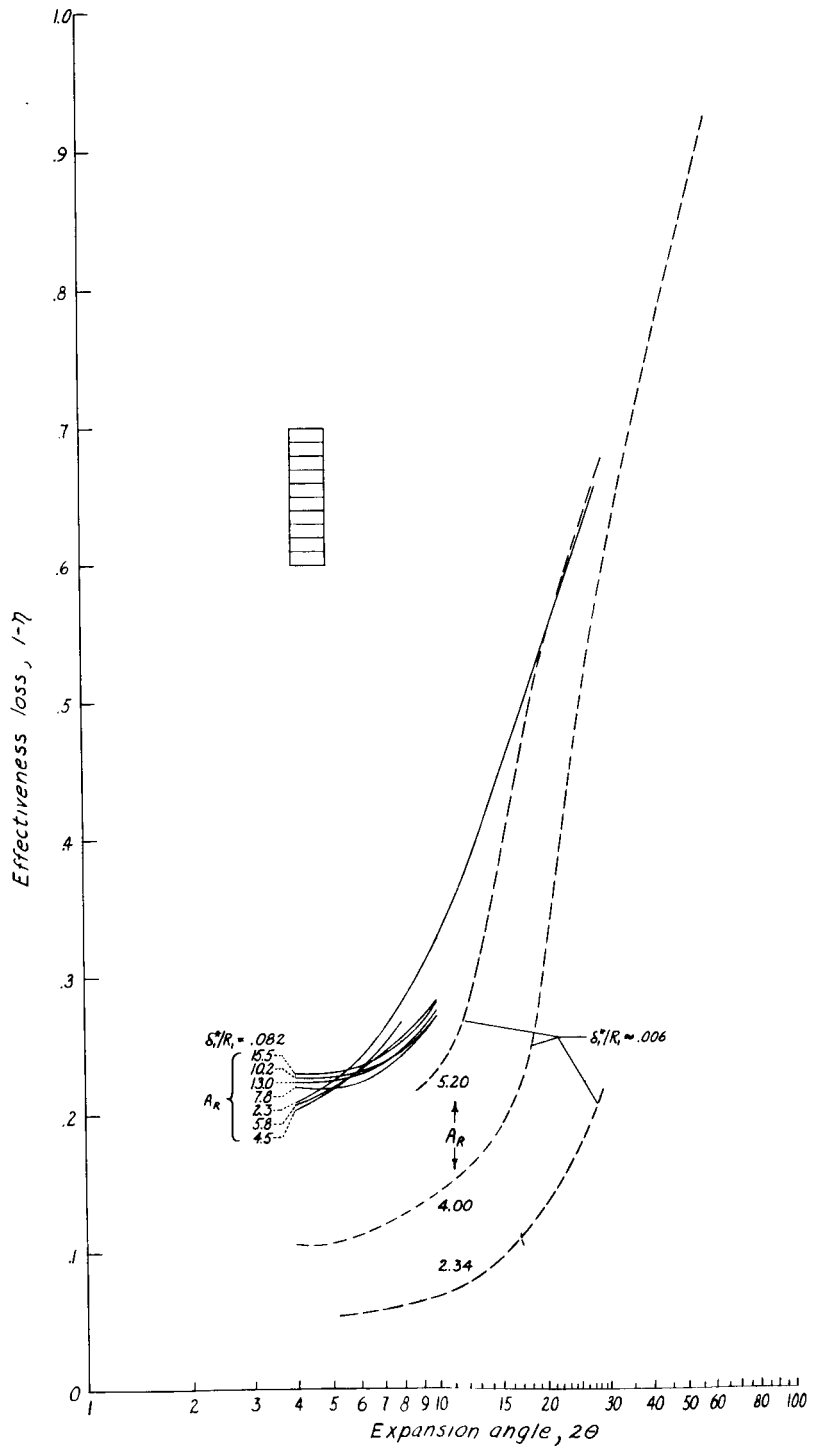

Figure 8.- Effectiveness loss. Conical diffusers; M_1 = 0.2 to 0.5.

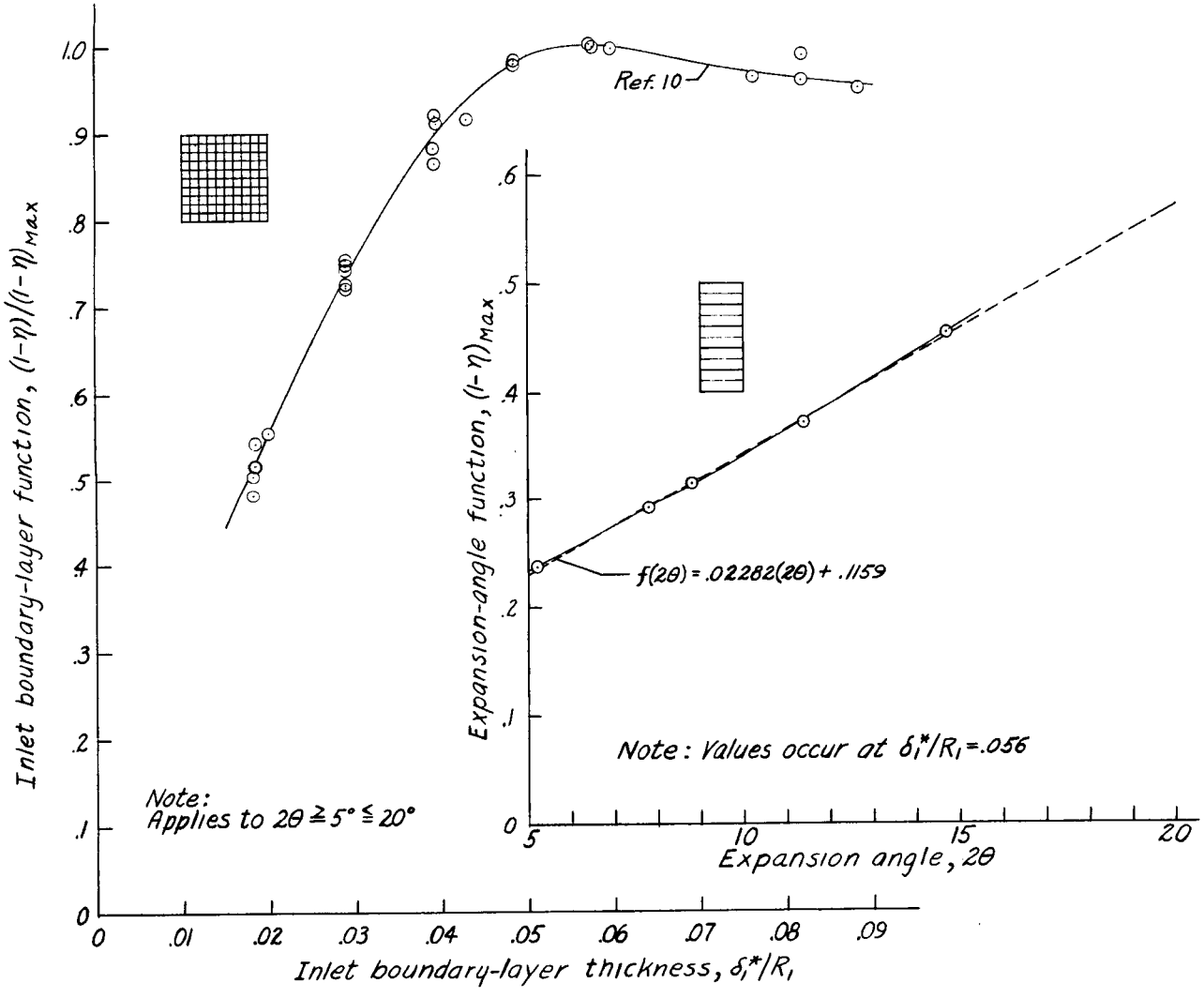

Figure 9.- Effectiveness-loss correlation. Conical diffusers; $A_R = 2.34$; $M_1 = 0.13$; reference 10.

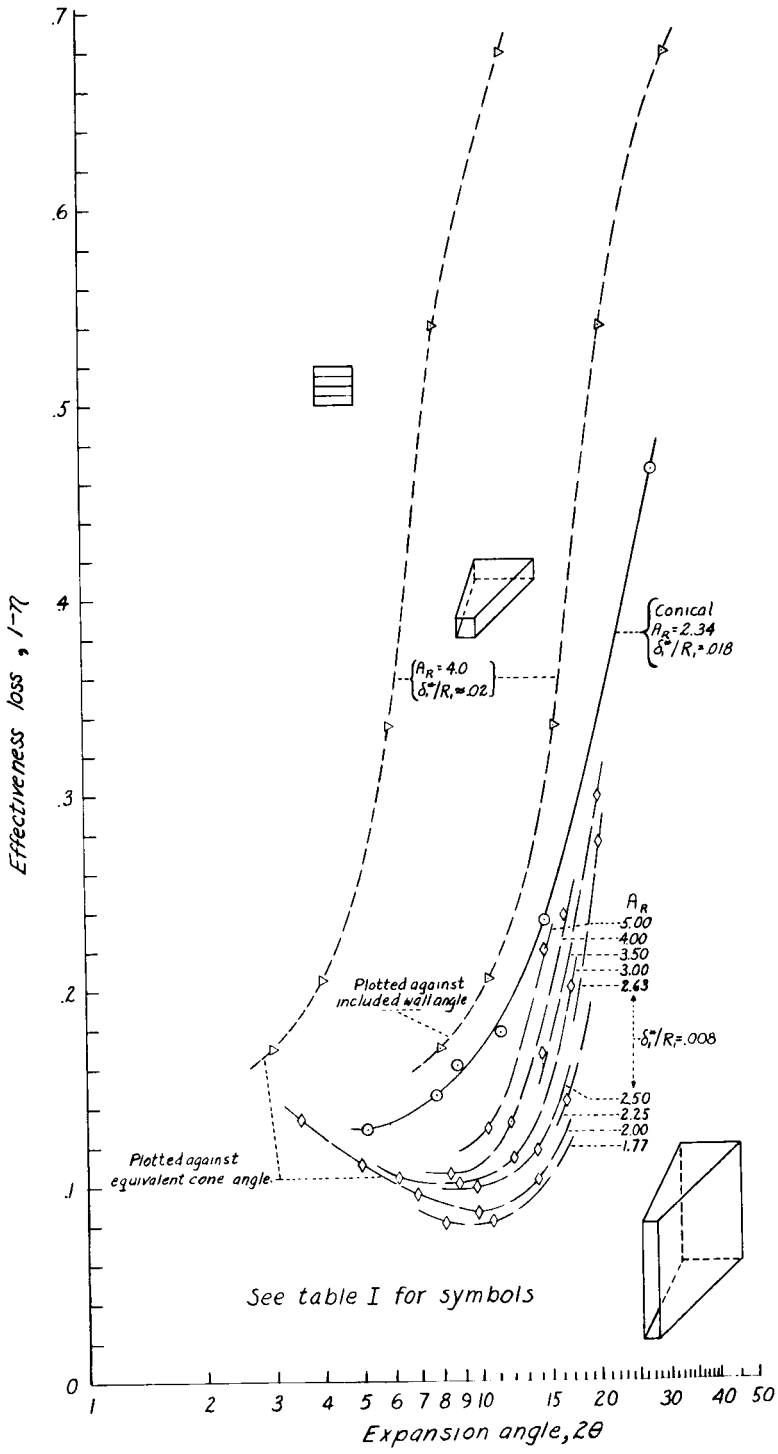

Figure 10.- Effectiveness loss. Rectangular diffusers; M_1 = 0.1 to 0.3.

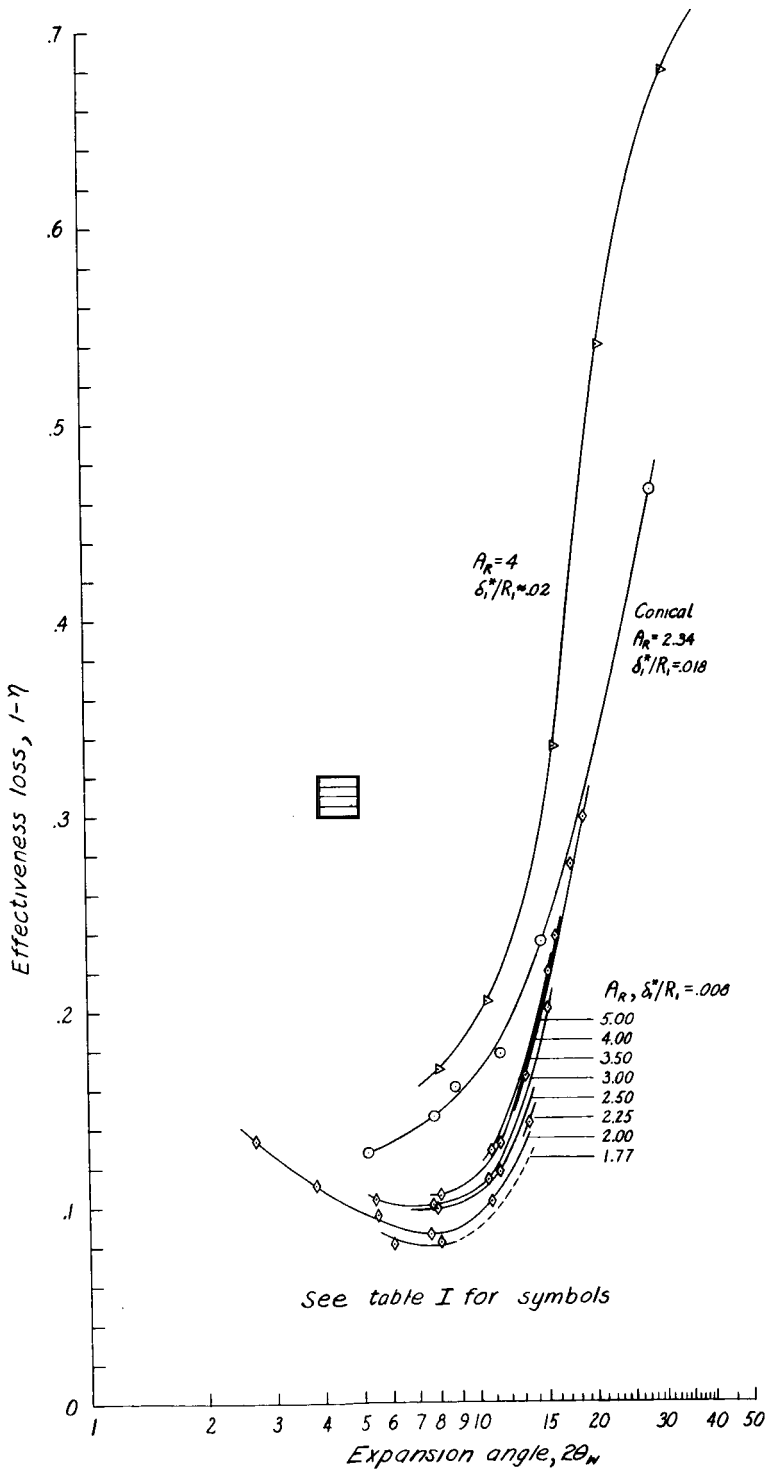

Figure 11.- Effectiveness loss. Rectangular diffusers; M_1 = 0.1 to 0.3.

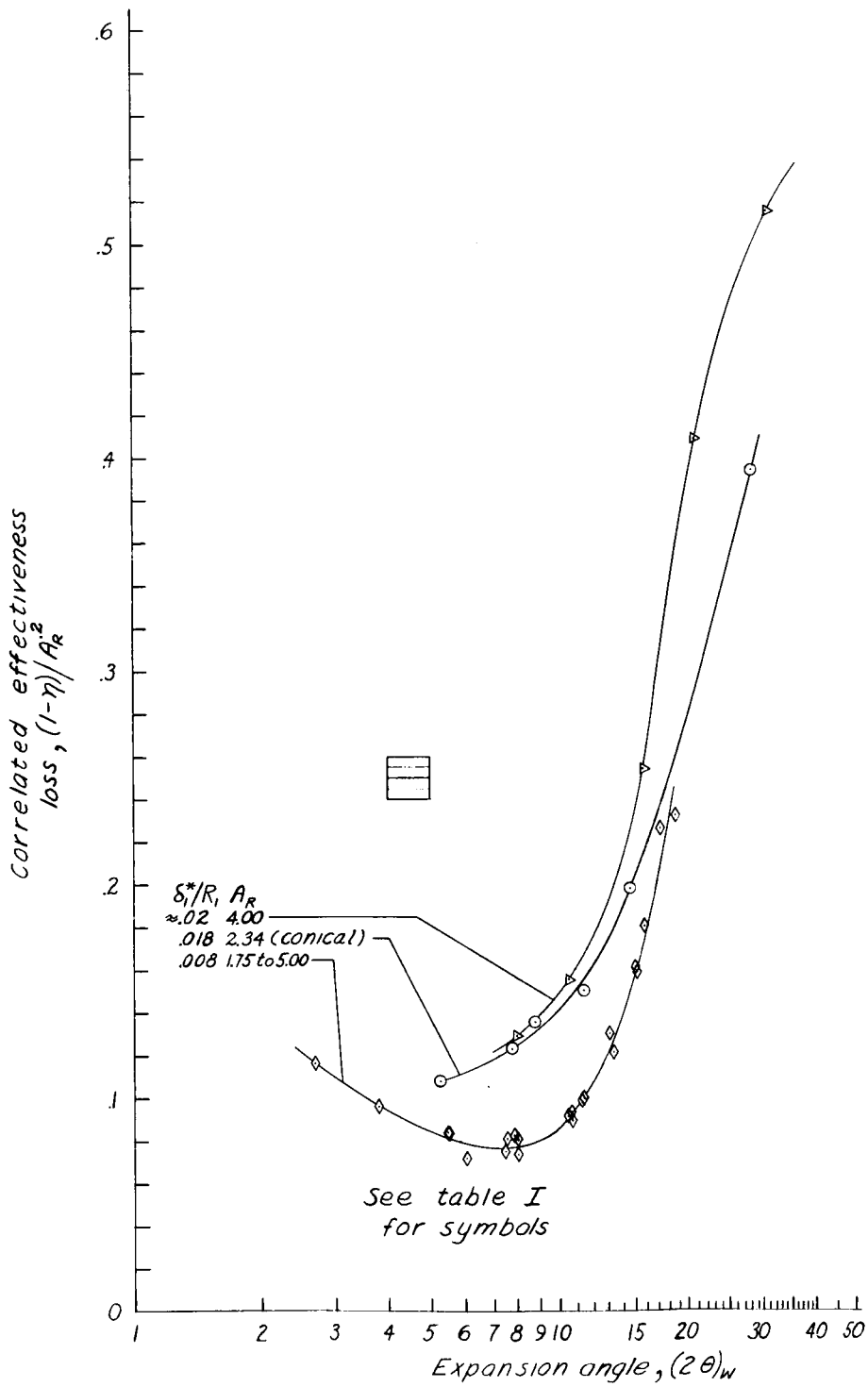

Figure 12.- Effectiveness loss. Rectangular diffusers; M_1 = 0.1 to 0.3.

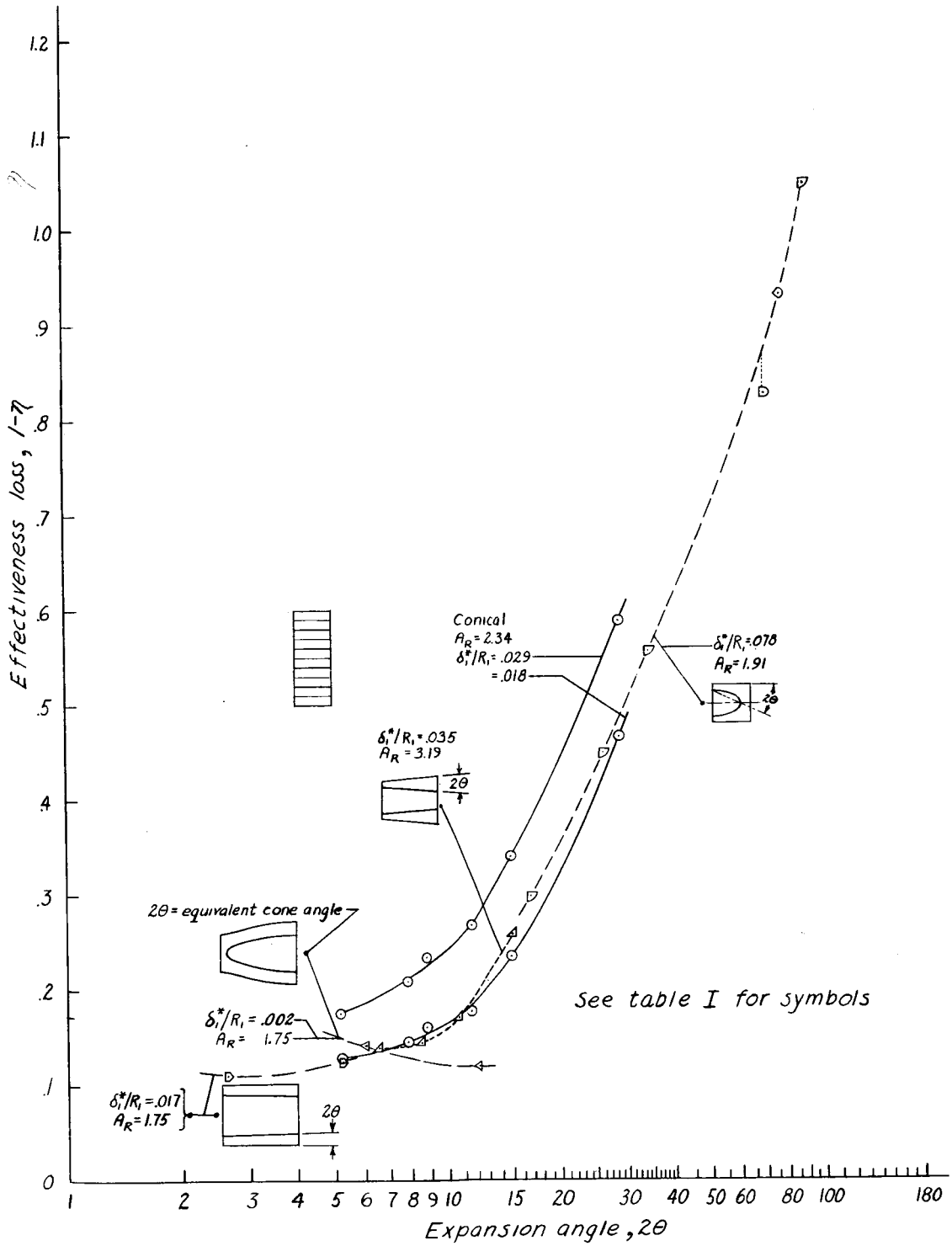

Figure 13.- Effectiveness loss. Annular diffusers; $M_1 \approx 0.2$.

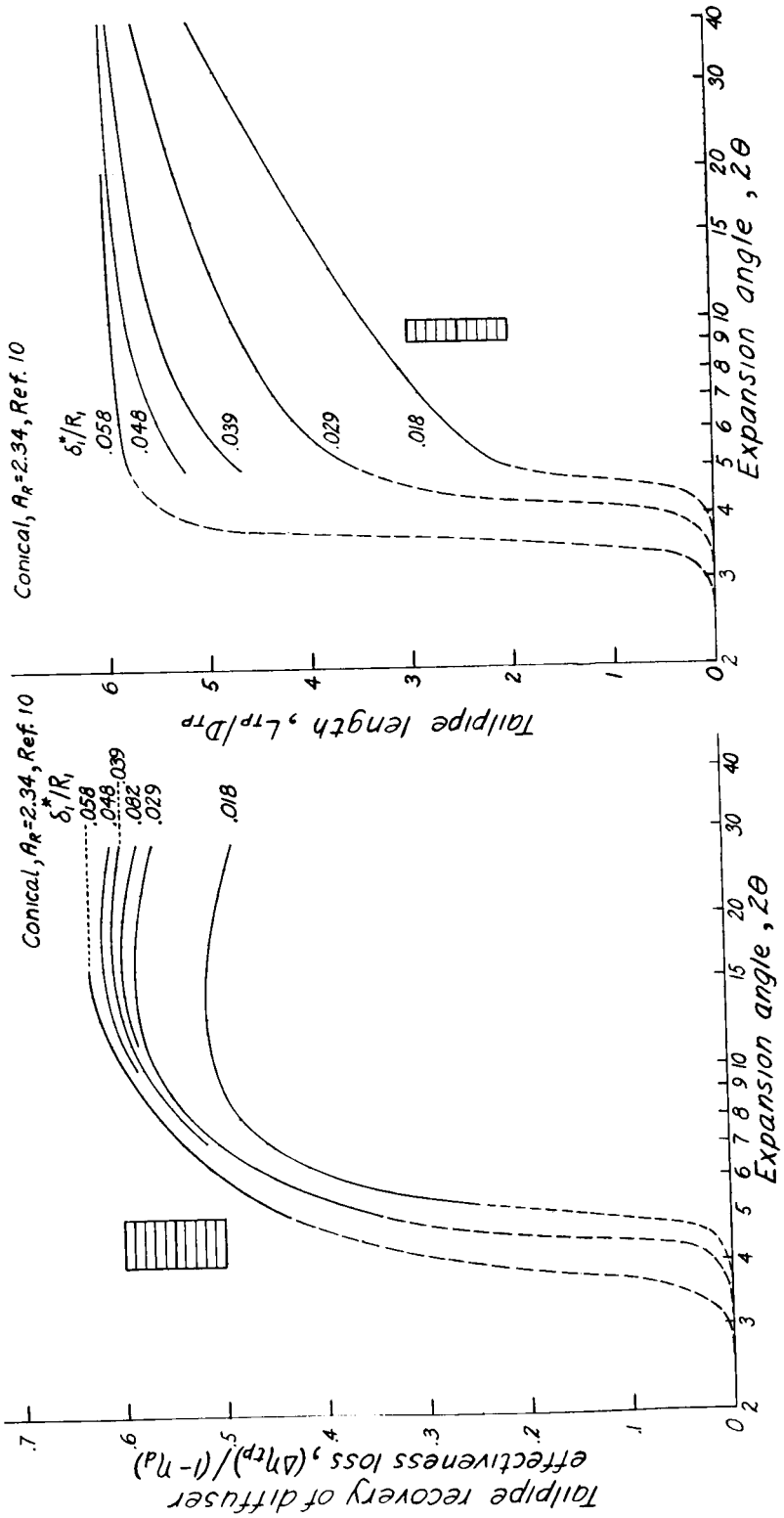

Figure 14.- Recovery of diffuser effectiveness in tailpipe. M_1 = 0.13.

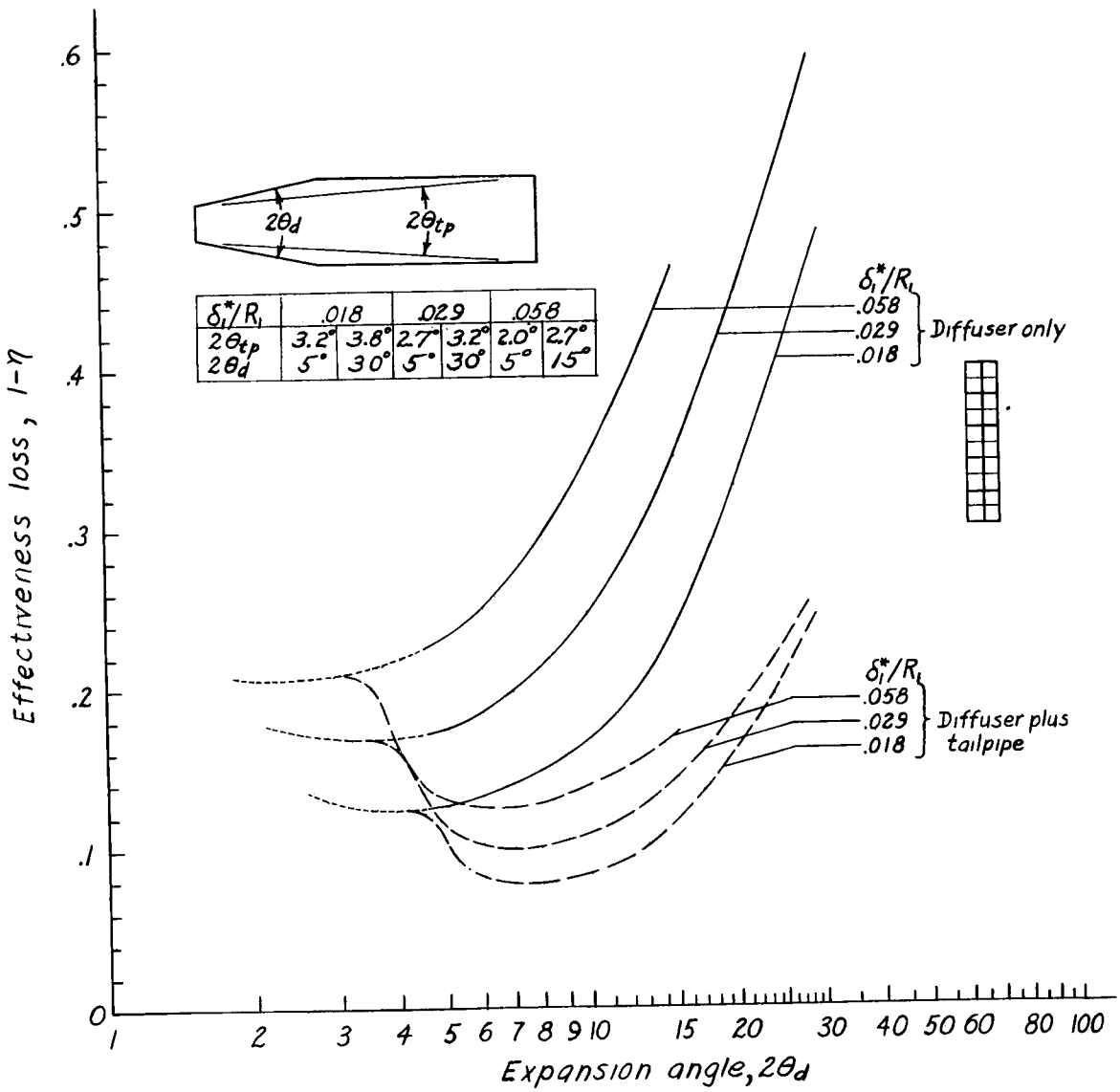

Figure 15.- Effectiveness loss. Conical-diffuser—tailpipe combinations; $A_R = 2.34$; $M_1 = 0.13$; reference 10.

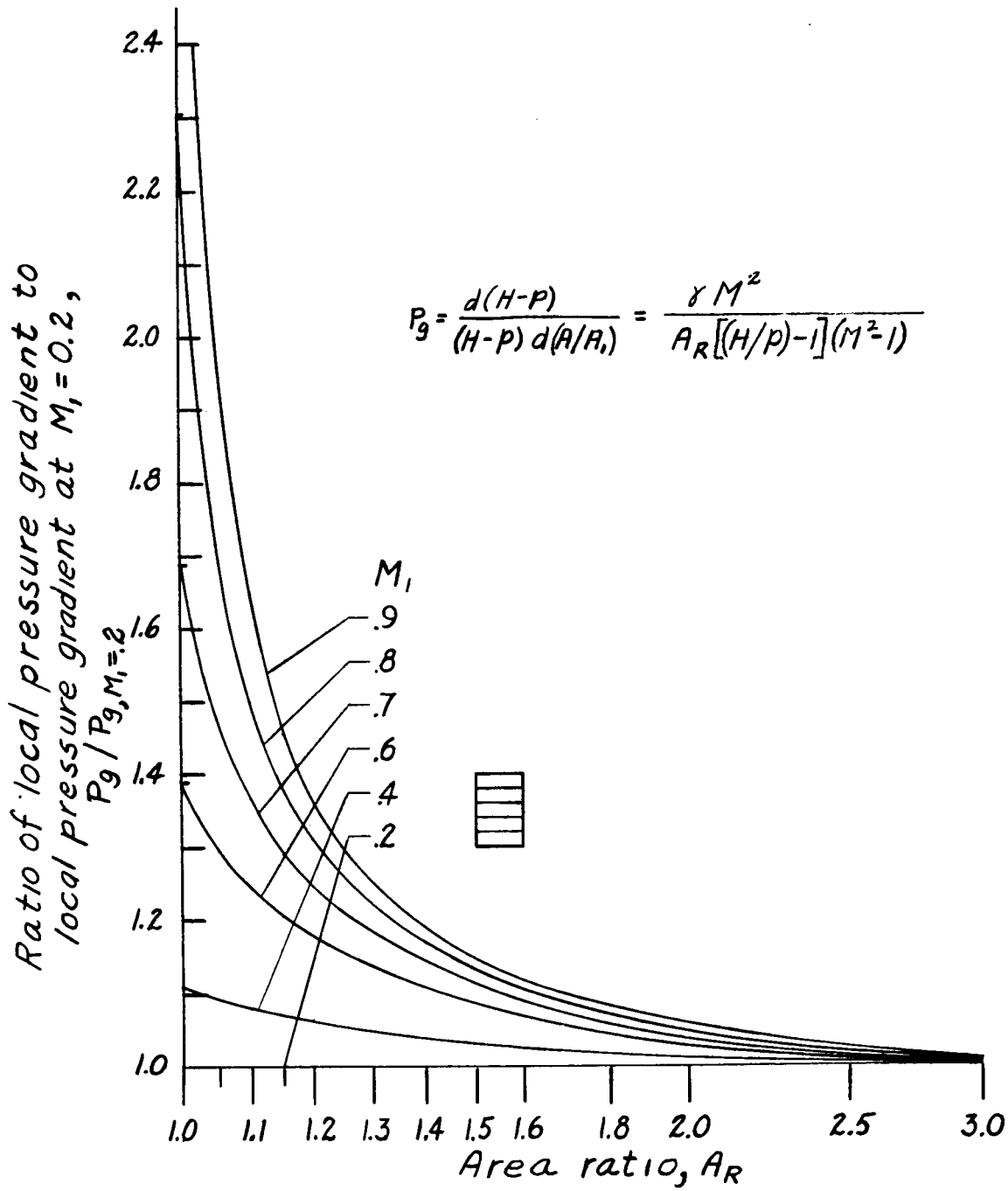

(a) Change in pressure gradient with Mach number.

Figure 16.- Compressibility effect on the ideal pressure gradient.

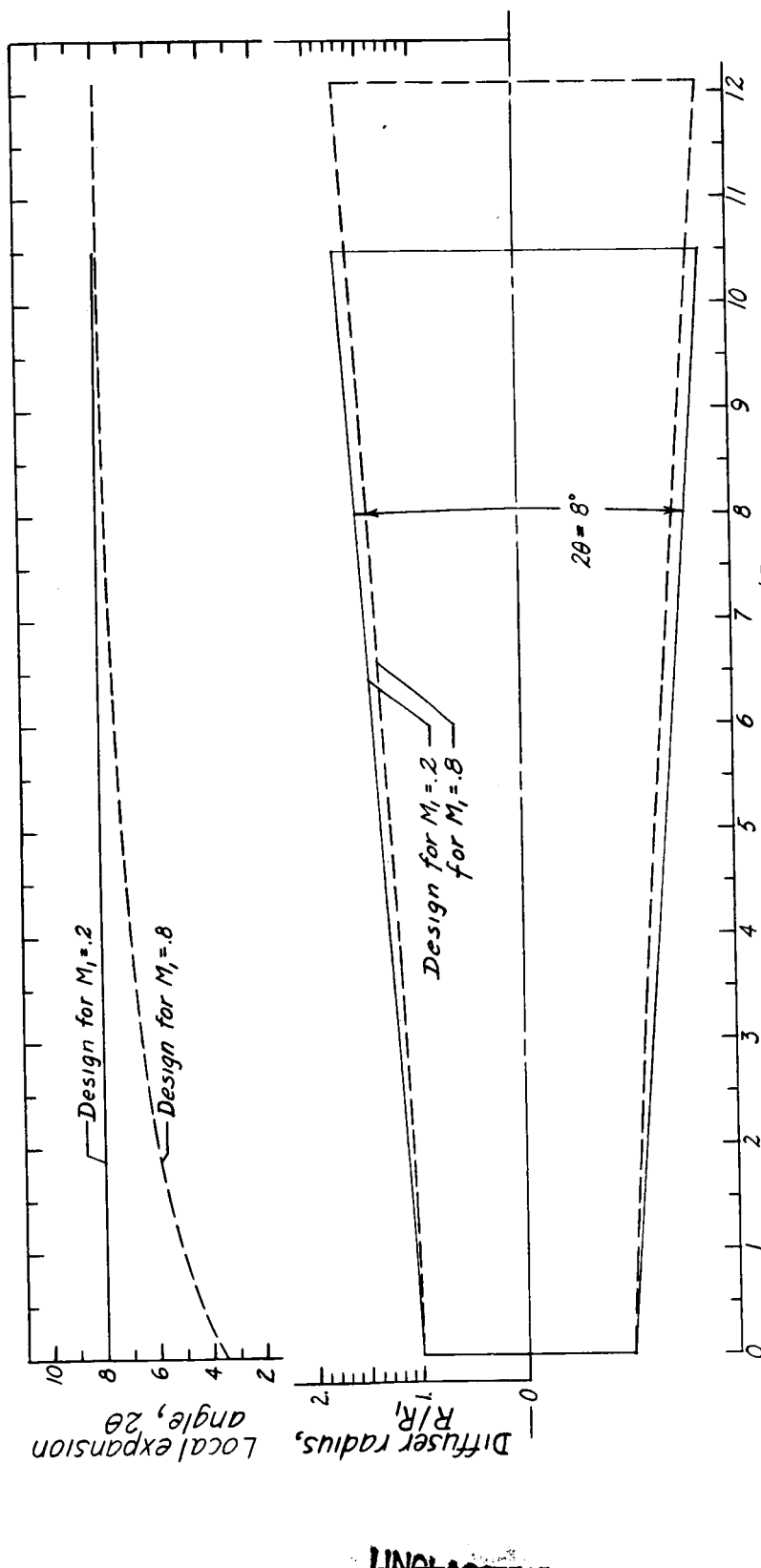

(b) Effect on design indicated by ideal pressure gradient.

Figure 16.- Concluded.

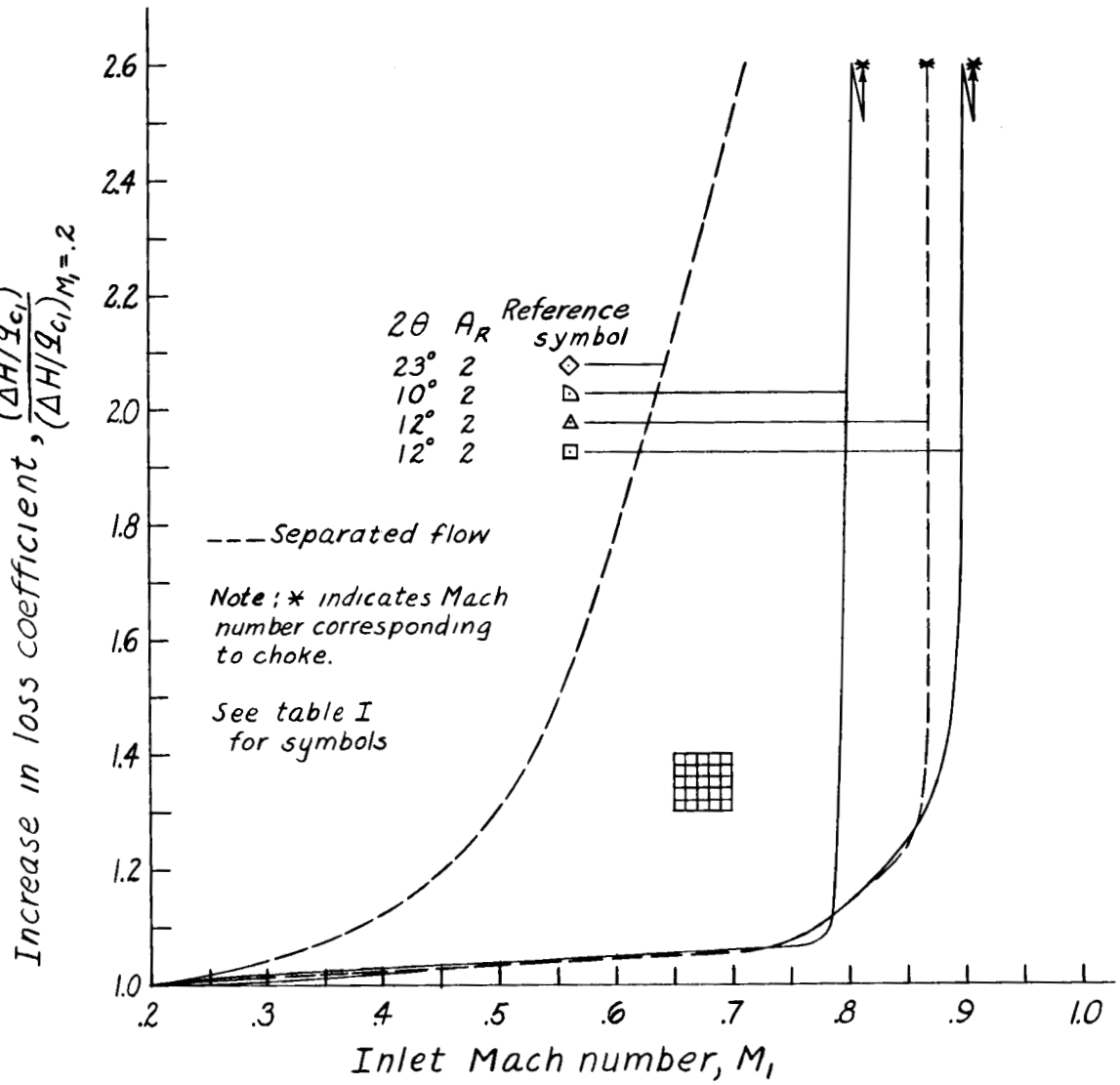

(a) Conical diffusers; δ^*_1/R_1 = 0.003 to 0.006.

Figure 17.- Inlet speed effects on loss coefficient.

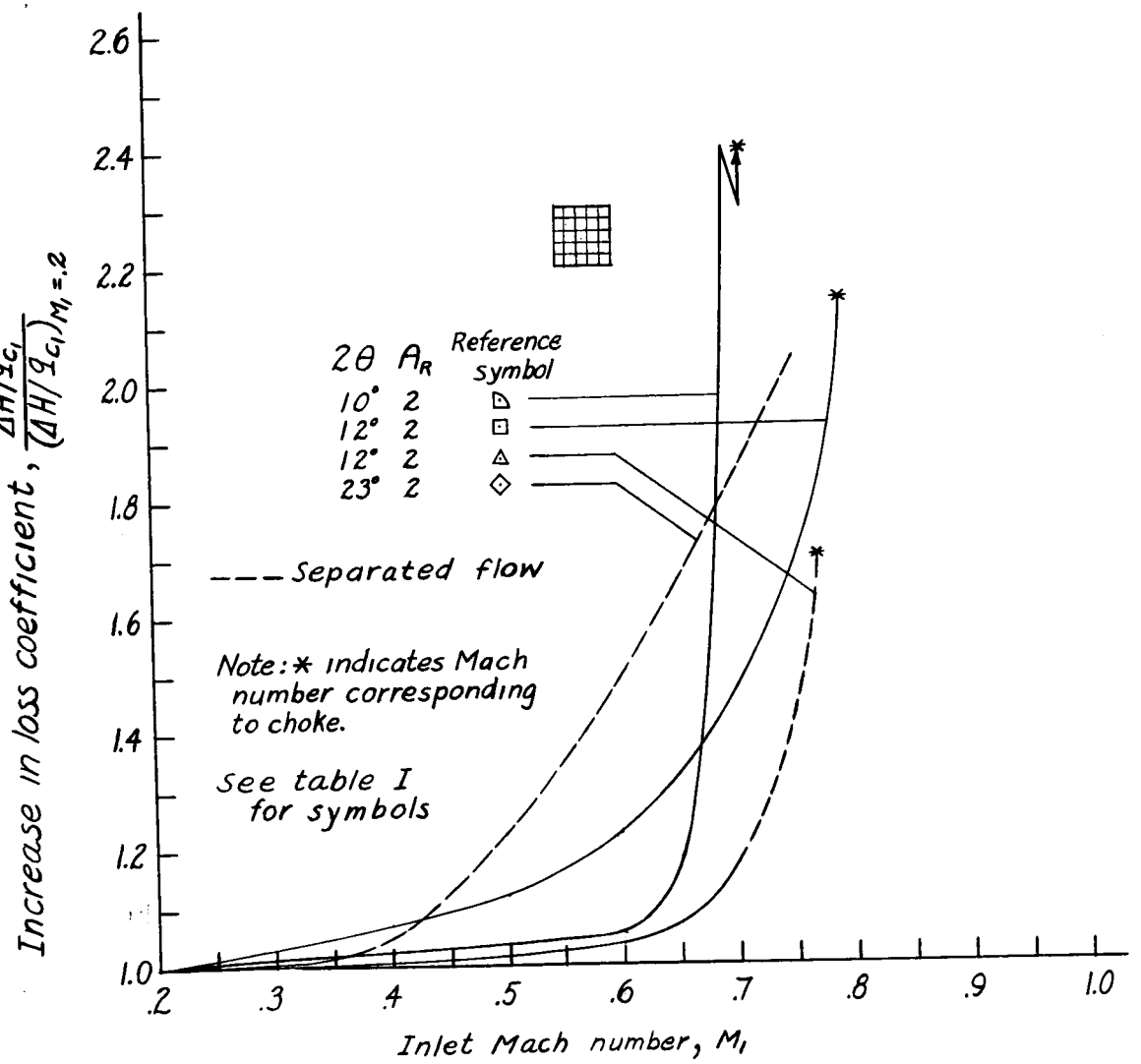

(b) Conical diffusers; δ^*_1/R_1 = 0.017 to 0.030.

Figure 17.- Continued.

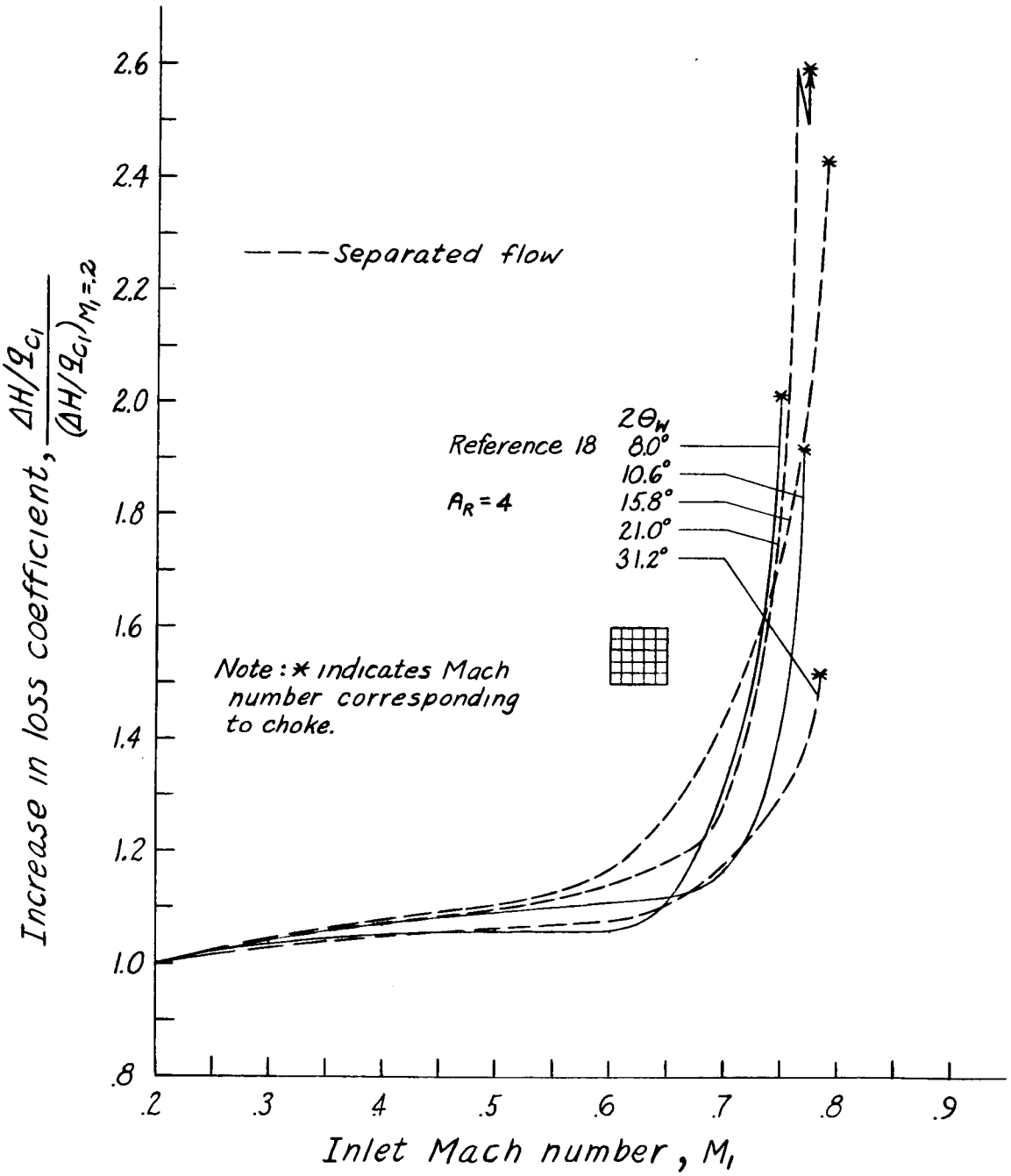

(c) Rectangular diffusers; $\delta^*_1/R_1 \approx 0.02$.

Figure 17.- Continued.

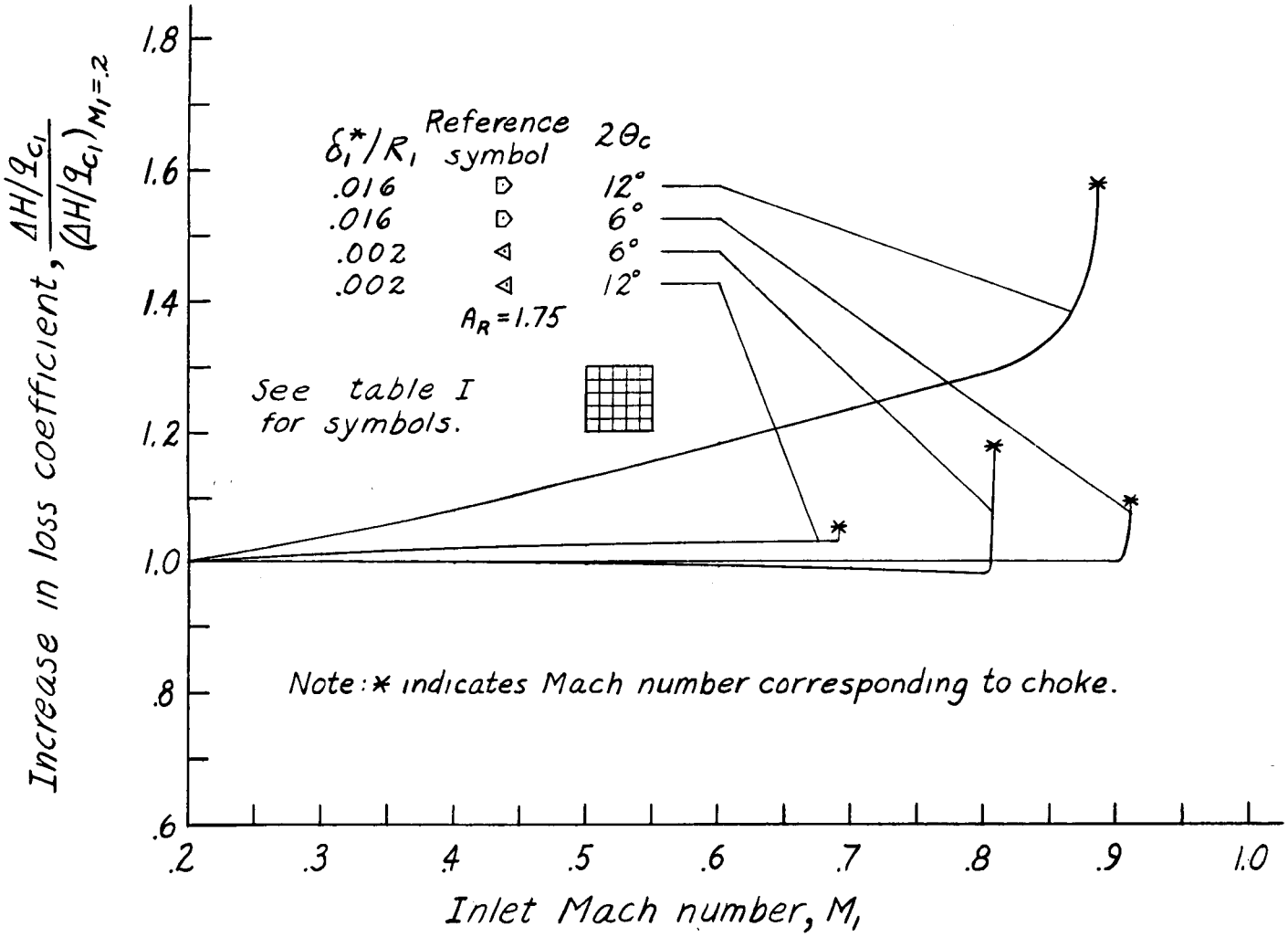

(d) Annular diffusers.

Figure 17.- Concluded.

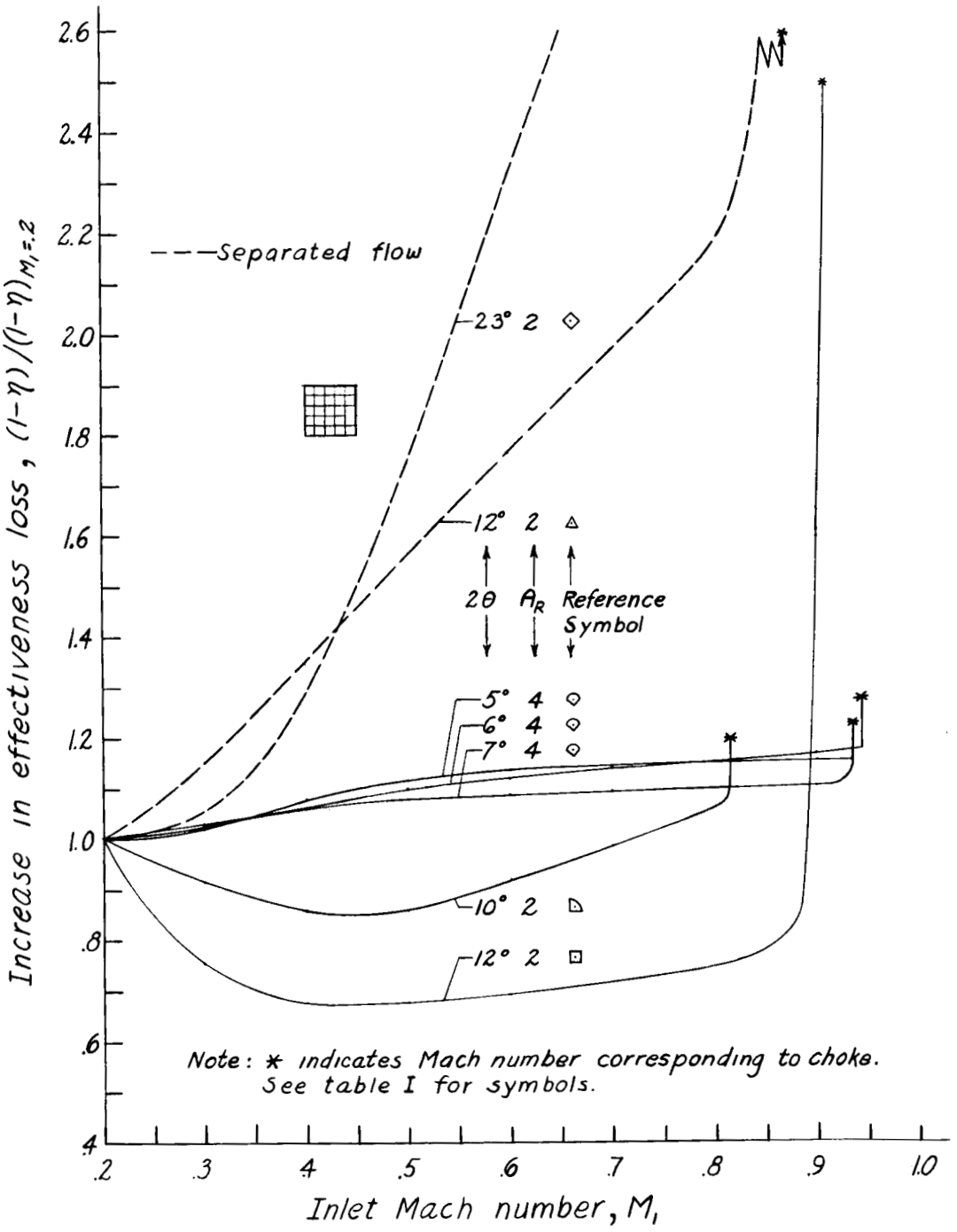

(a) Conical diffusers; δ^*_1/R_1 = 0.003 to 0.006.

Figure 18.- Inlet speed effect on effectiveness loss.

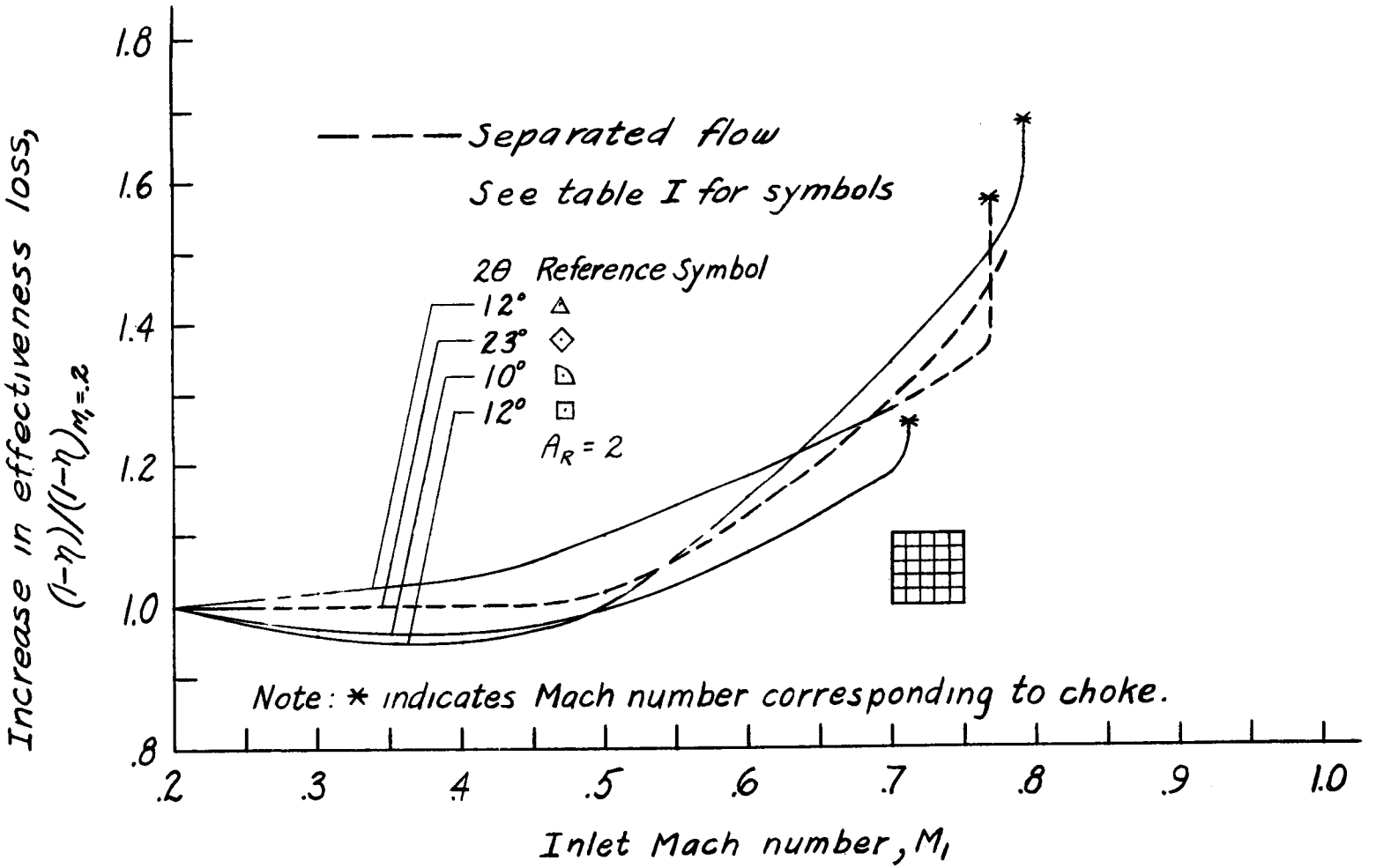

(b) Conical diffusers; δ^*_1/R_1 = 0.017 to 0.030.

Figure 18.- Continued.

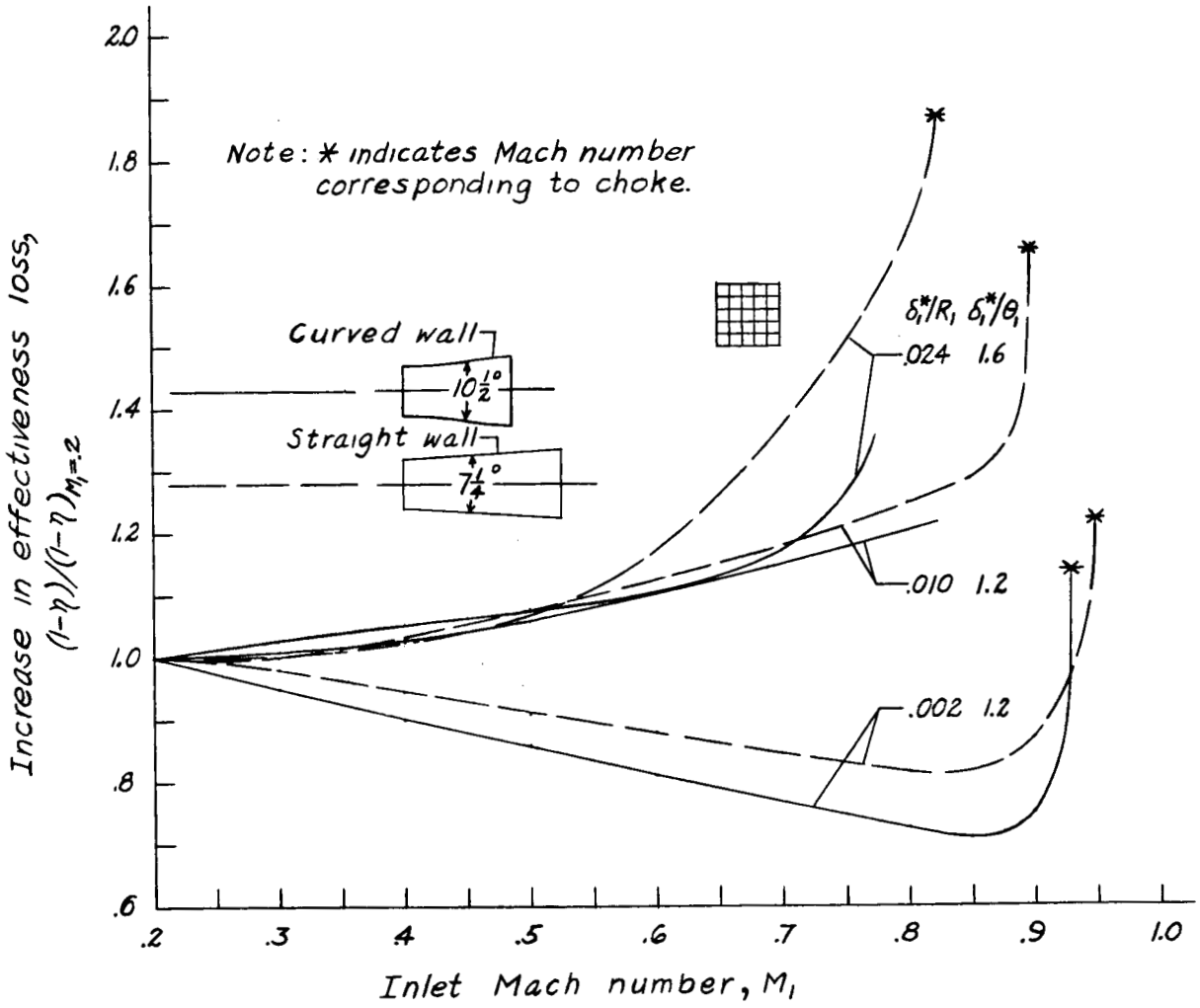

(c) Conical diffusers; δ^*_1/R_1 = 0.002 to 0.024; A_R = 1.96; reference 20.

Figure 18.- Continued.

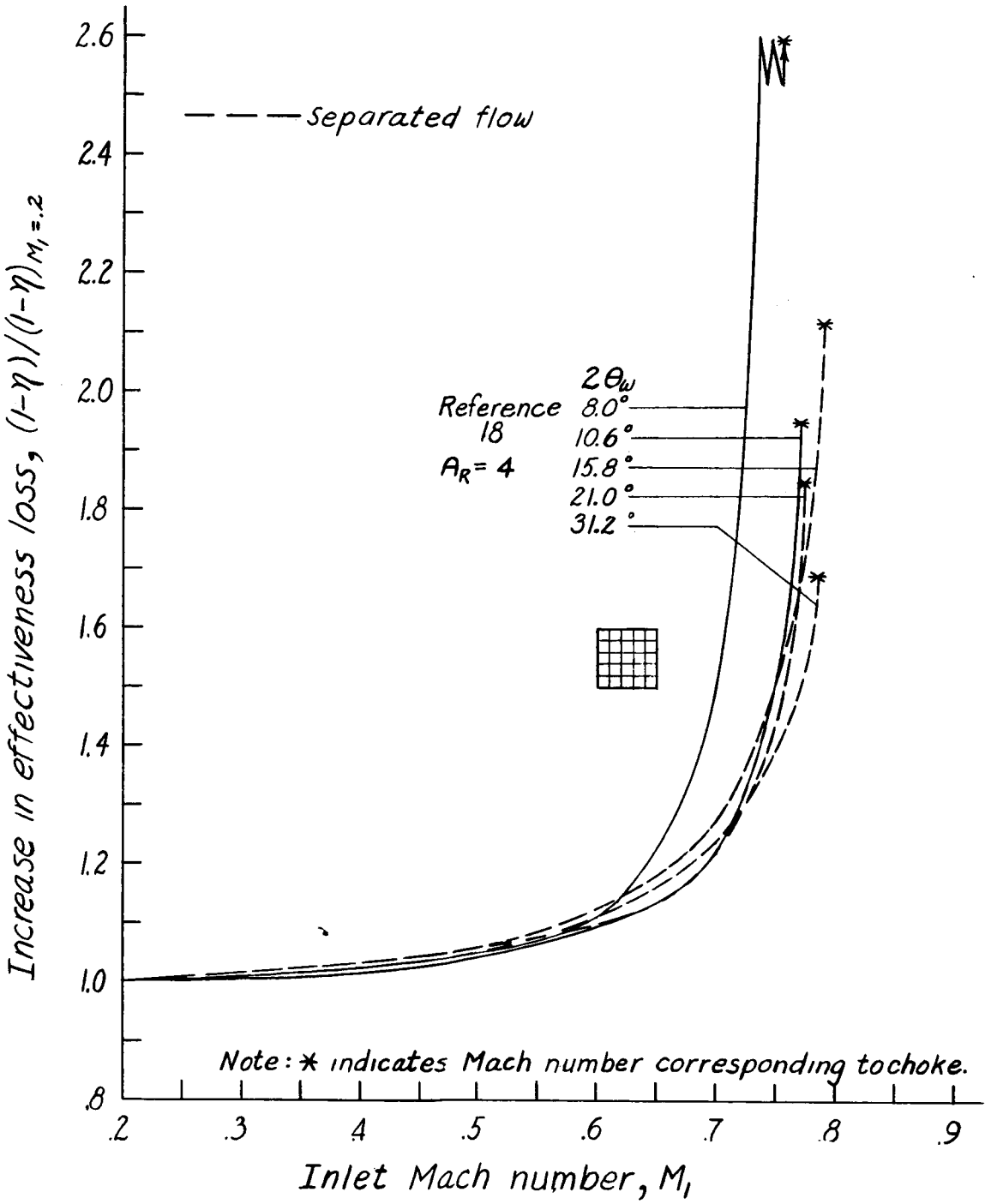

(d) Rectangular diffusers; $\delta^*_1/R_1 \approx 0.02$.

Figure 18.- Continued.

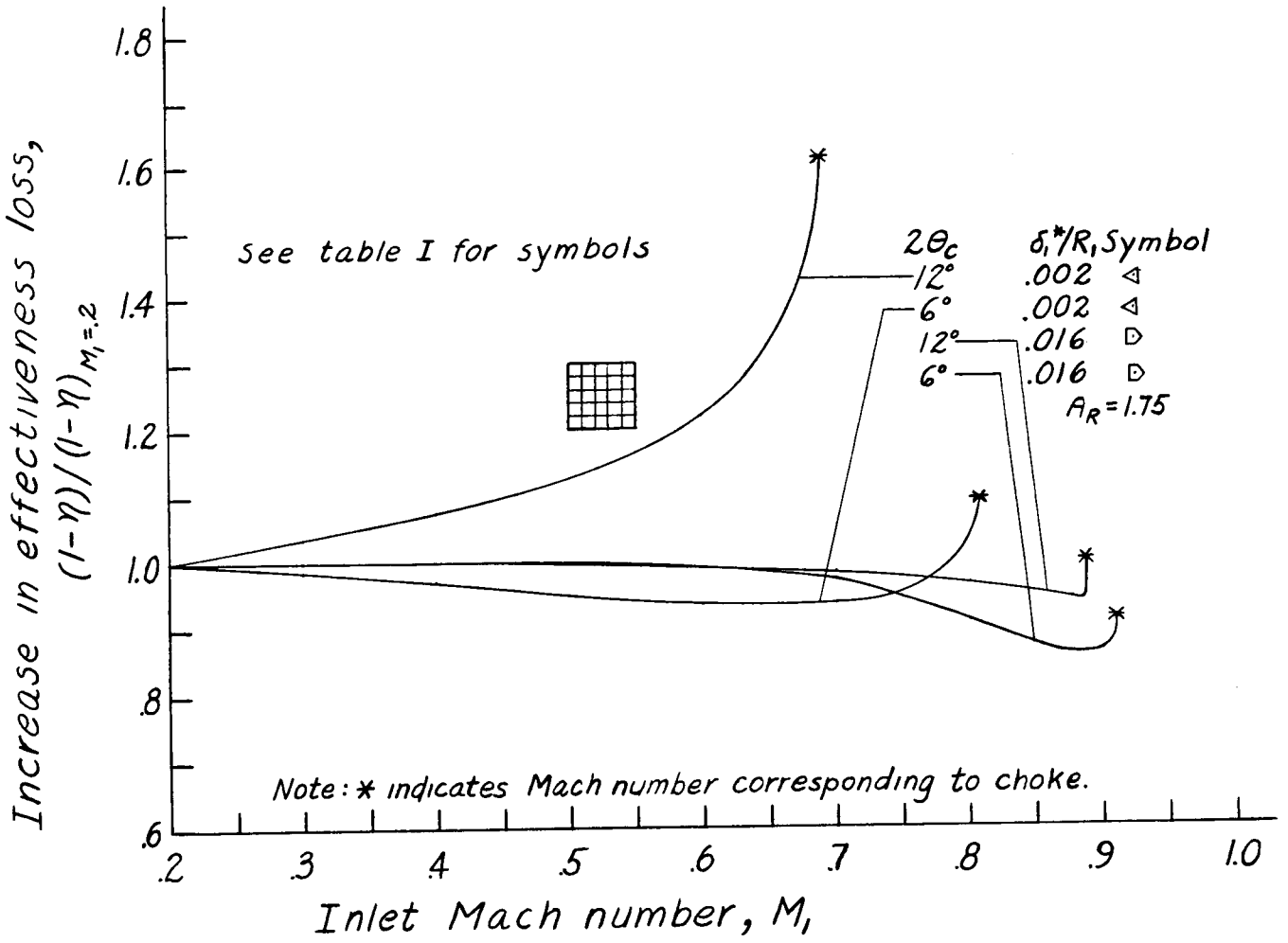

(e) Annular diffusers.

Figure 18.- Concluded.

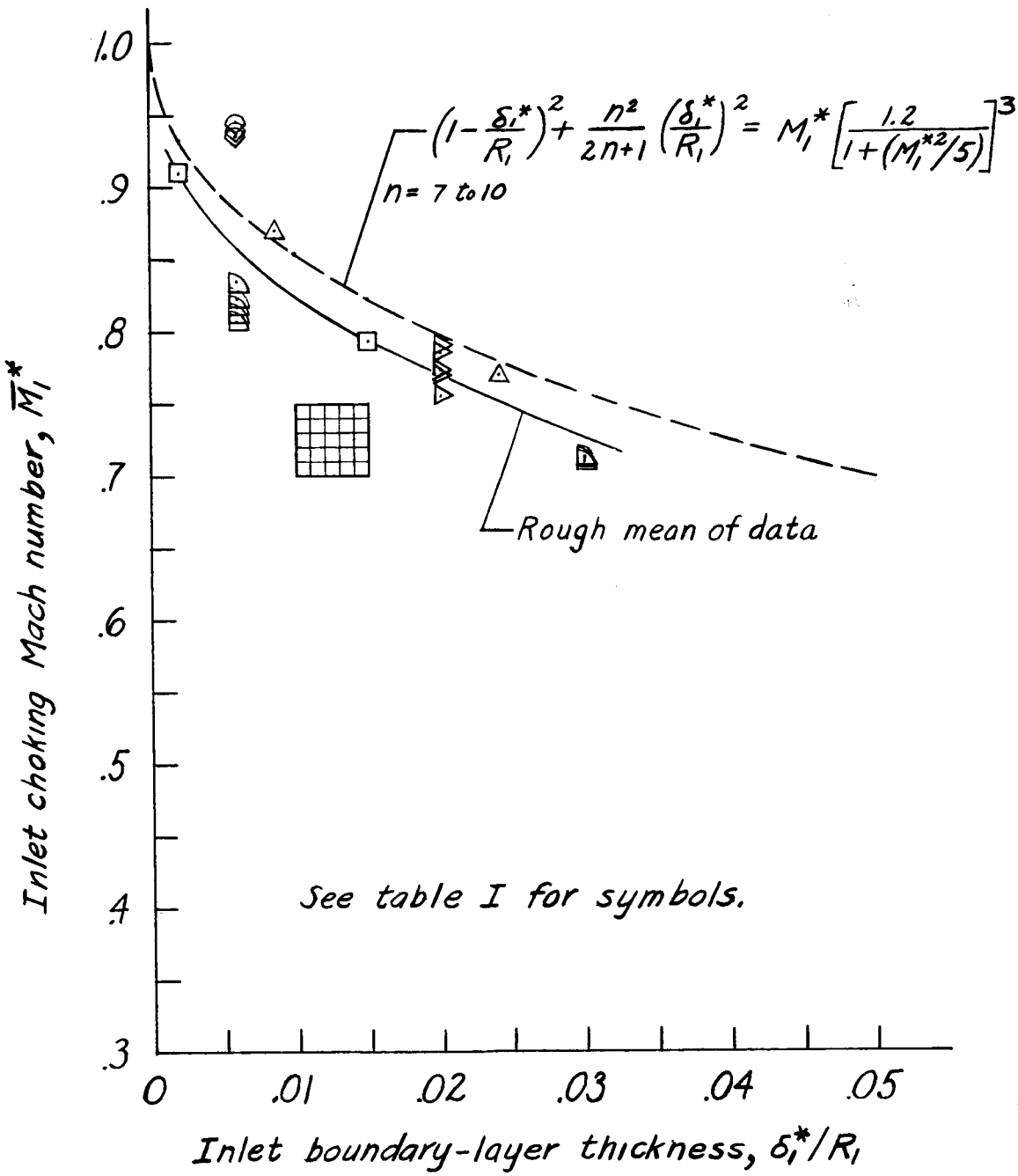

Figure 19.- Typical values of diffuser choking Mach number.

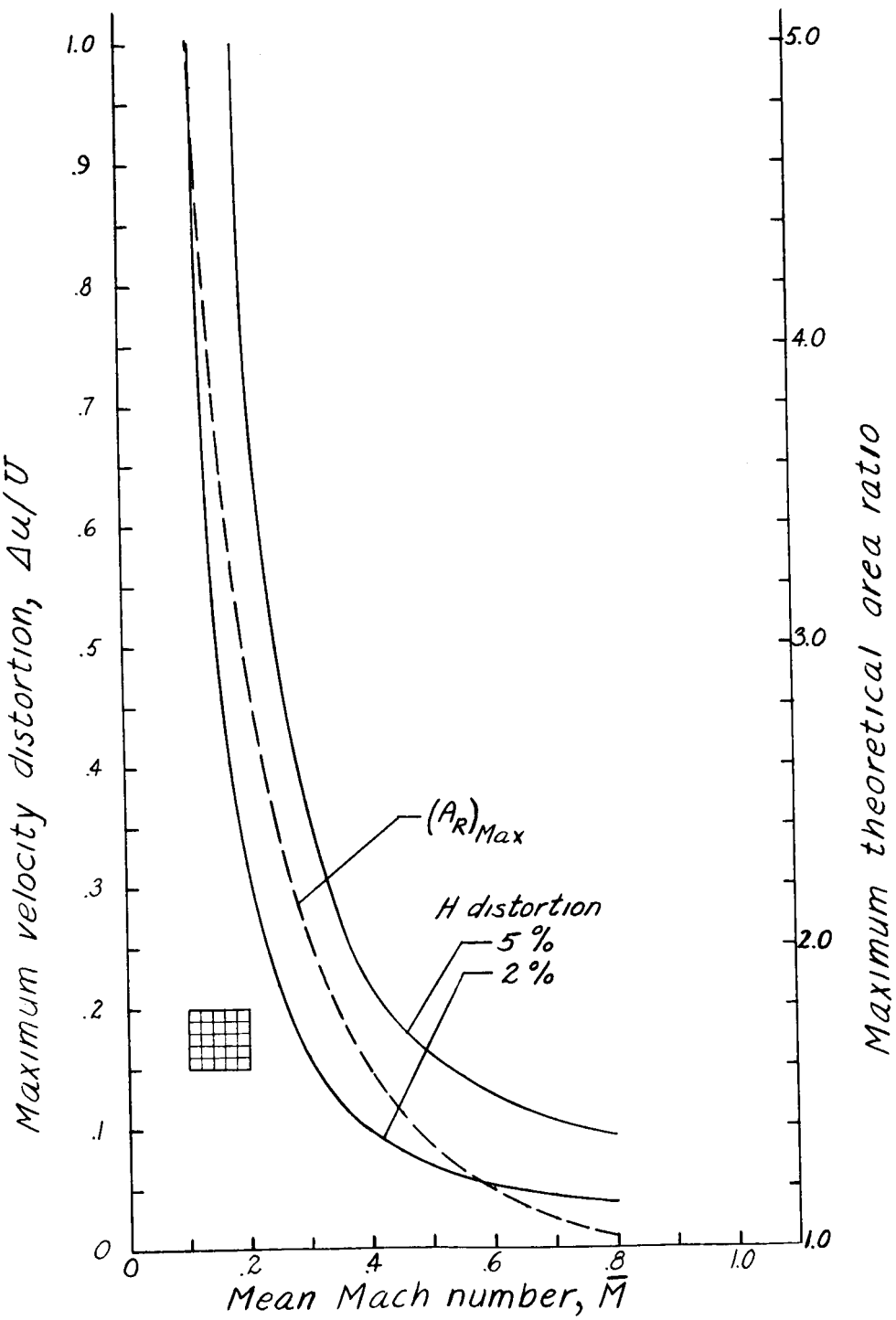

Figure 20.- Calculated velocity distortions for given values of total-pressure distortion.

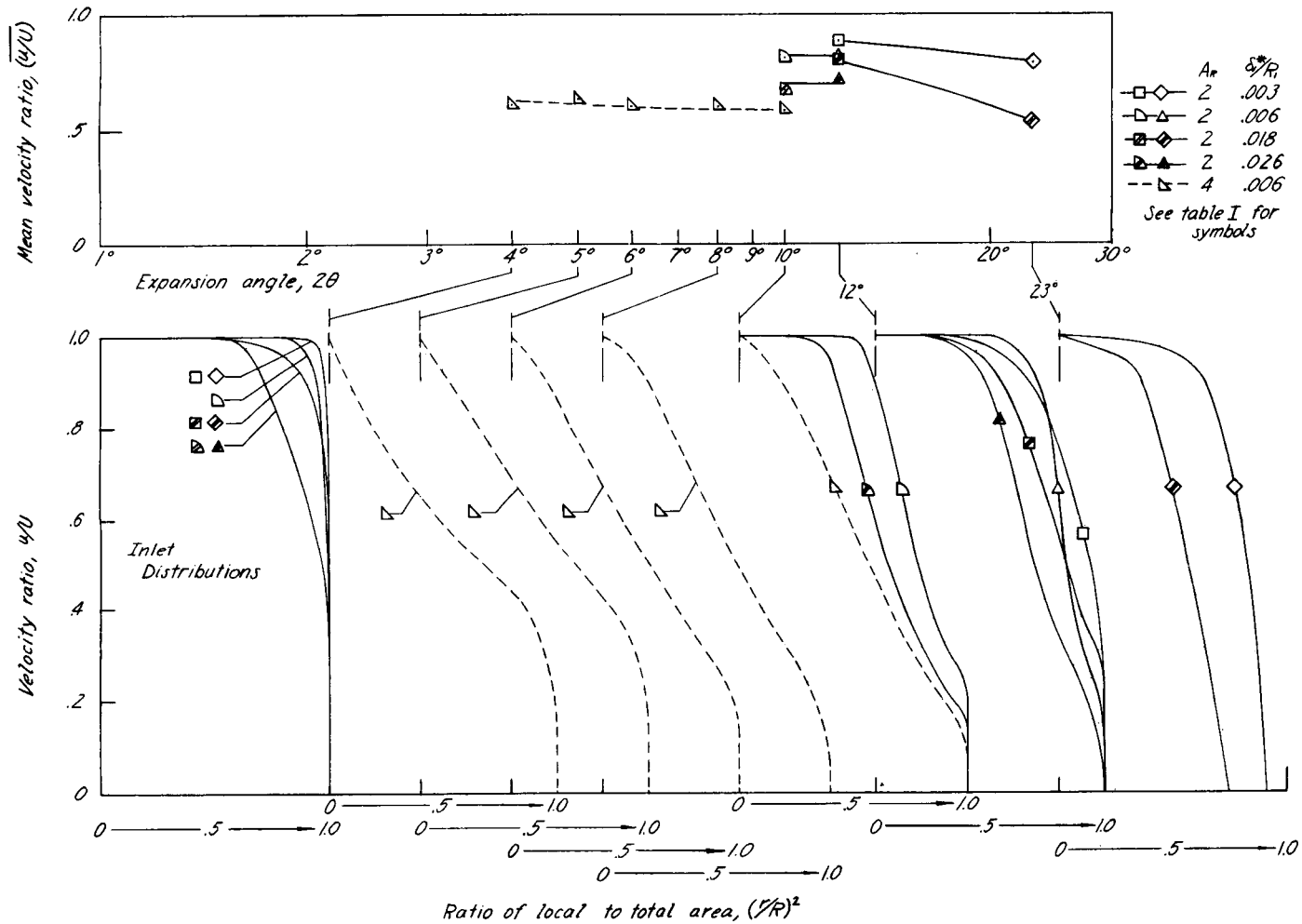

(a) Conical diffusers; thin inlet boundary layers; $M_1 \approx 0.20$.

Figure 21.- Exit flow distributions.

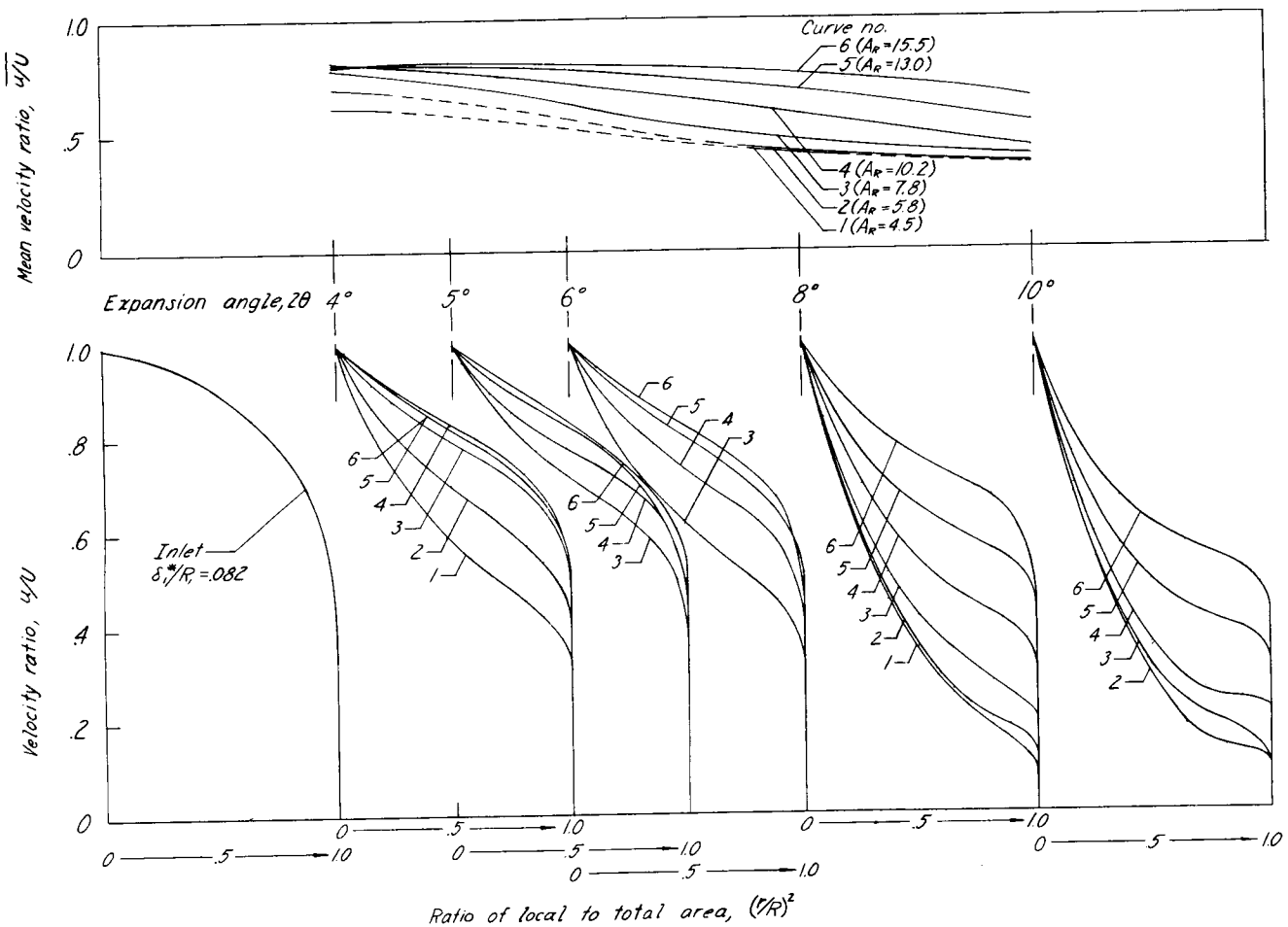

(b) Conical diffusers; thick inlet boundary layer; $\delta^*_1/R_1 = 0.082$; $M_1 = 0.45$; reference 15.

Figure 21.- Continued.

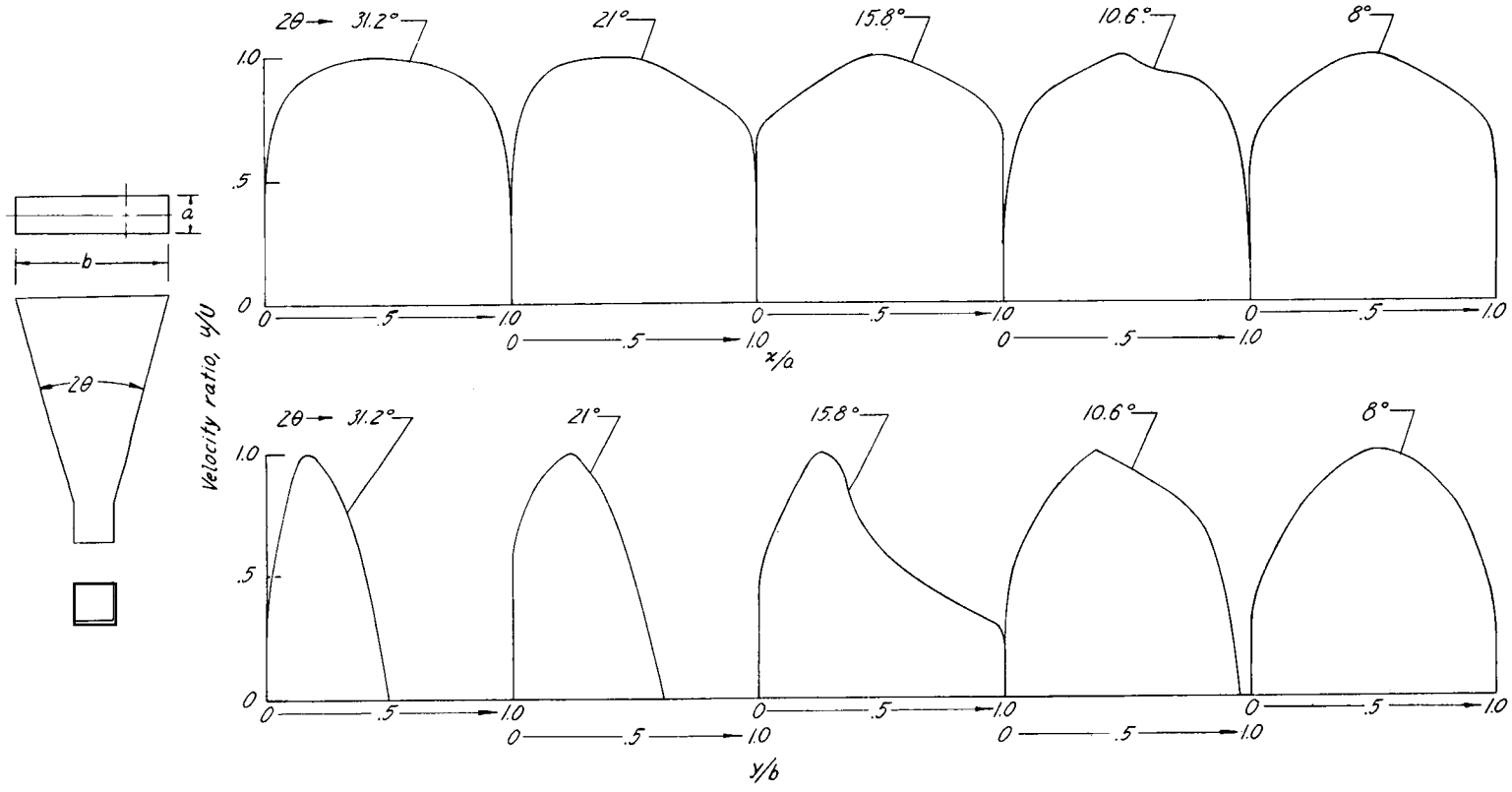

Note: Velocity distributions along line (a) located at peak velocity point on line (b), which is a center line.

(c) Rectangular diffusers; thin inlet boundary layer; $\delta^*_1/R_1 \approx 0.02$; $A_R = 4.0$; $M_1 \approx 0.2$; reference 18.

Figure 21.- Continued.

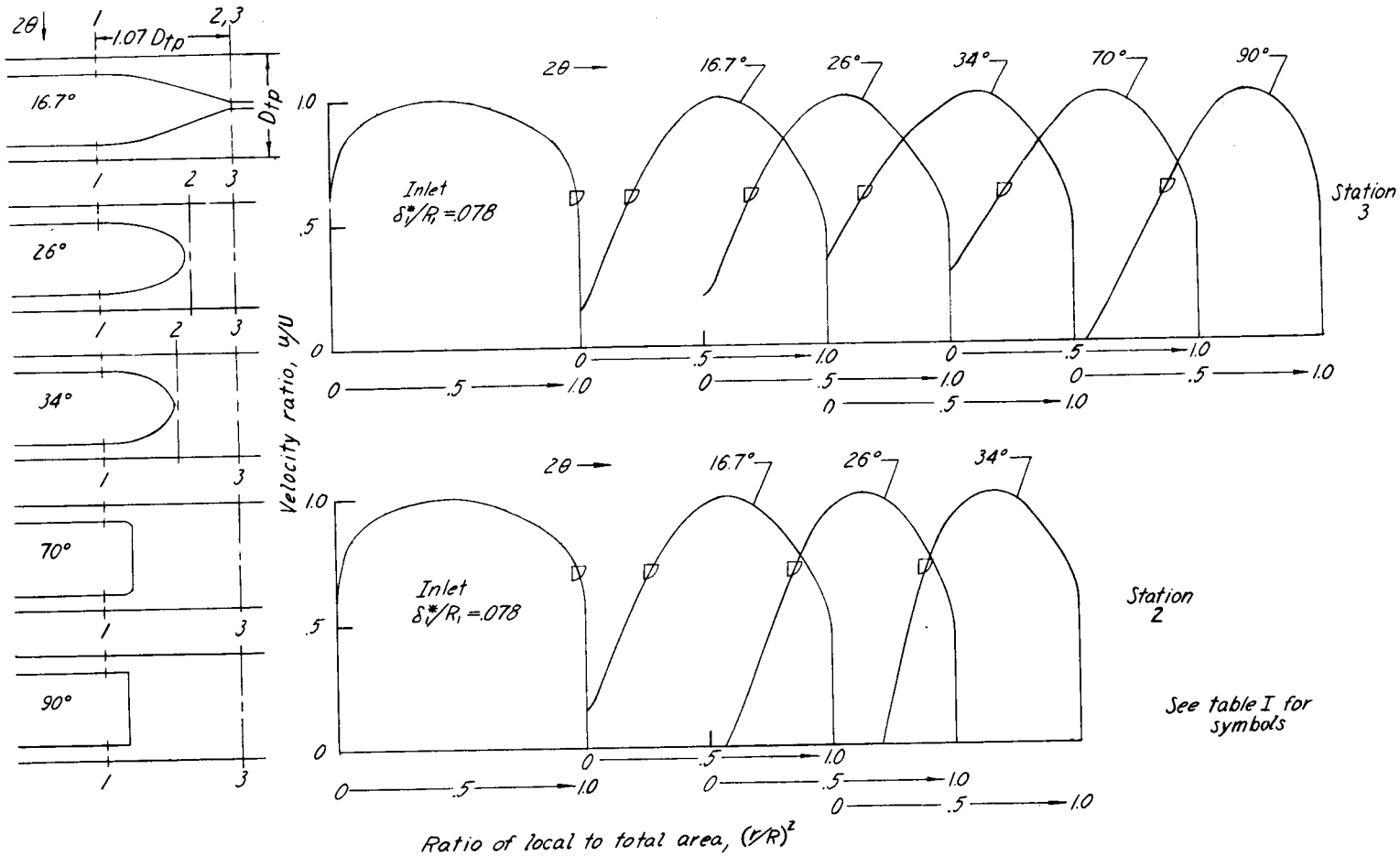

(d) Annular diffusers; thick inlet boundary layer; $A_R = 1.91$; $M_1 \approx 0.25$.

Figure 21.- Concluded.

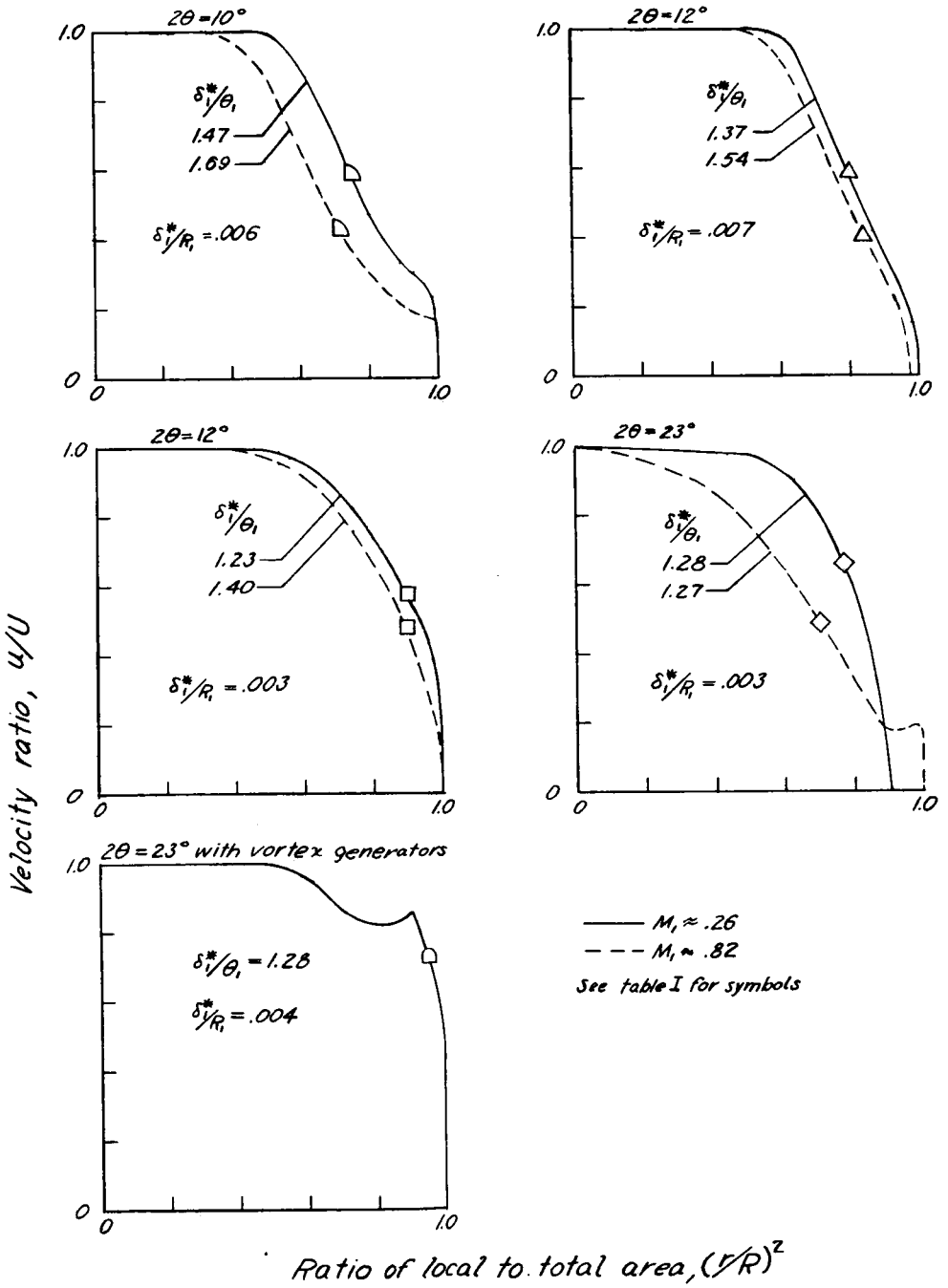

(a) Conical diffusers; thin boundary layer; δ^*_1/R_1 = 0.003 to 0.007; A_R = 2.00.

Figure 22.- Effect of inlet speed on exit flow distributions.

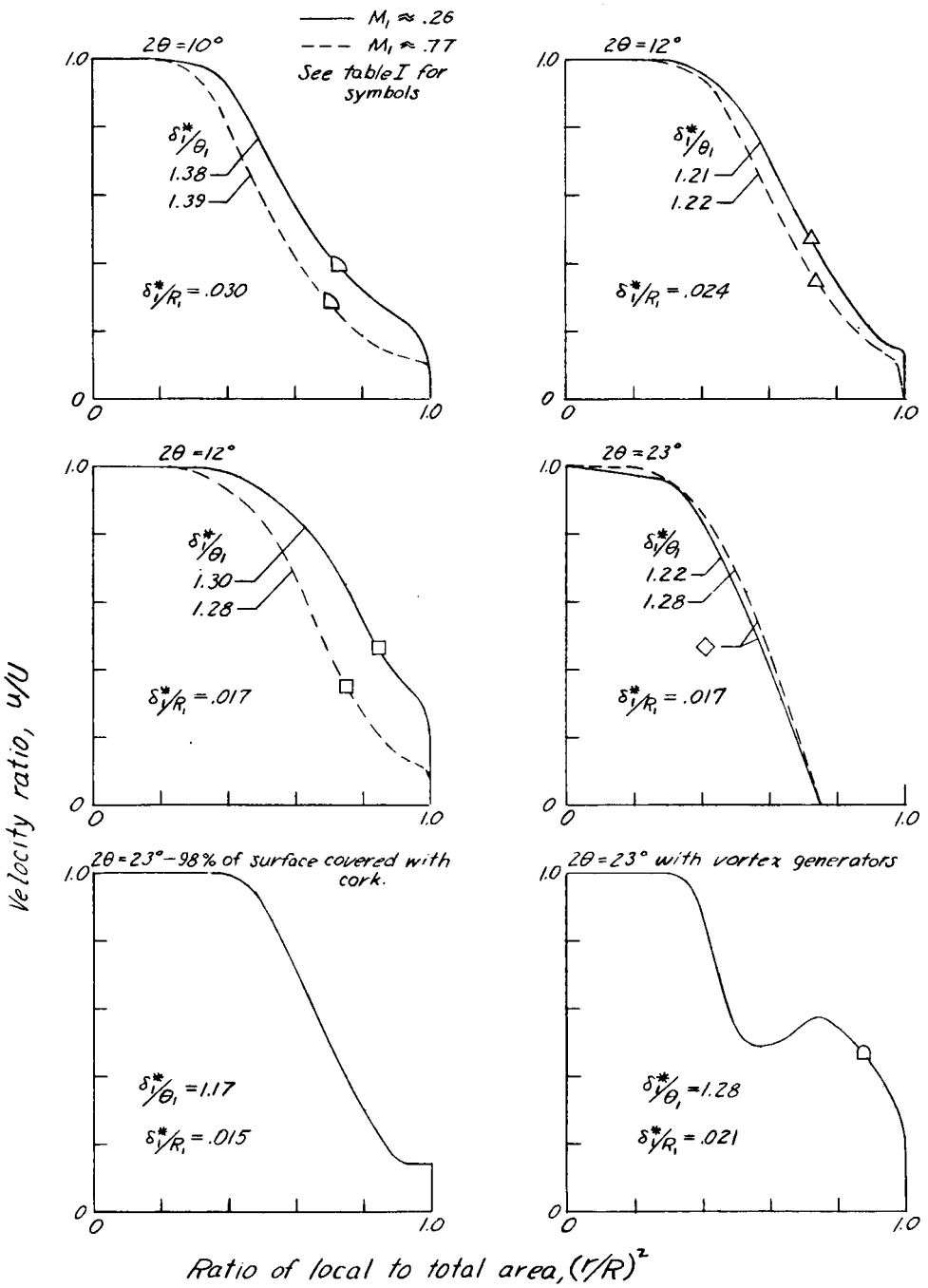

(b) Conical diffusers; thin boundary layer; δ^*_1/R_1 = 0.015 to 0.030; A_R = 2.0.

Figure 22.- Continued.

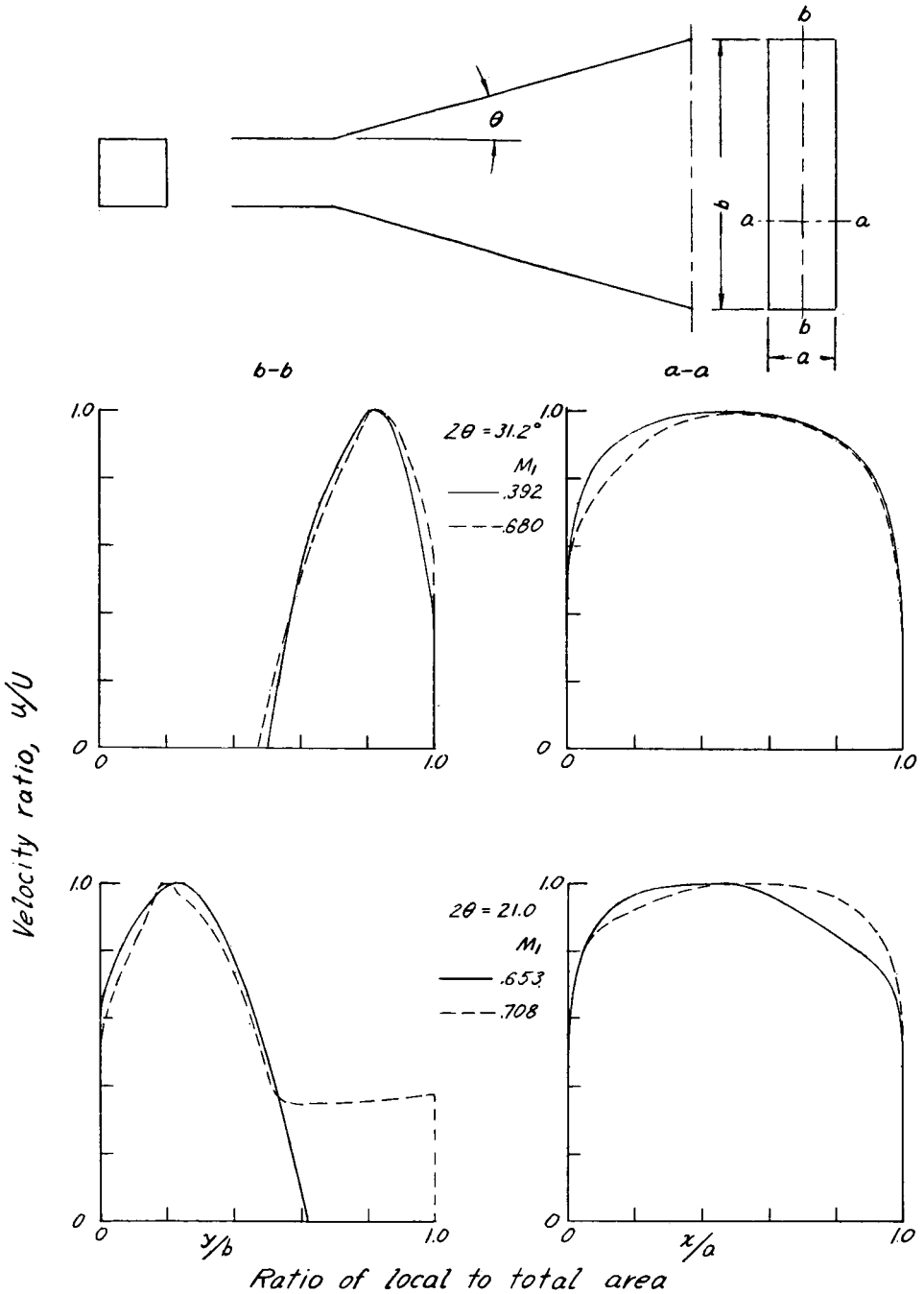

(c) Rectangular diffusers; thin inlet boundary layer; $\delta^*_1/R_1 \approx 0.02$; $A_R = 4.0$; reference 18.

Figure 22.- Continued.

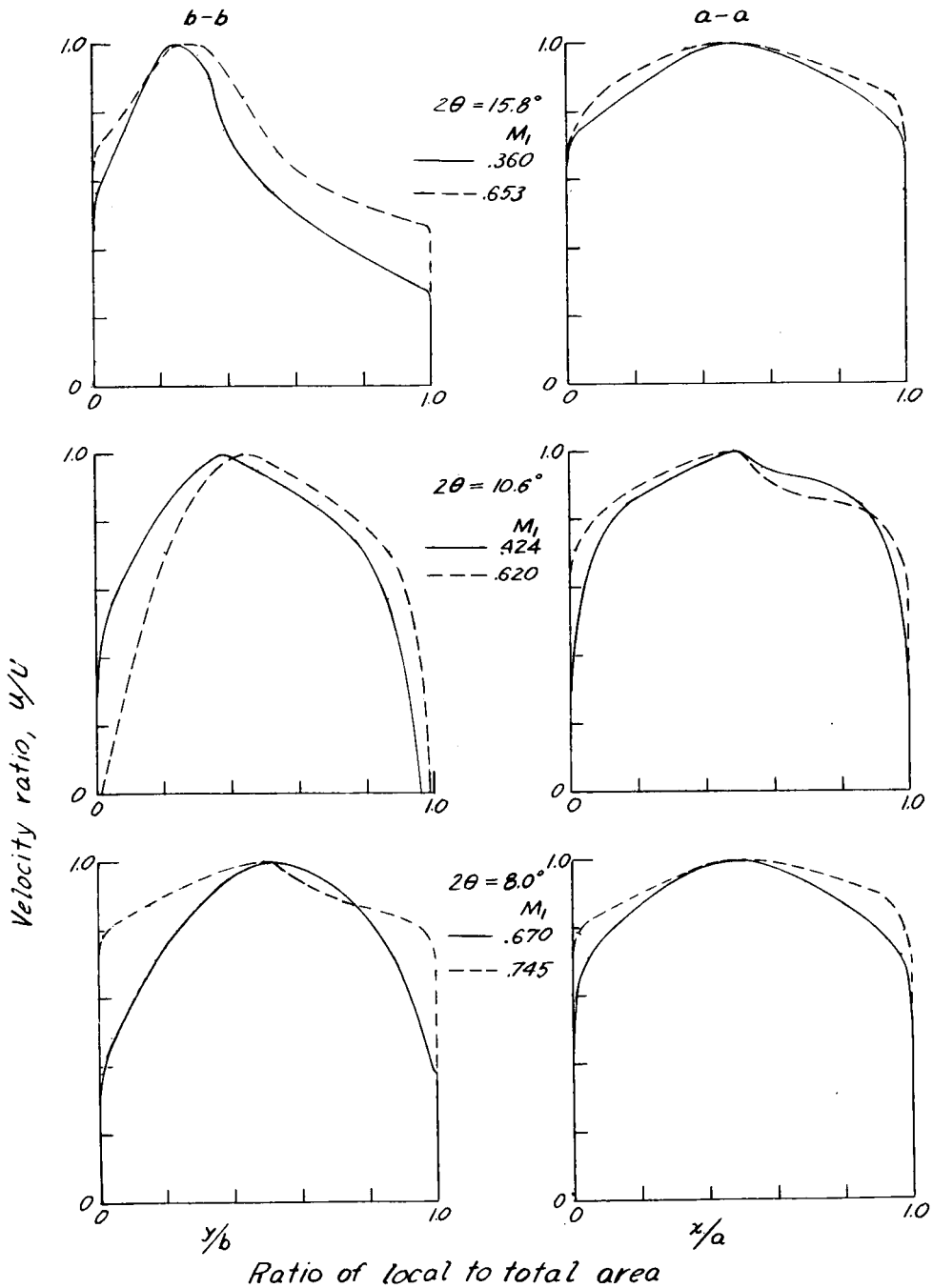

(d) Rectangular diffusers; thin boundary layer; $\delta^*_1/R_1 \approx 0.02$; $A_R = 4.0$; reference 18.

Figure 22.- Concluded.

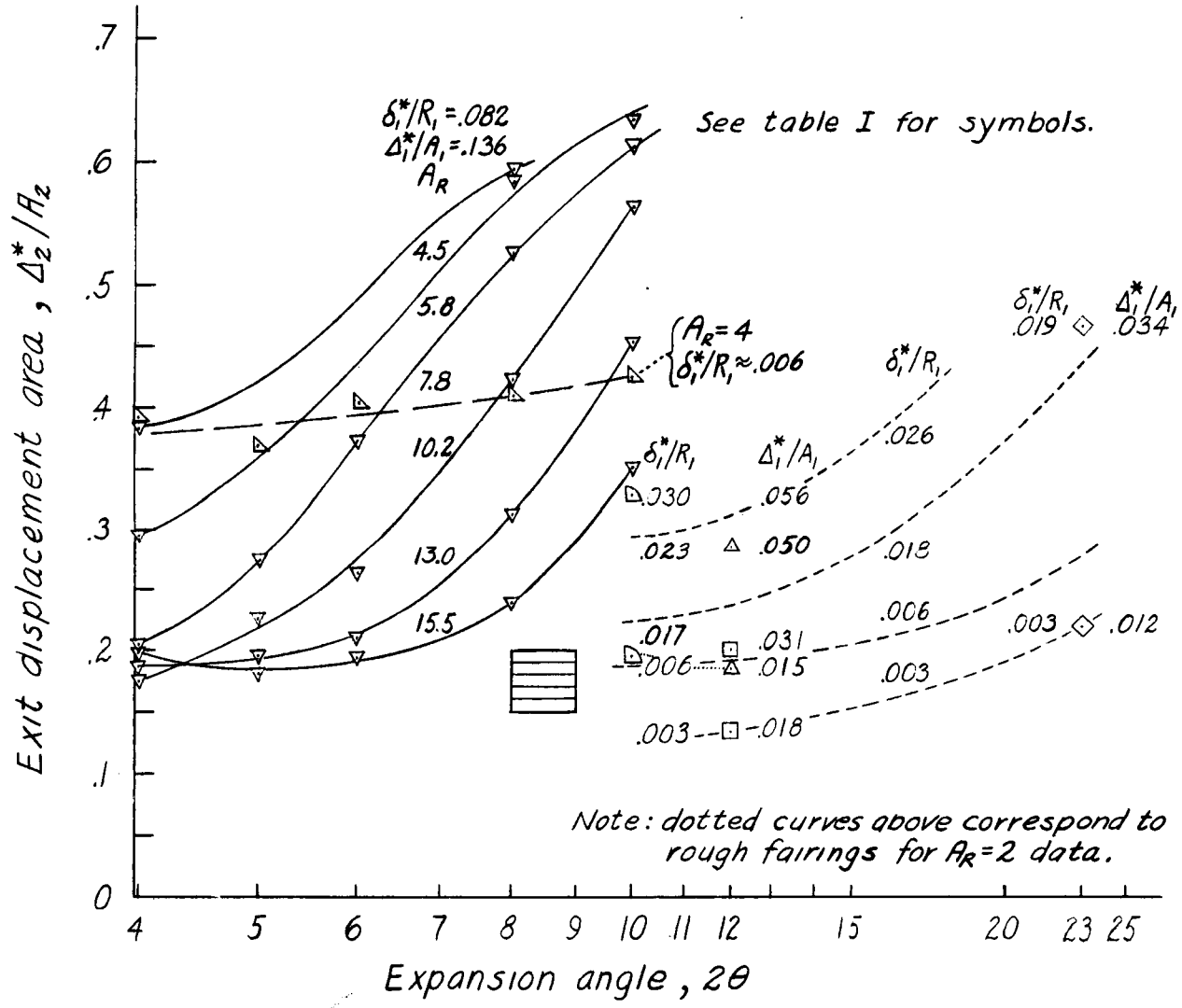

Figure 23.- Exit displacement area. Conical diffusers; M_1 = 0.2 to 0.45.

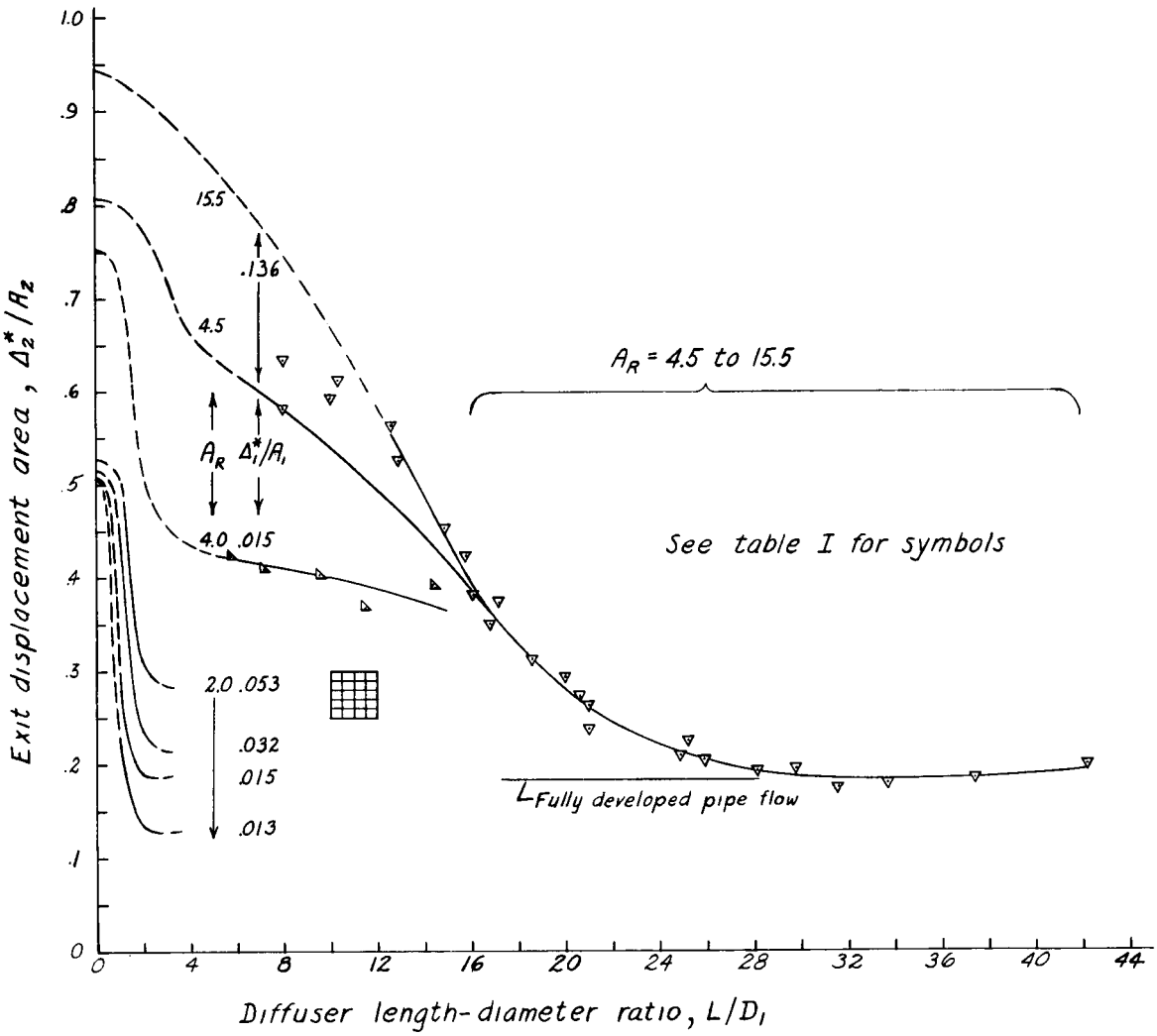

Figure 24.- Exit displacement area; conical diffusers; M_1 = 0.2 to 0.45;

$$\left(\frac{\Delta^*_2}{A_2}\right)_{L/D_1=0} = 1 - \frac{1 - (\Delta^*_1/A_1)}{A_R}.$$

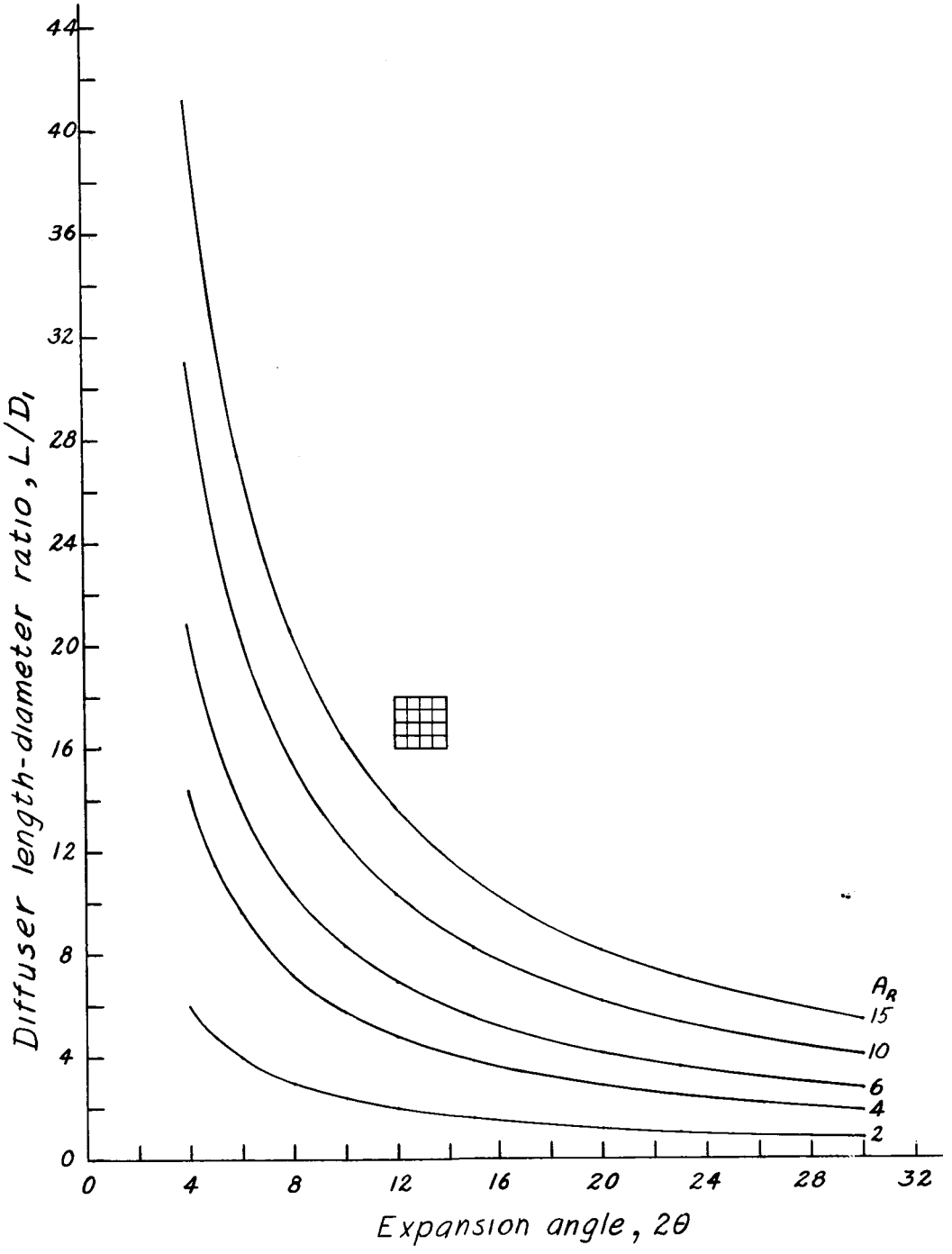

Figure 25.- Variation of length-diameter ratio with area ratio and expansion angle. Conical diffusers; $L/D_1 = \frac{\sqrt{A_R} - 1}{2 \tan \theta}$.

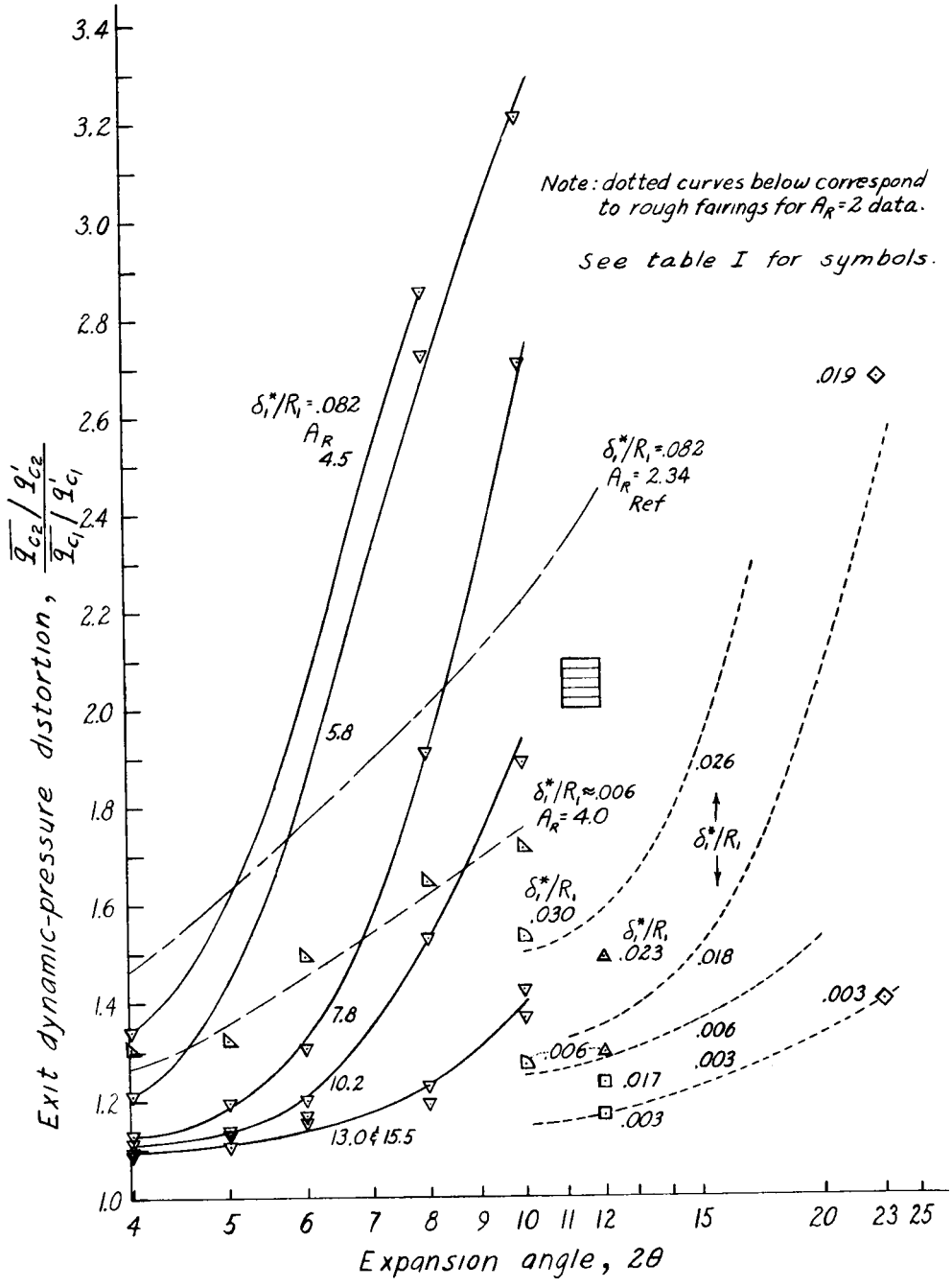

(a) Mean dynamic pressure as a function of 2θ.

Figure 26.- Exit flow-distribution factors. Conical diffusers; M_1 = 0.20 to 0.45.

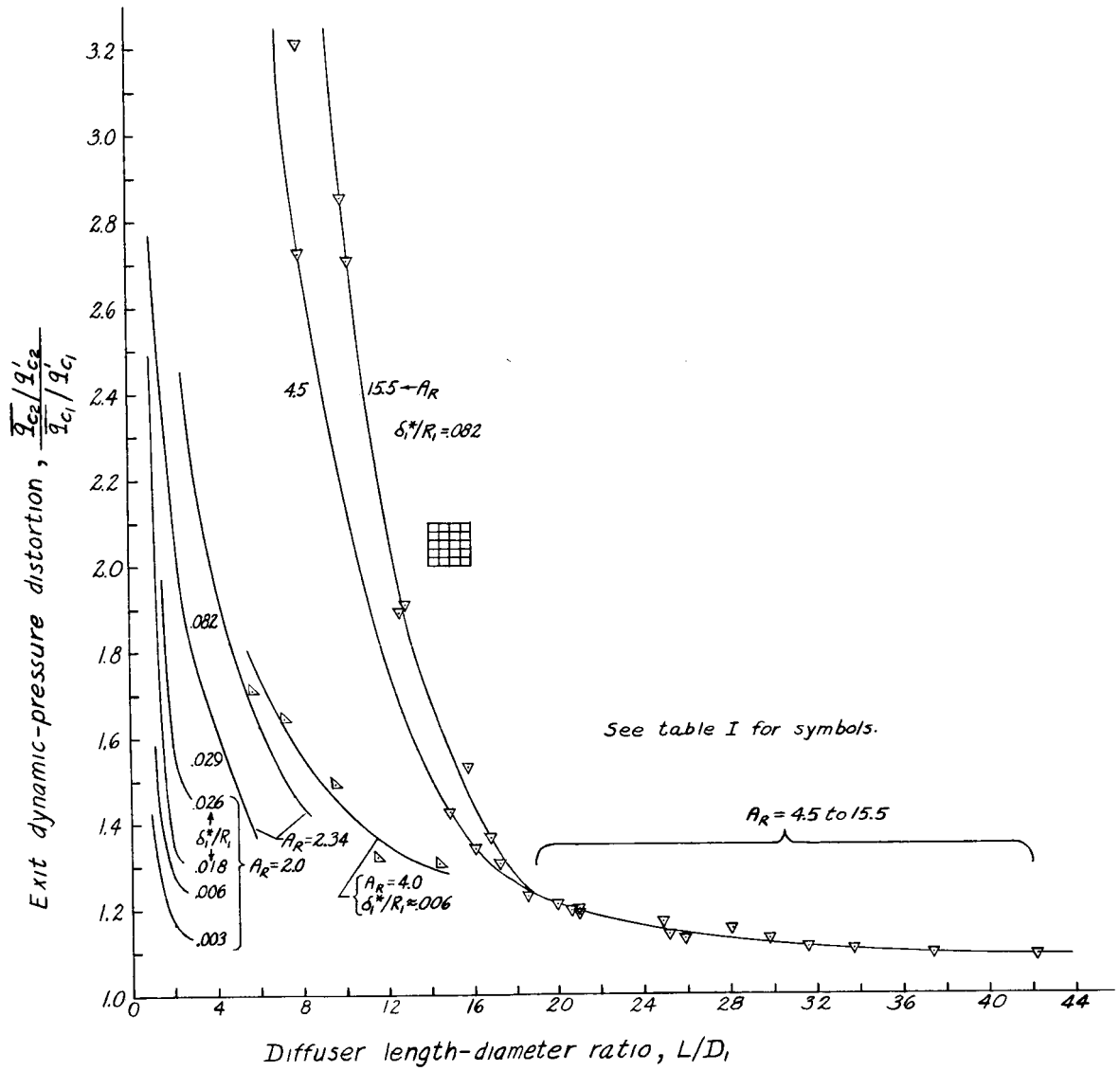

(b) Mean dynamic pressure as a function of L/D_1.

Figure 26.- Continued.

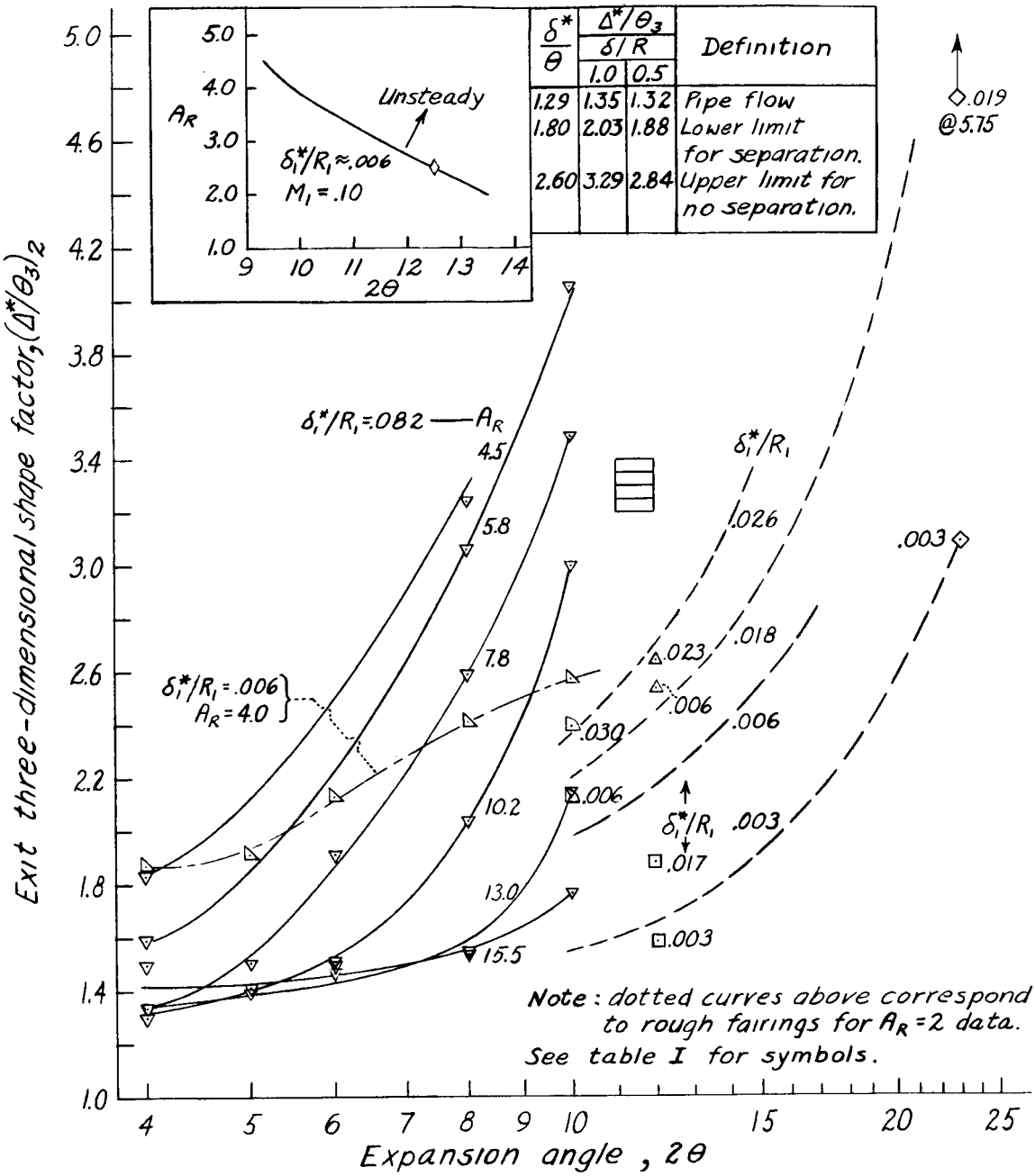

(c) Three-dimensional shape factor.

Figure 26.- Concluded.

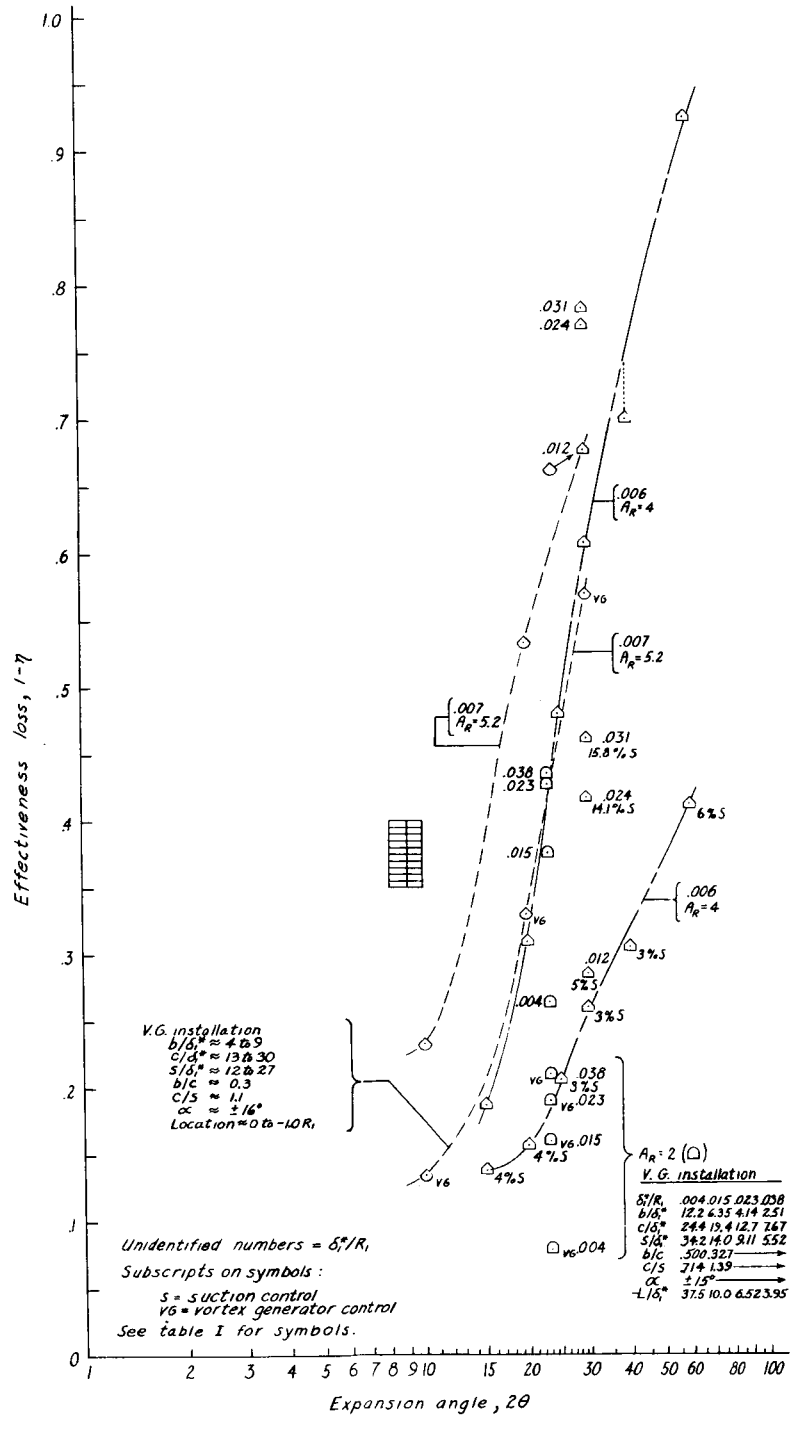

Figure 27.- Reductions in $1 - \eta$ obtained with boundary-layer control. Conical diffusers; $M_1 = 0.18$ to 0.50.

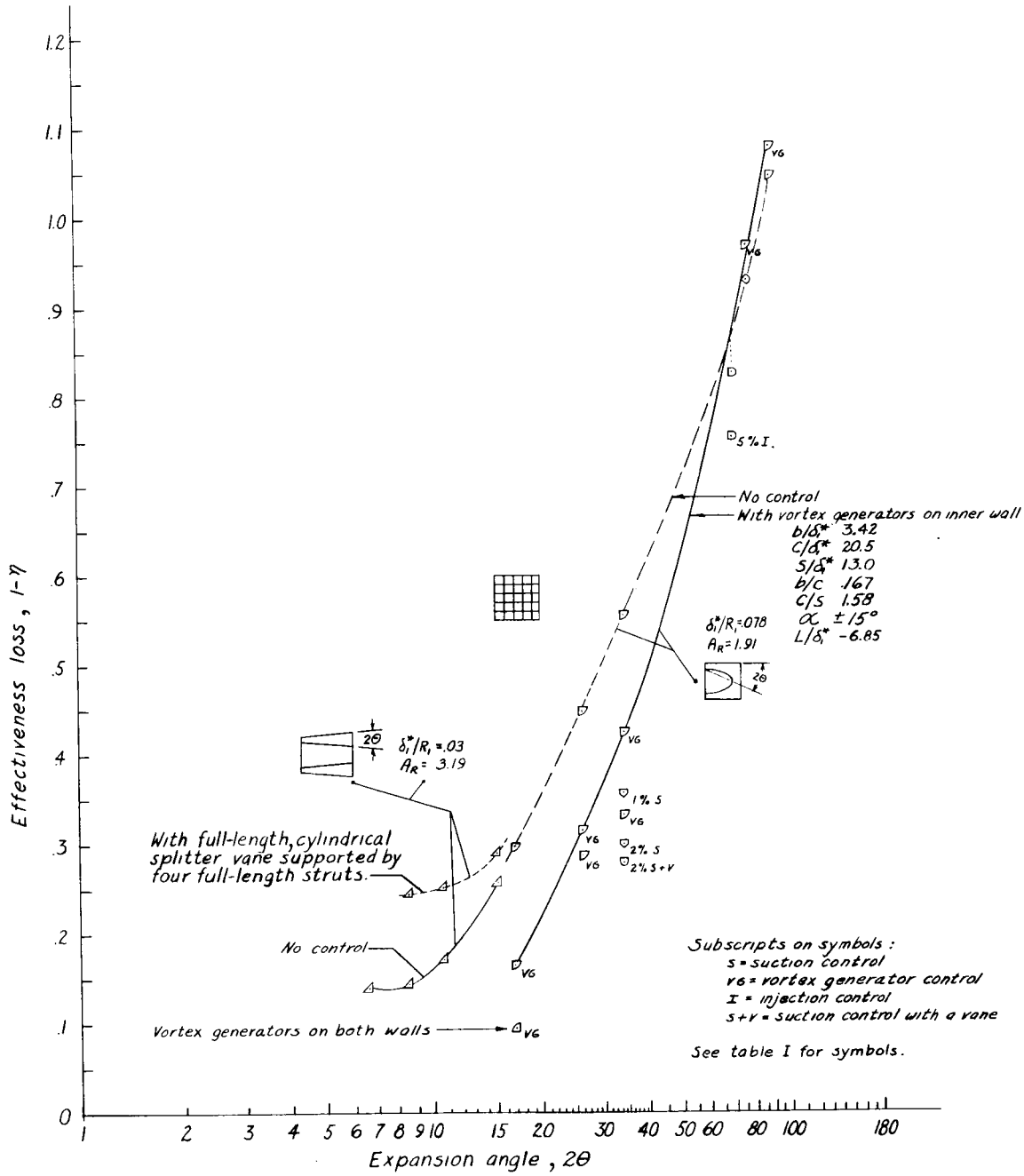

Figure 28.- Reductions in $1 - \eta$ obtained with boundary-layer control. Annular diffusers; $M_1 = 0.25$ to 0.30.

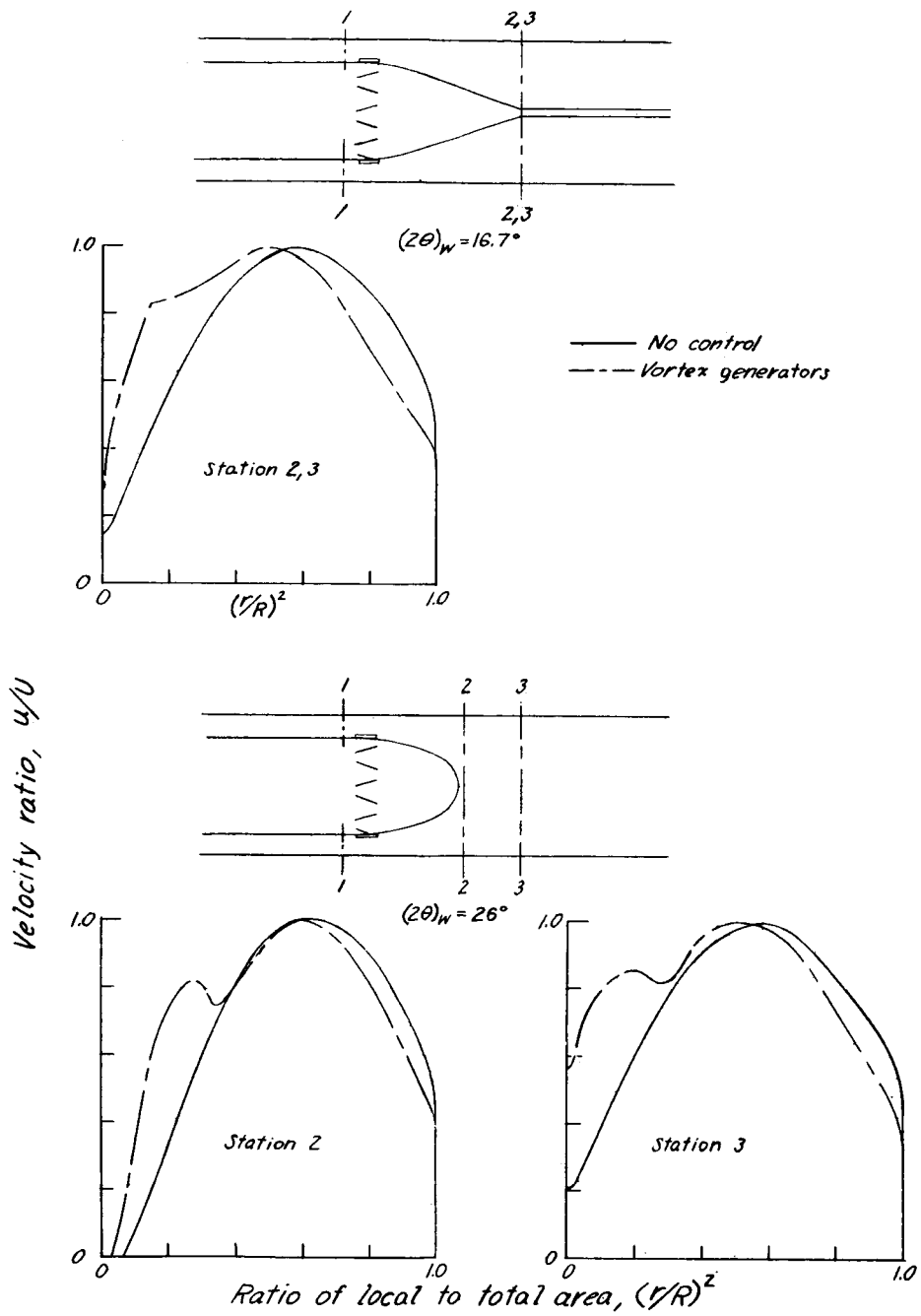

(a) $2\theta_w = 16.7^\circ$ and 26°.

Figure 29.- Effect of boundary-layer control with vortex generators on the exit velocity distribution. Annular diffusers; $\delta^*_1/R_1 = 0.078$; $A_R = 1.91$; $\overline{M_1} \approx 0.26$; reference 12.

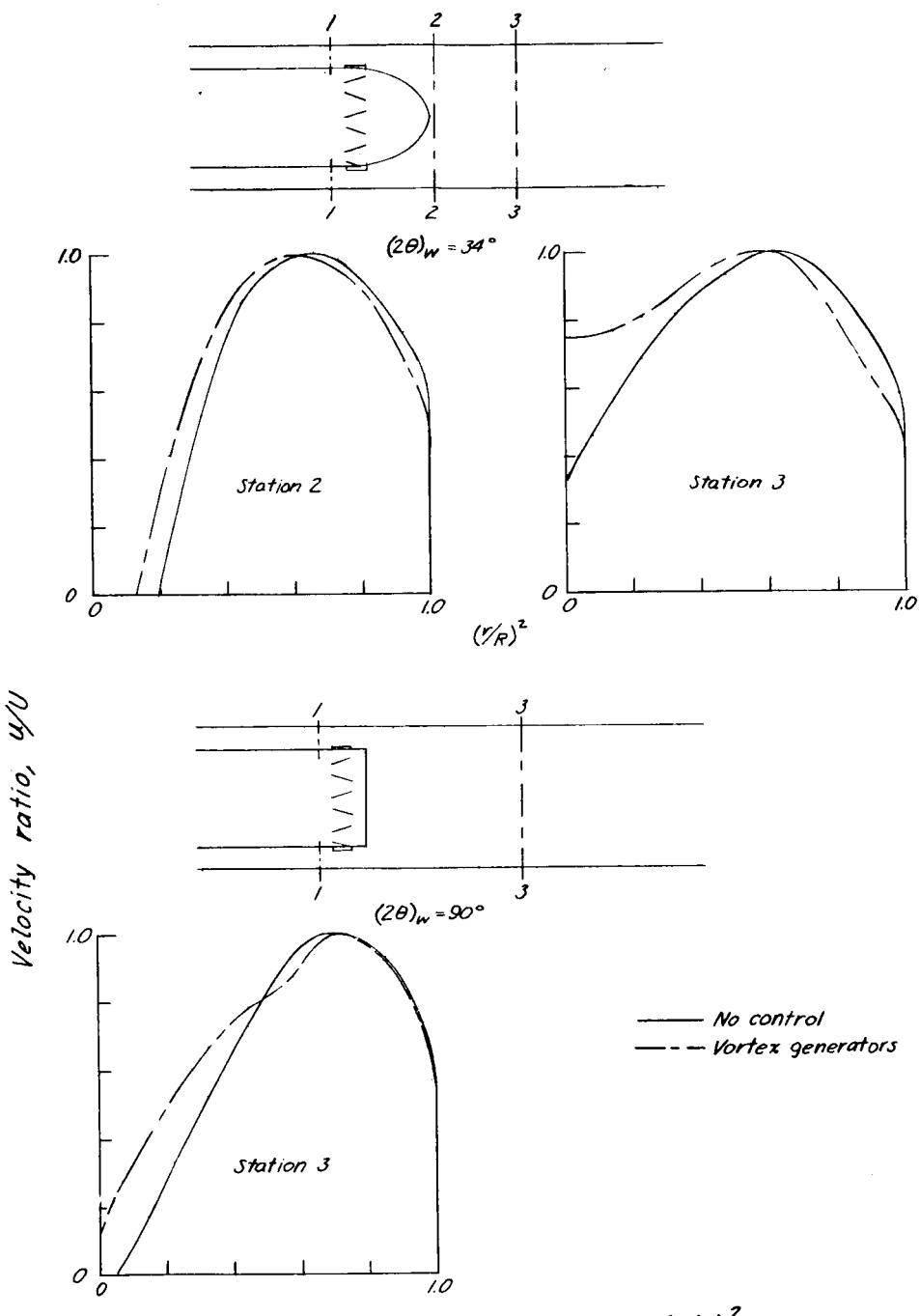

(b) $2\theta_w = 34^\circ$ and 90°.

Figure 29.- Concluded.

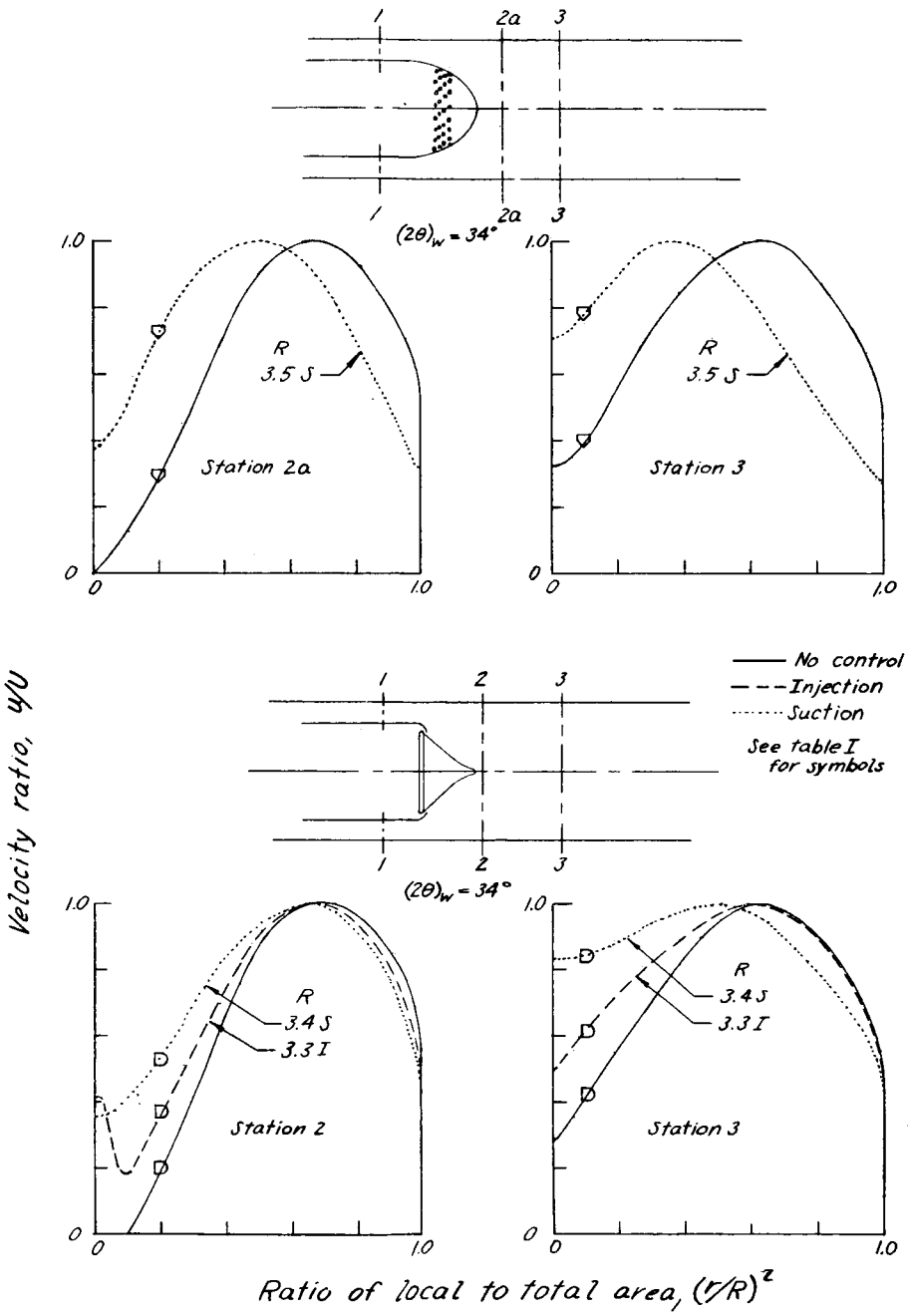

(a) $2\theta_w = 34^\circ$; suction and injection.

Figure 30.- Effect of suction, injection, and vanes on the exit velocity distribution. Annular diffusers; $\delta^*_1/R_1 = 0.078$; $A_R = 1.91$; $M_1 \approx 0.26$.

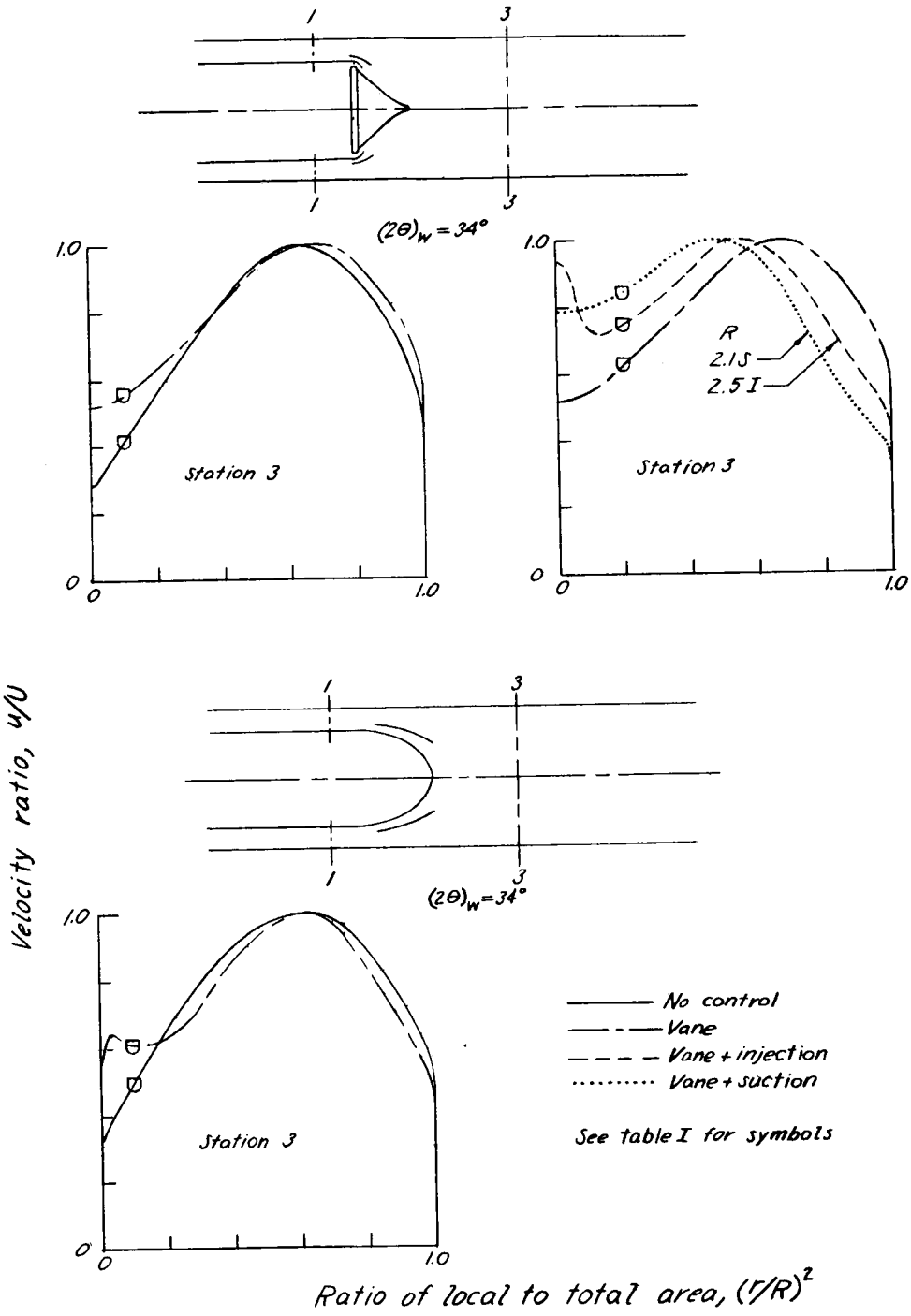

(b) $2\theta_w = 34^o$; vanes, suction, and injection.

Figure 30.- Continued.

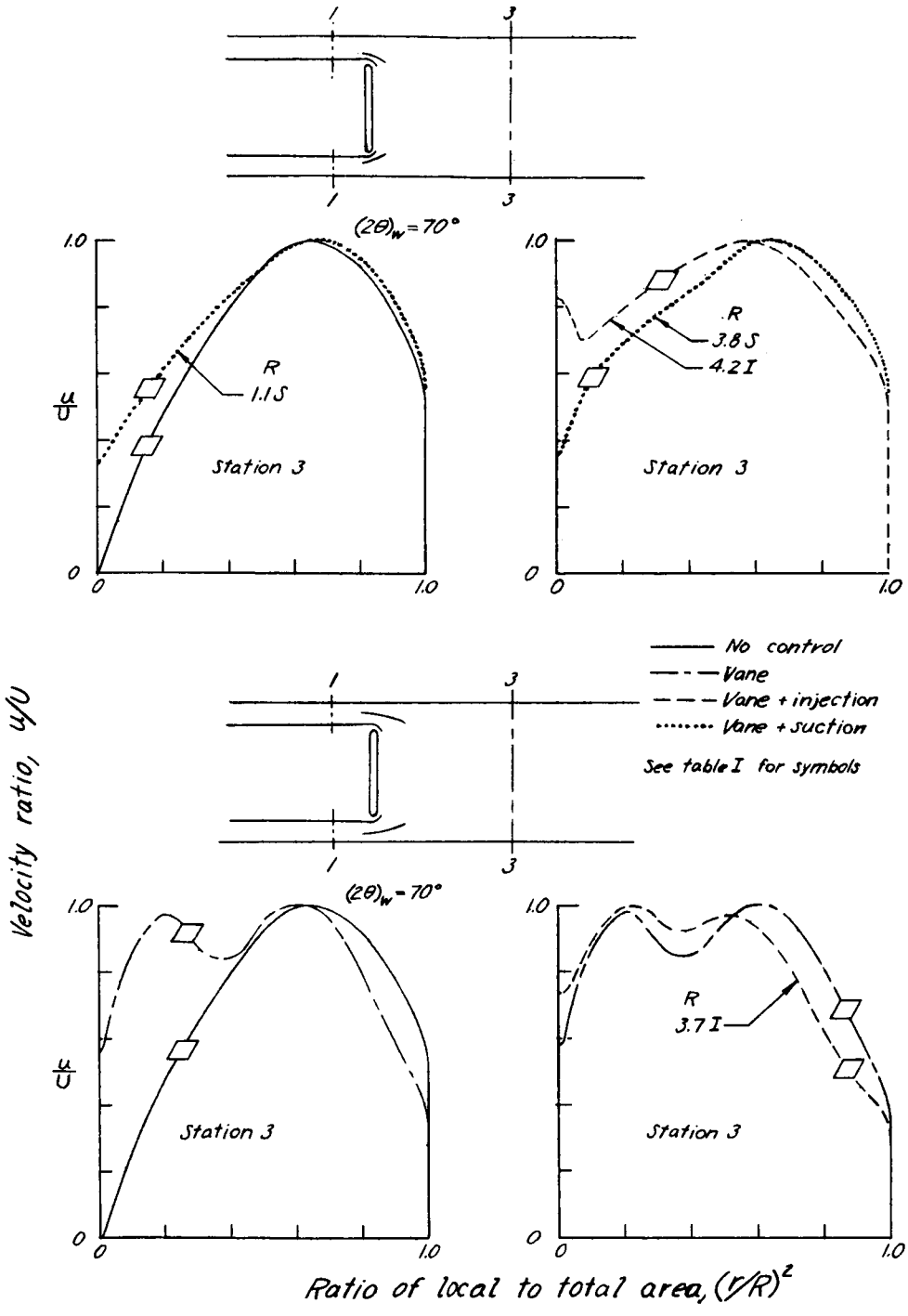

(c) $2\theta_w = 70°$; vane, suction, and injection.

Figure 30.- Continued.

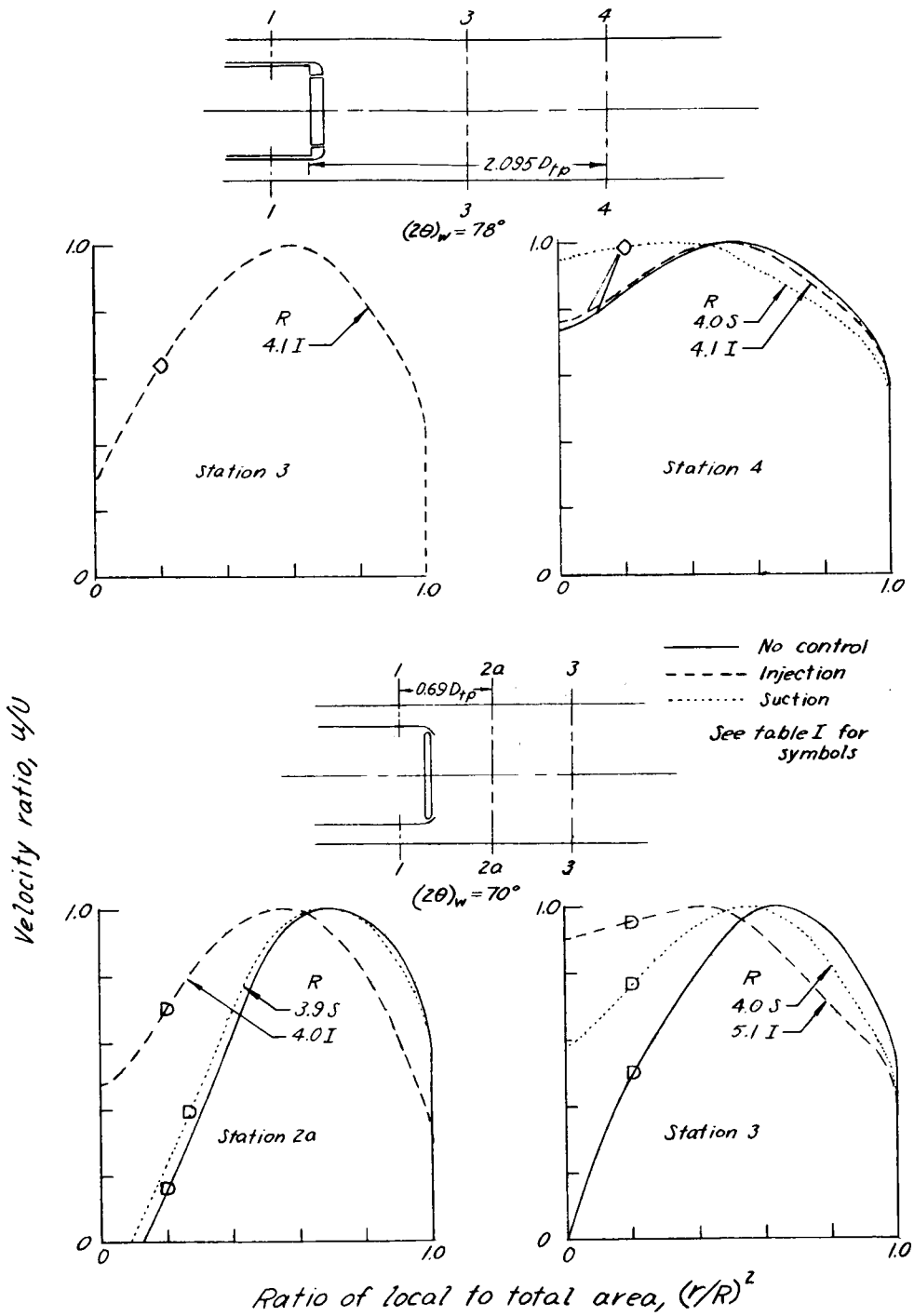

(d) $2\theta_w = 70°$ and $78°$; suction and injection.

Figure 30.- Concluded.

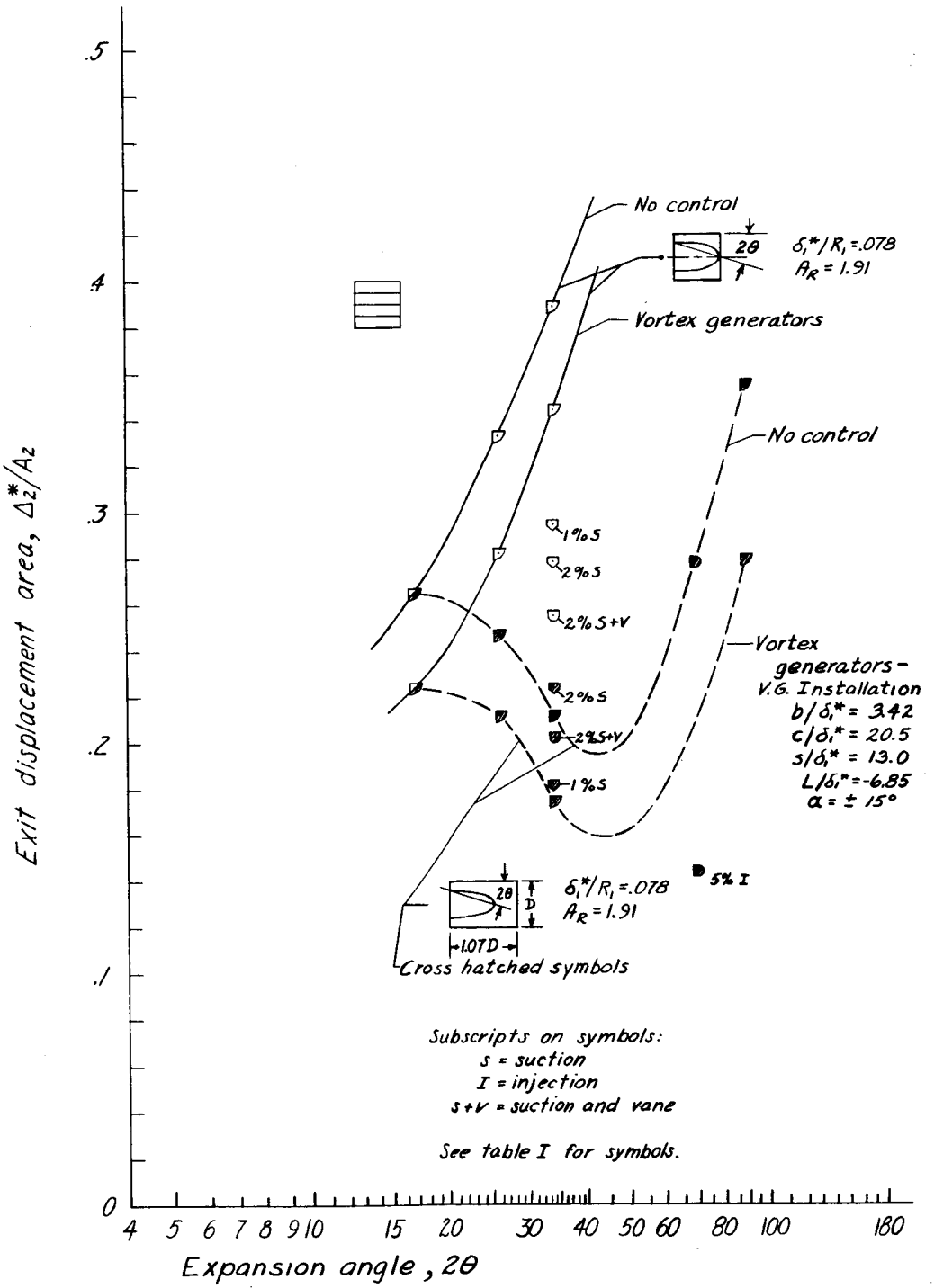

Figure 31.- Effect of boundary-layer controls on exit displacement area. Annular diffusers; $M_1 = 0.25$ to 0.30.

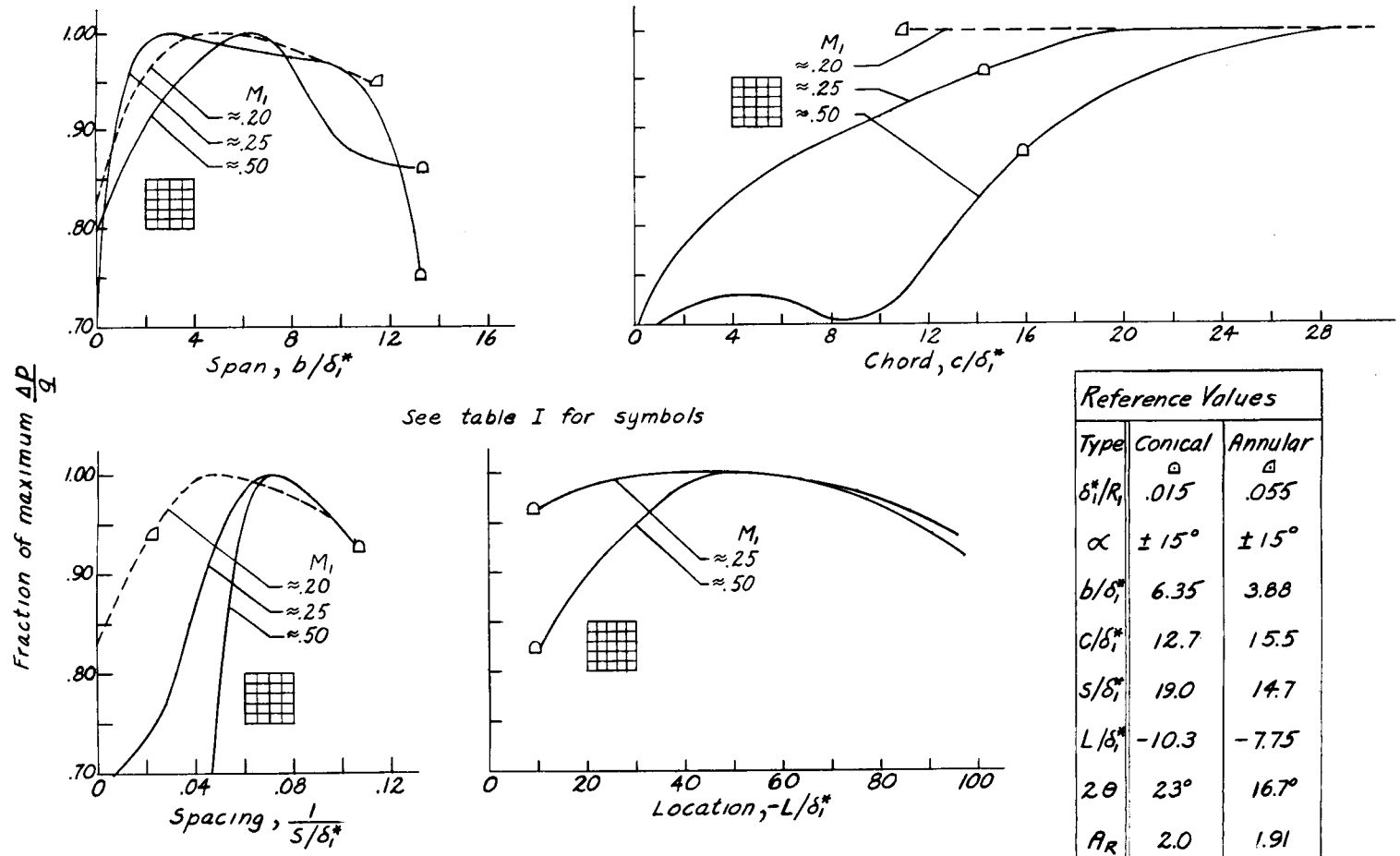

Reference Values		
Type	Conical ◻	Annular ◿
δ_1^*/R_1	.015	.055
α	± 15°	± 15°
b/δ_1^*	6.35	3.88
c/δ_1^*	12.7	15.5
s/δ_1^*	19.0	14.7
L/δ_1^*	-10.3	-7.75
2θ	23°	16.7°
A_R	2.0	1.91

Figure 32.- Effects of several vortex-generator geometric variables on diffuser performance. Conical and annular diffusers.

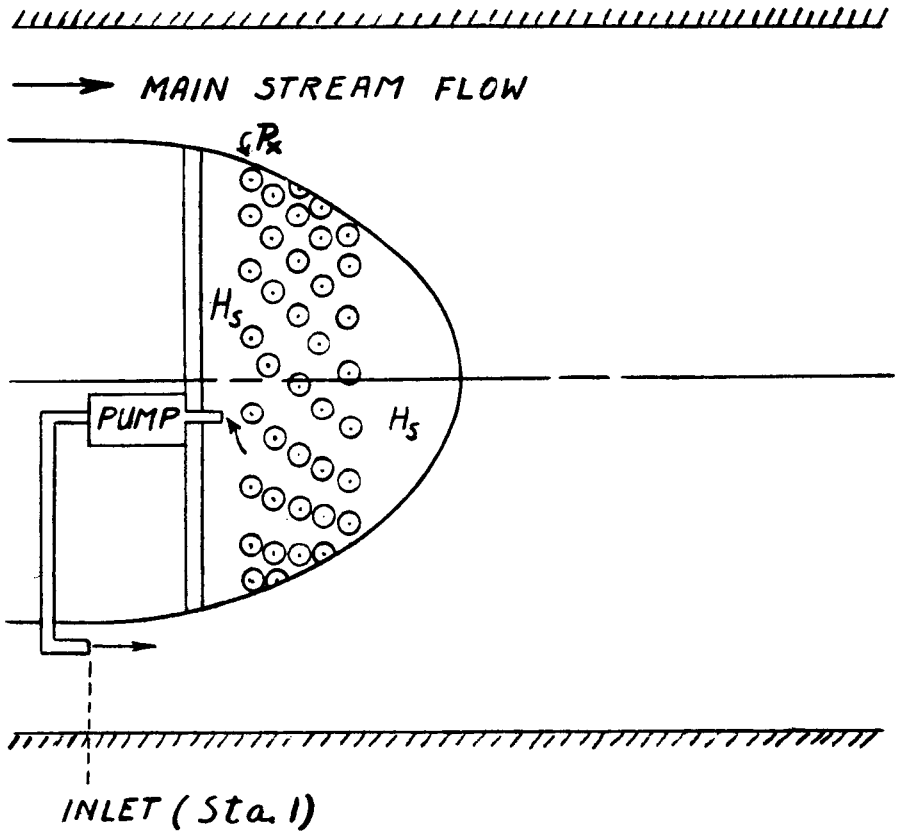

SUCTION PUMPING POWER COEFFICIENT =

$$P_s = \frac{R}{100} \frac{\bar{H}_1 - H_s}{\bar{q}_{c_1}}$$

Figure 33.- Hypothetical auxiliary-flow system for evaluating suction power.

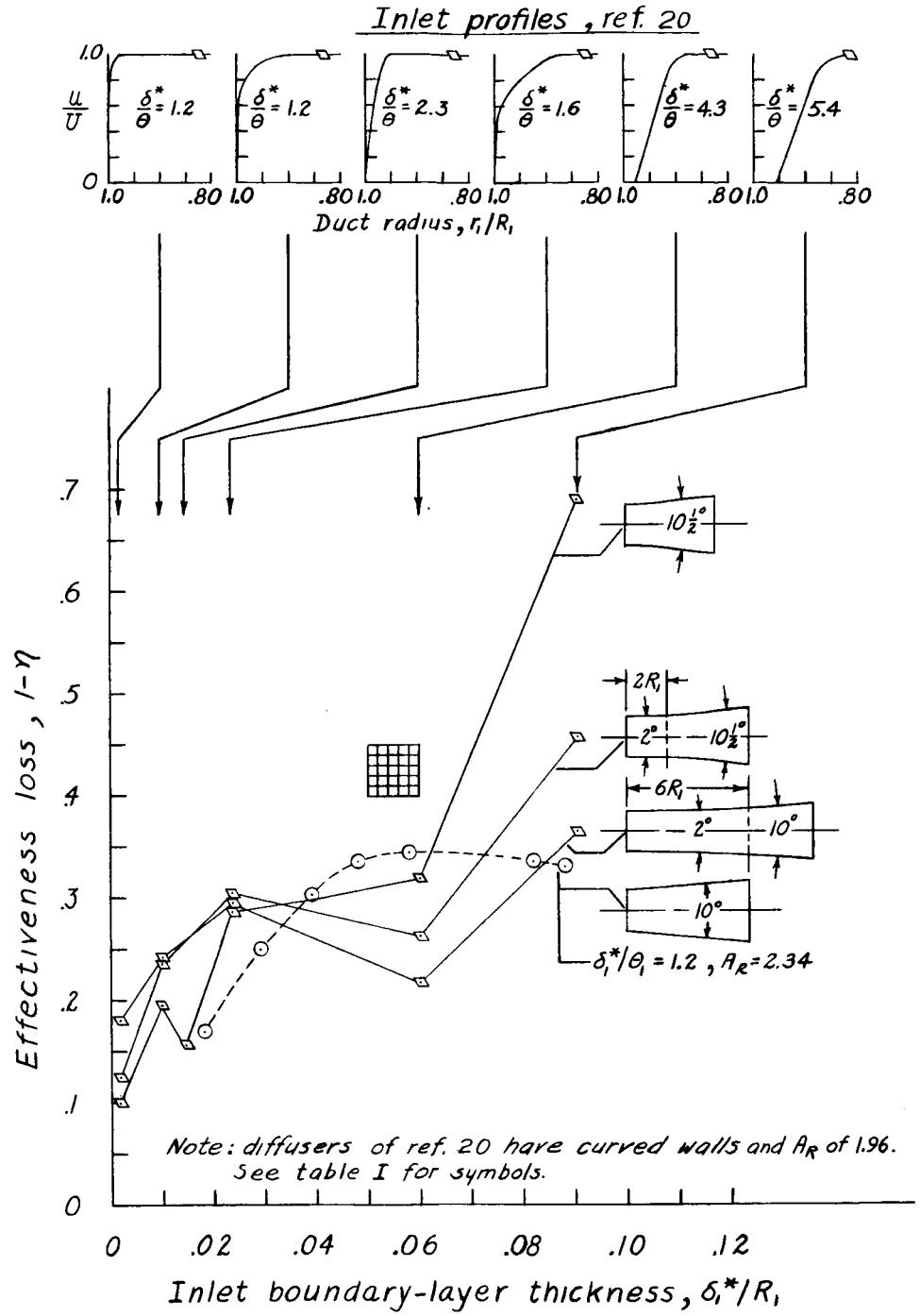

(a) Conical diffusers; $M_1 \approx 0.2$.

Figure 34.- Effect of inlet velocity distribution on $1 - \eta$.

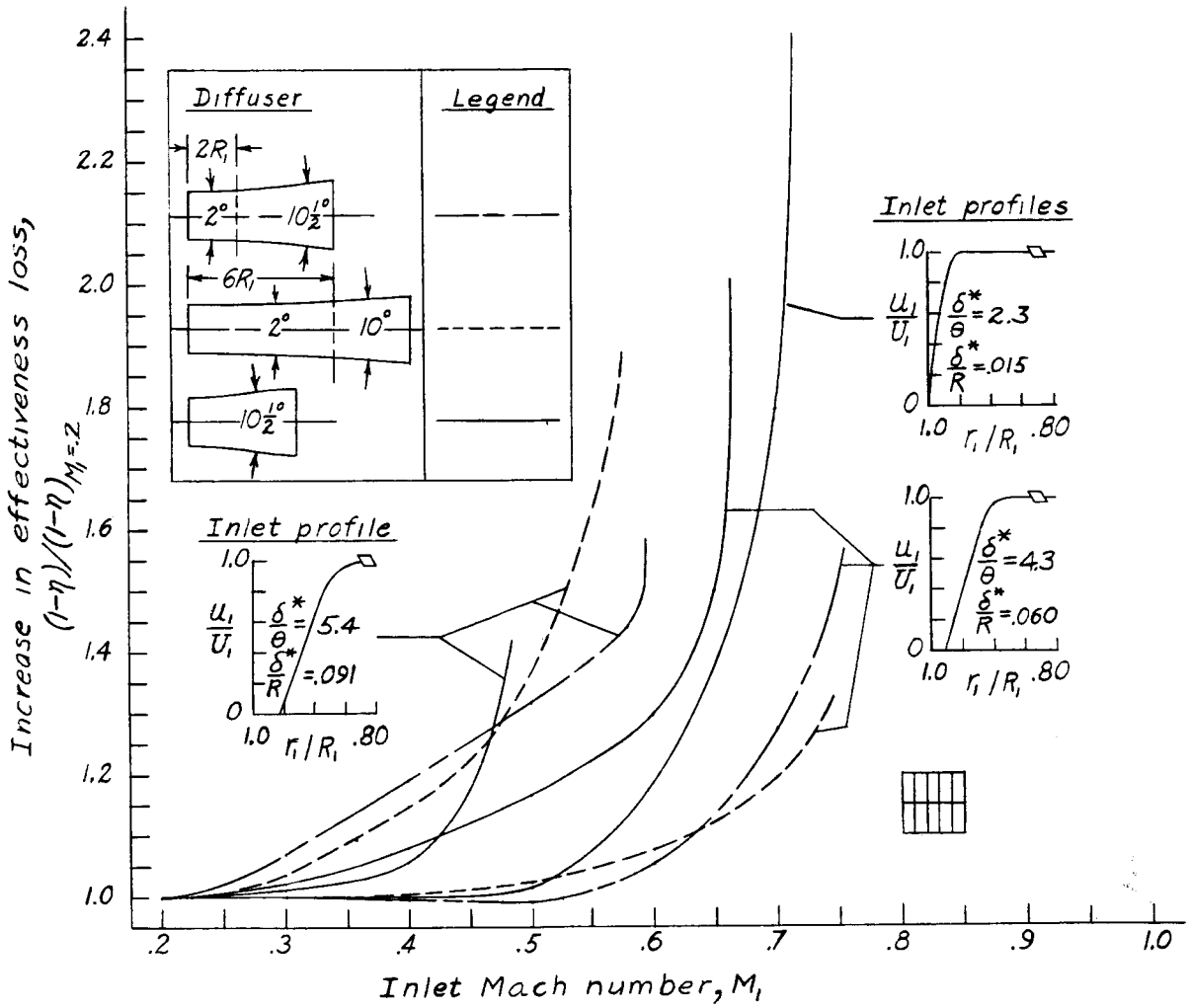

(b) Curved-wall conical diffusers; A_R = 1.96; reference 20.

Figure 34.- Continued.

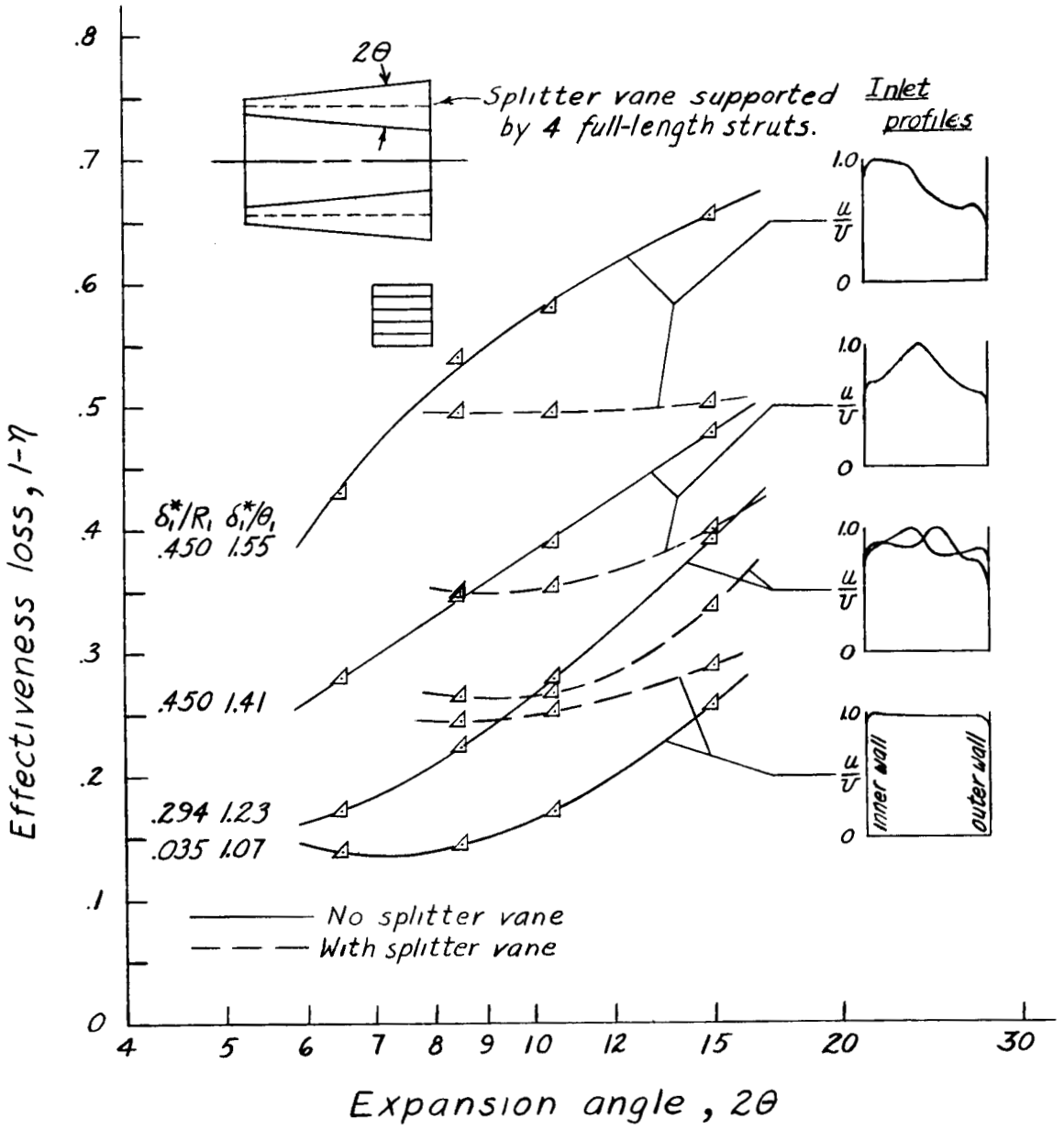

(c) Annular diffusers; A_R = 3.19; M_1 = 0.30; reference 28.

Figure 34.- Concluded.

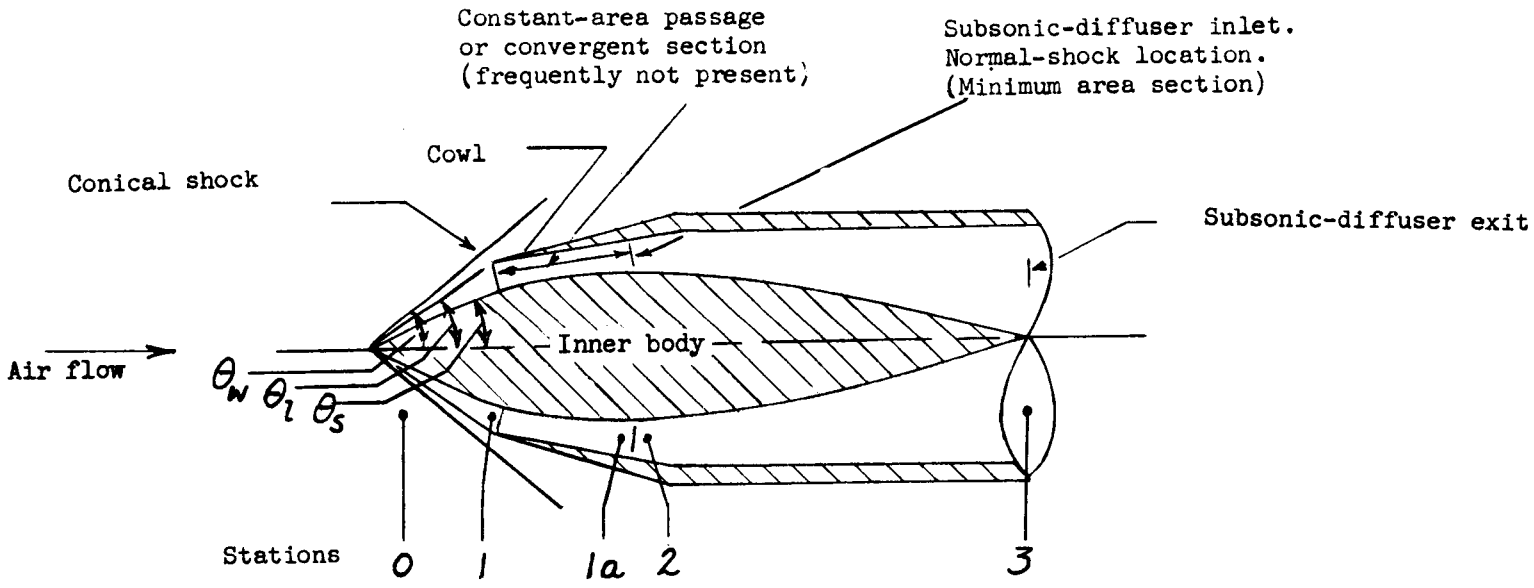

Figure 35.- Diagram of a typical supersonic inlet.

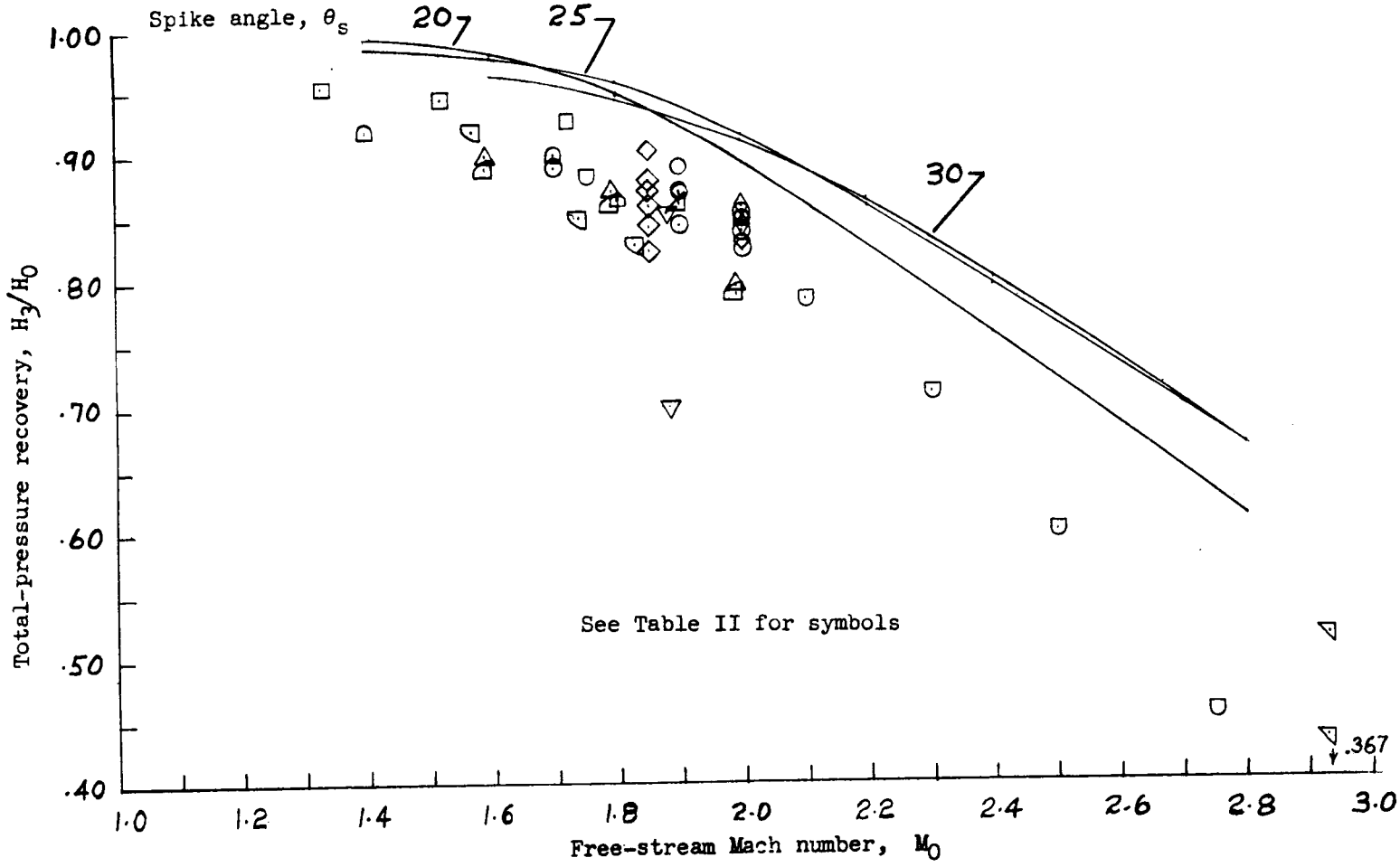

Figure 36.- Experimental and theoretical variations of pressure recovery with Mach number for supersonic spike inlets having no internal contraction.

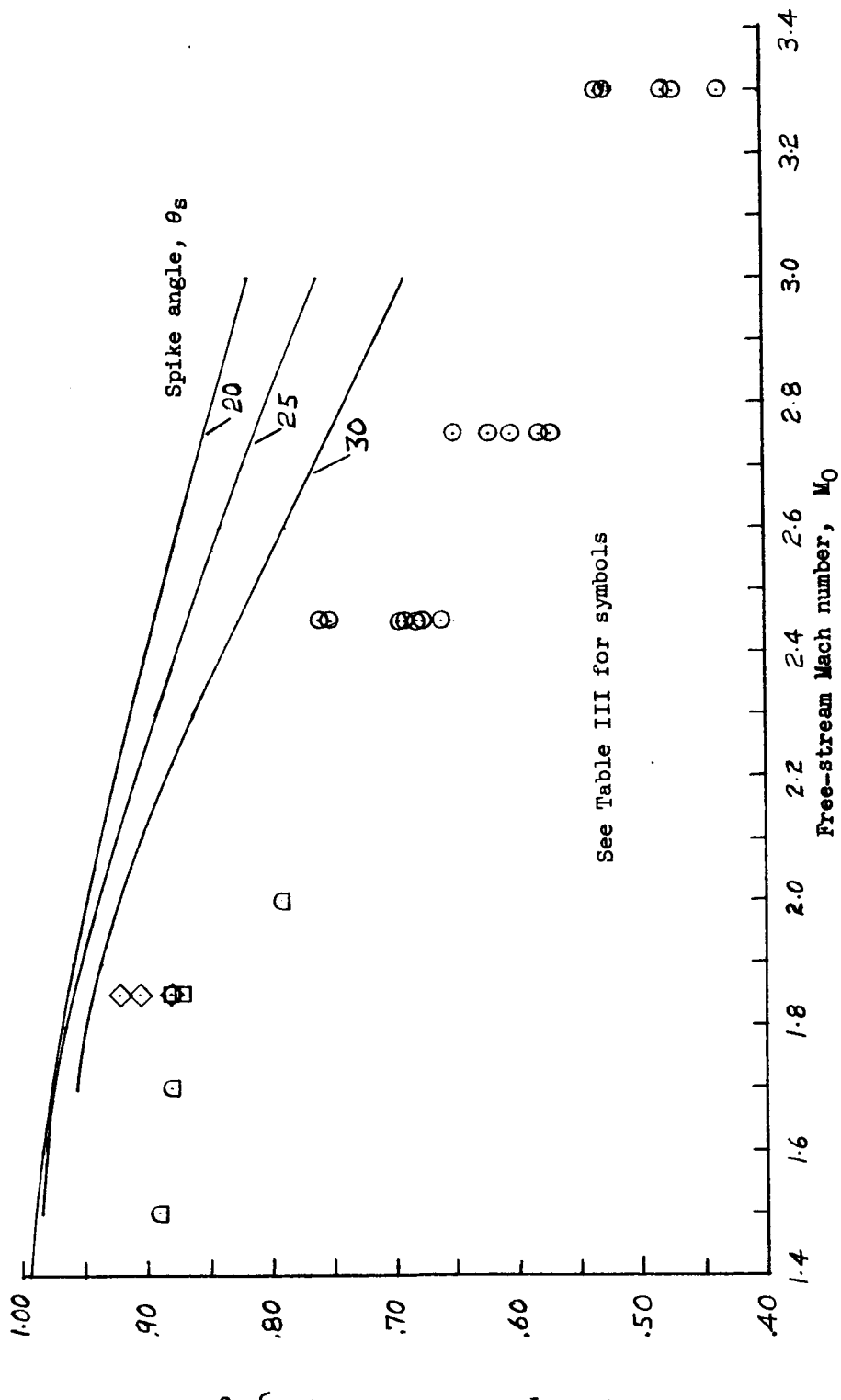

Figure 37.- Experimental and theoretical variations of pressure recovery with Mach number for supersonic spike inlets having internal contraction.

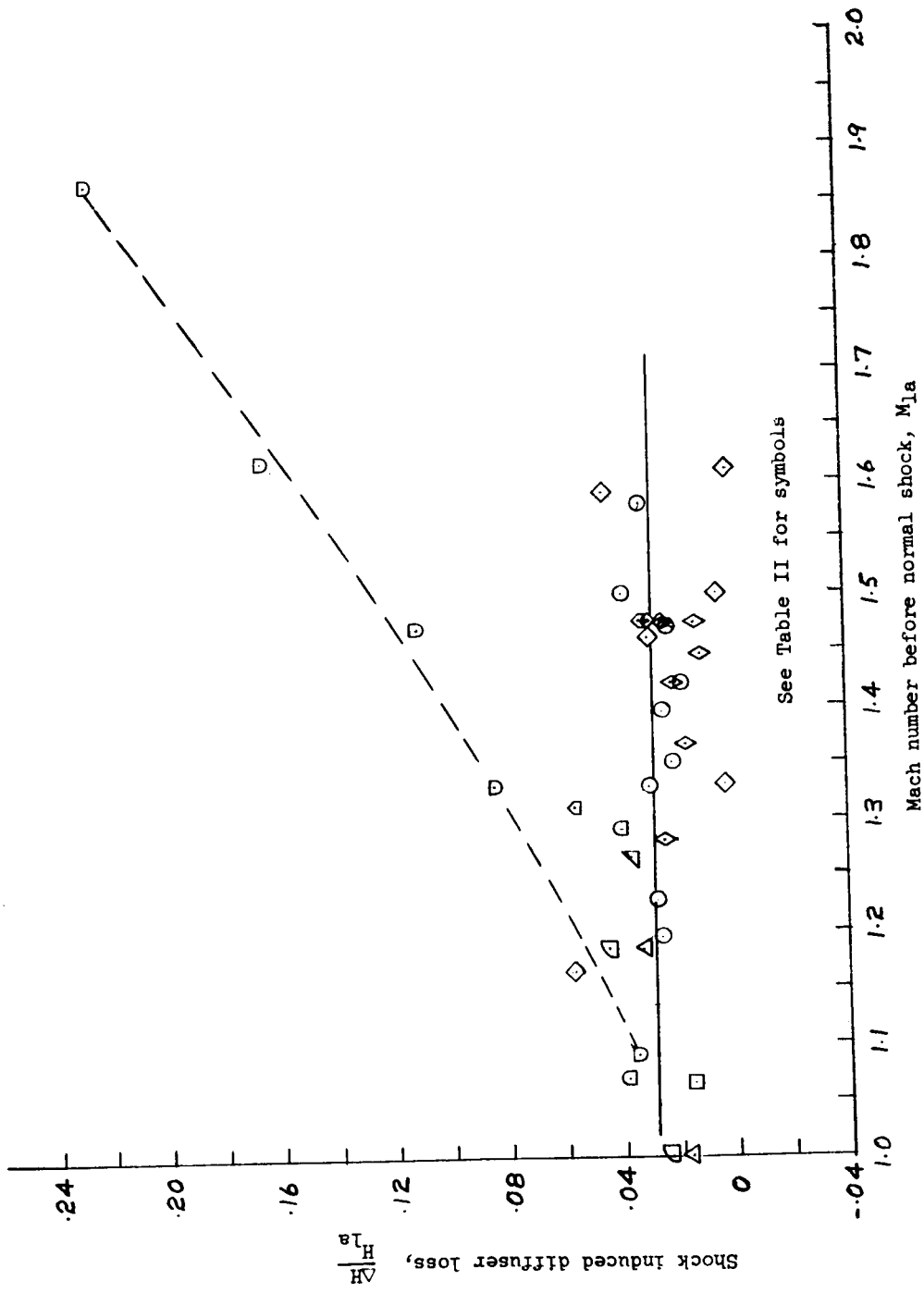

Figure 38.- Variations with Mach number of the shock-induced loss in the diffuser section of supersonic spike inlets having no internal contraction.

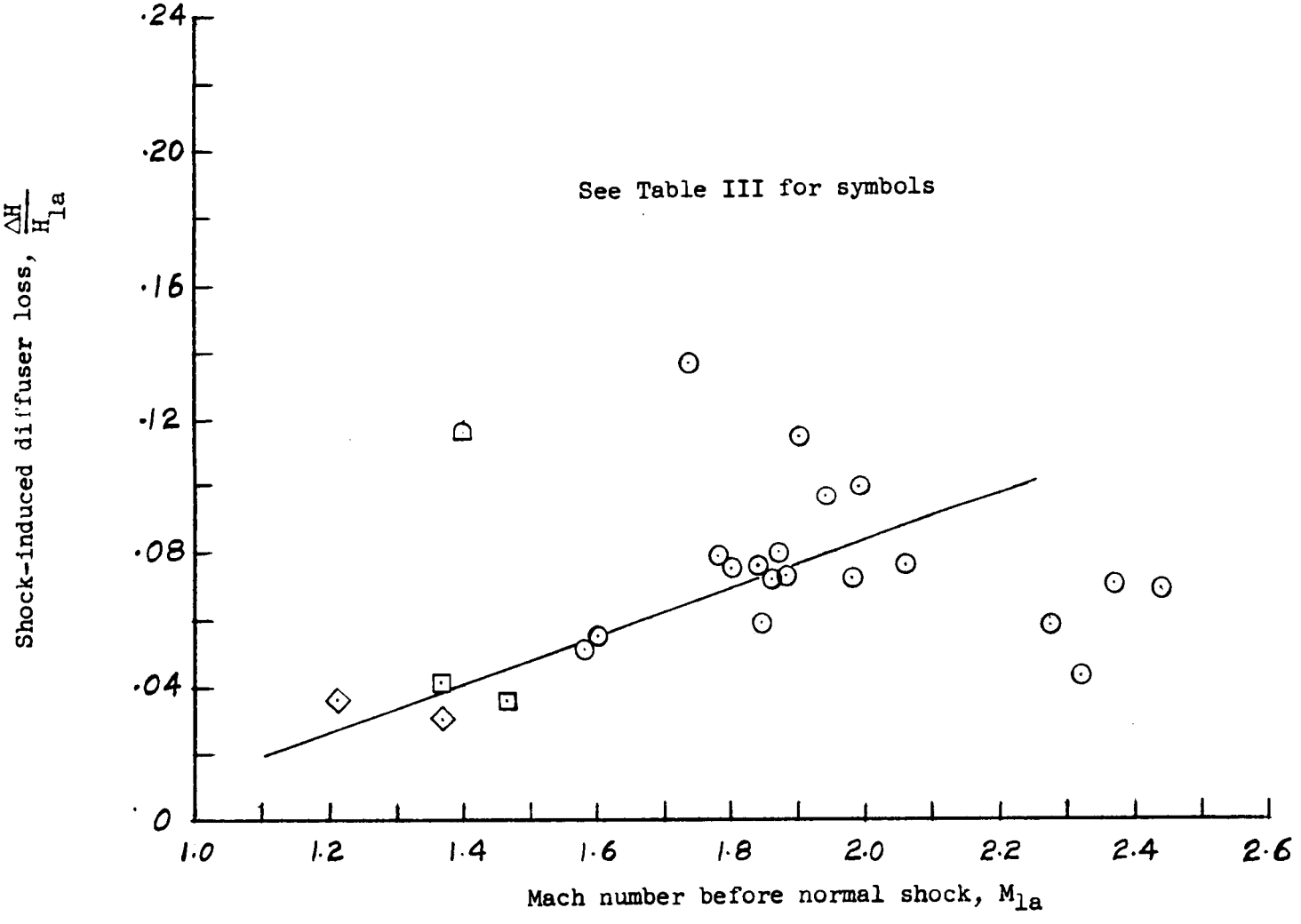

Figure 39.- Variations with Mach number of the shock-induced loss in the diffuser section of supersonic spike inlets having internal contraction.

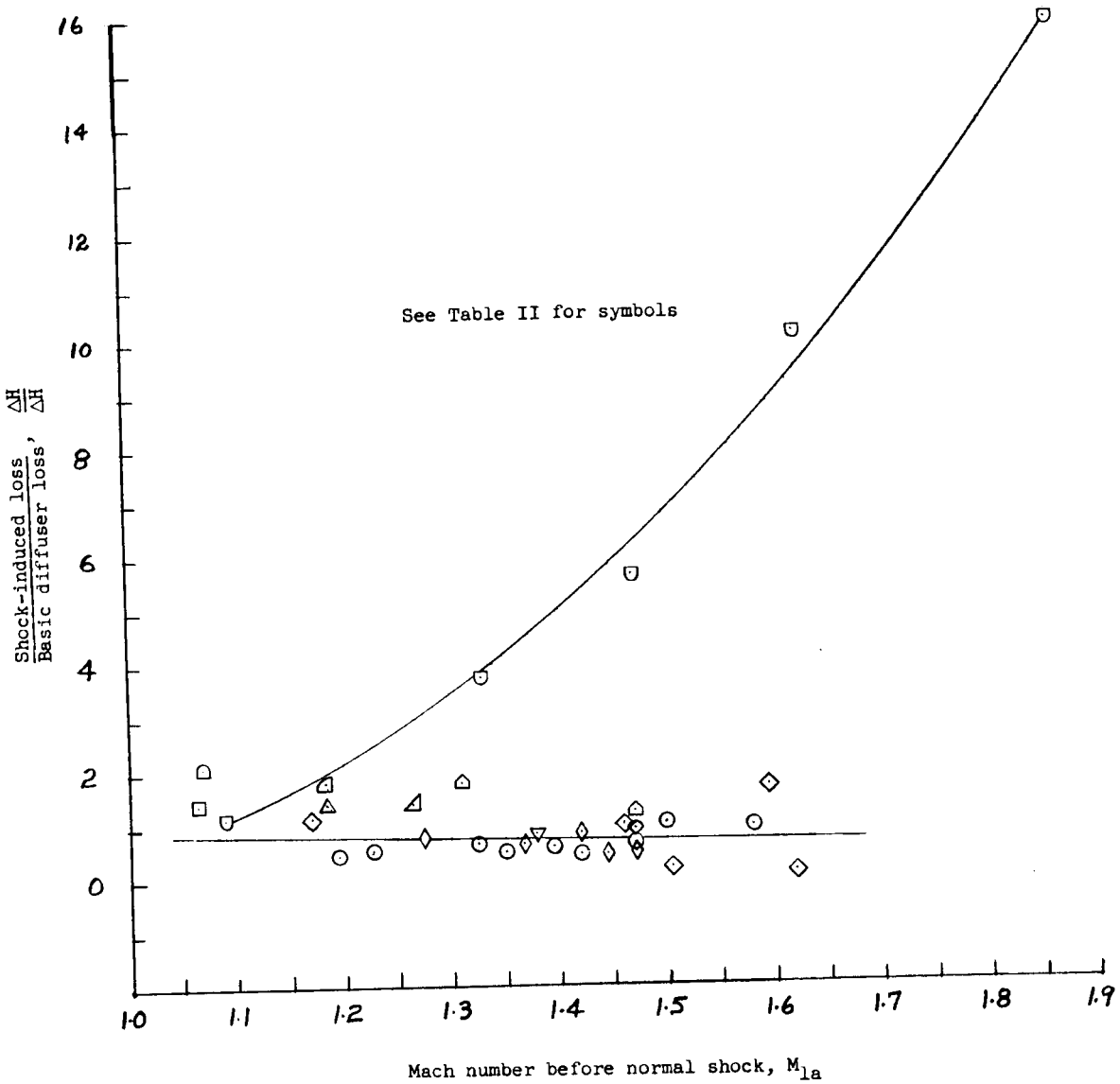

Figure 40.- Variation of the ratio of the shock-induced loss to the basic subsonic-diffuser loss with Mach number for supersonic spike inlets having no contraction.

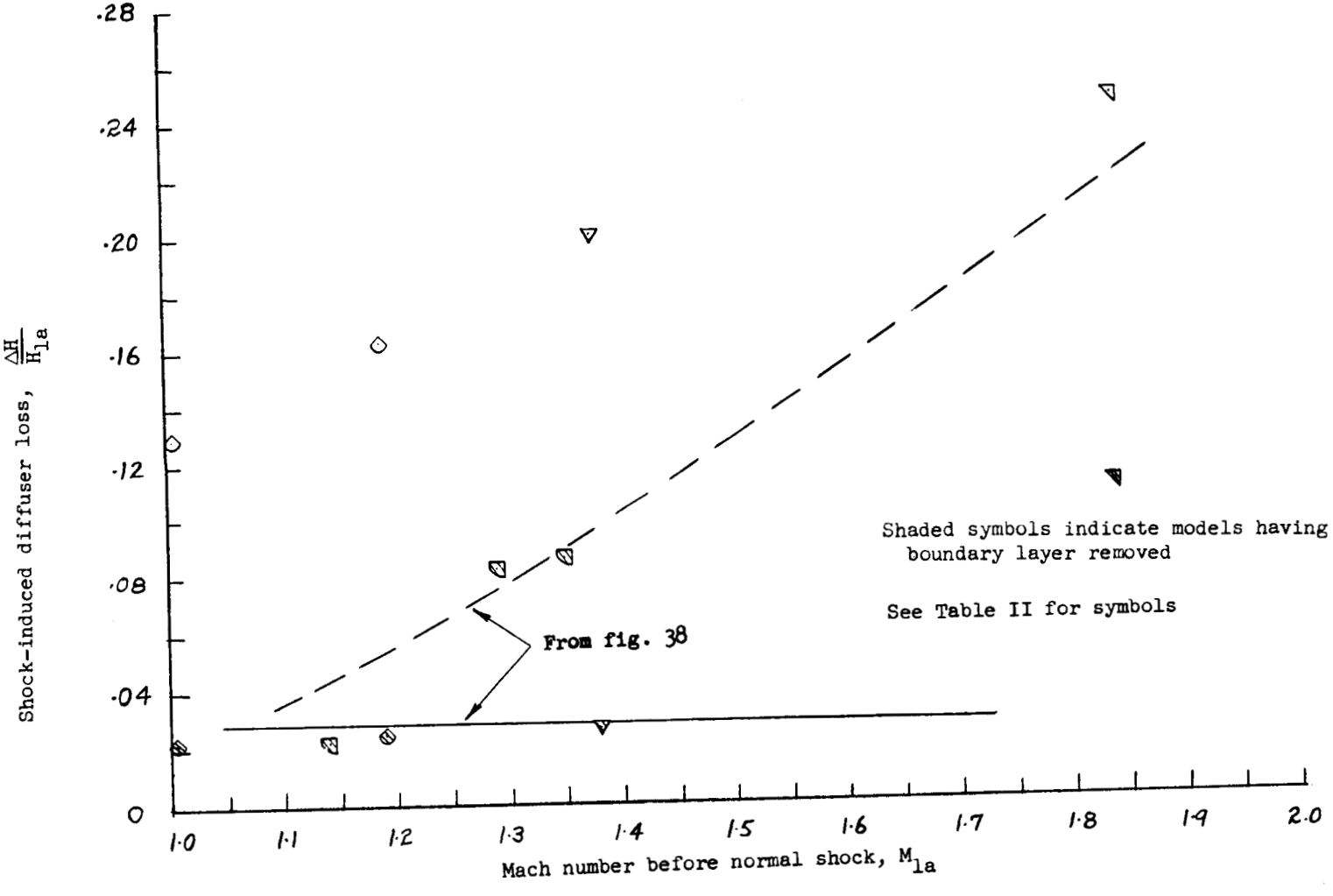

Figure 41.- Effects of inlet boundary-layer thickness on the shock-induced loss in the subsonic-diffuser section of supersonic spike inlets having no contraction.

Figure 42.- Variations with Mach number of the shock-induced loss in the diffuser section of a supersonic convergent-divergent inlet.

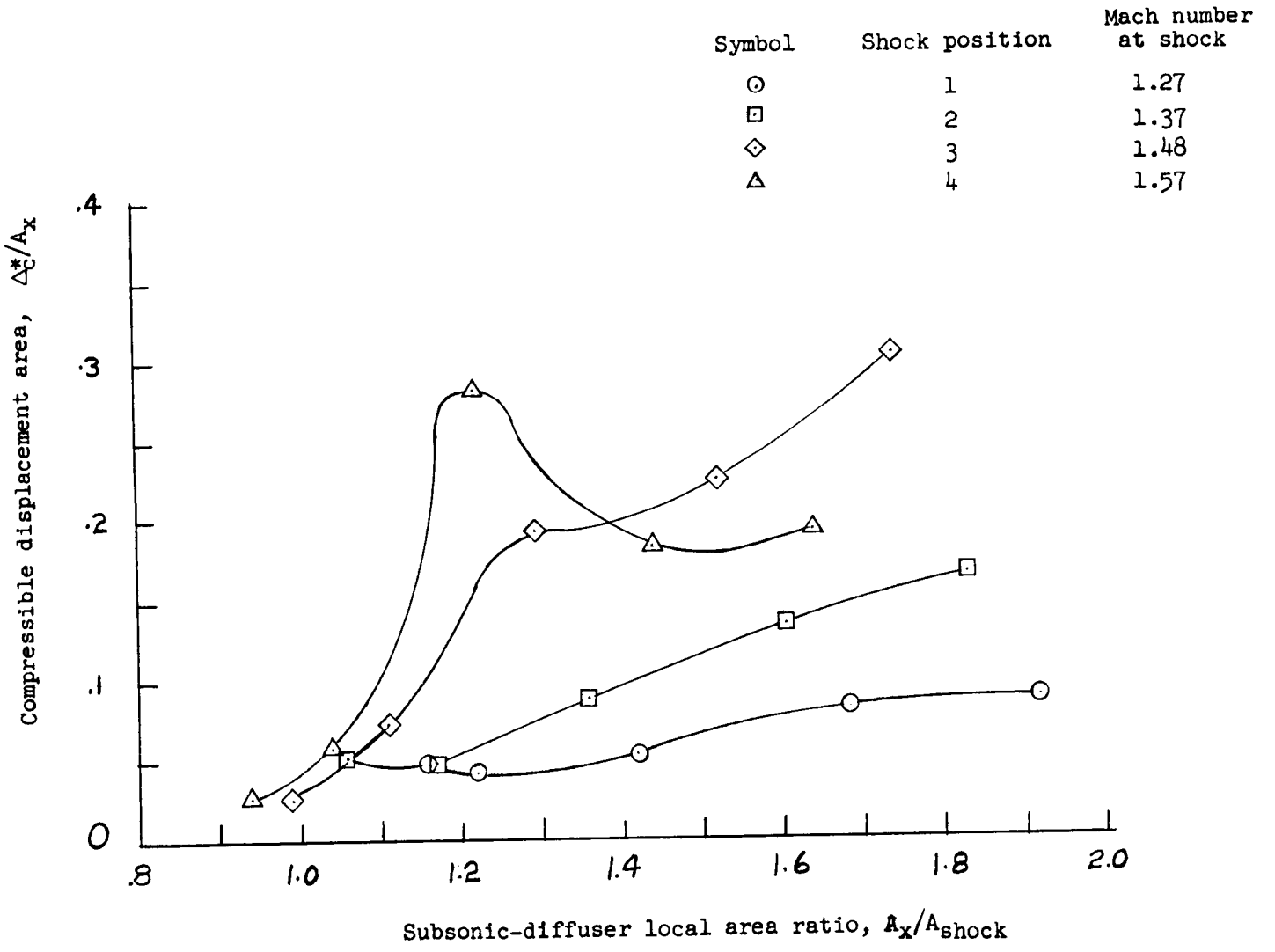

Figure 43.- Compressible three-dimensional displacement area as a function of survey location for various shock positions.

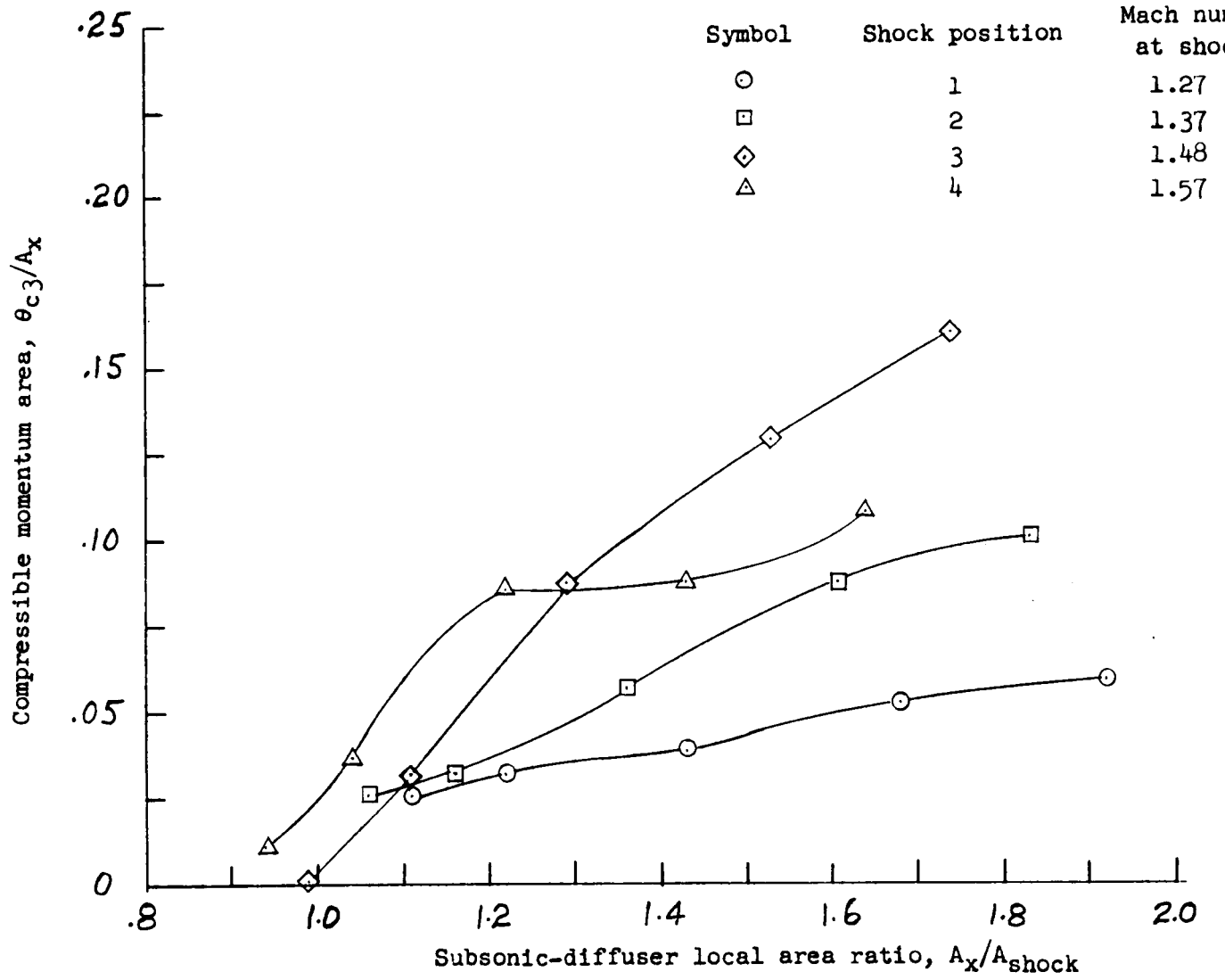

Figure 44.- Compressible three-dimensional momentum area as a function of survey location for various shock positions.

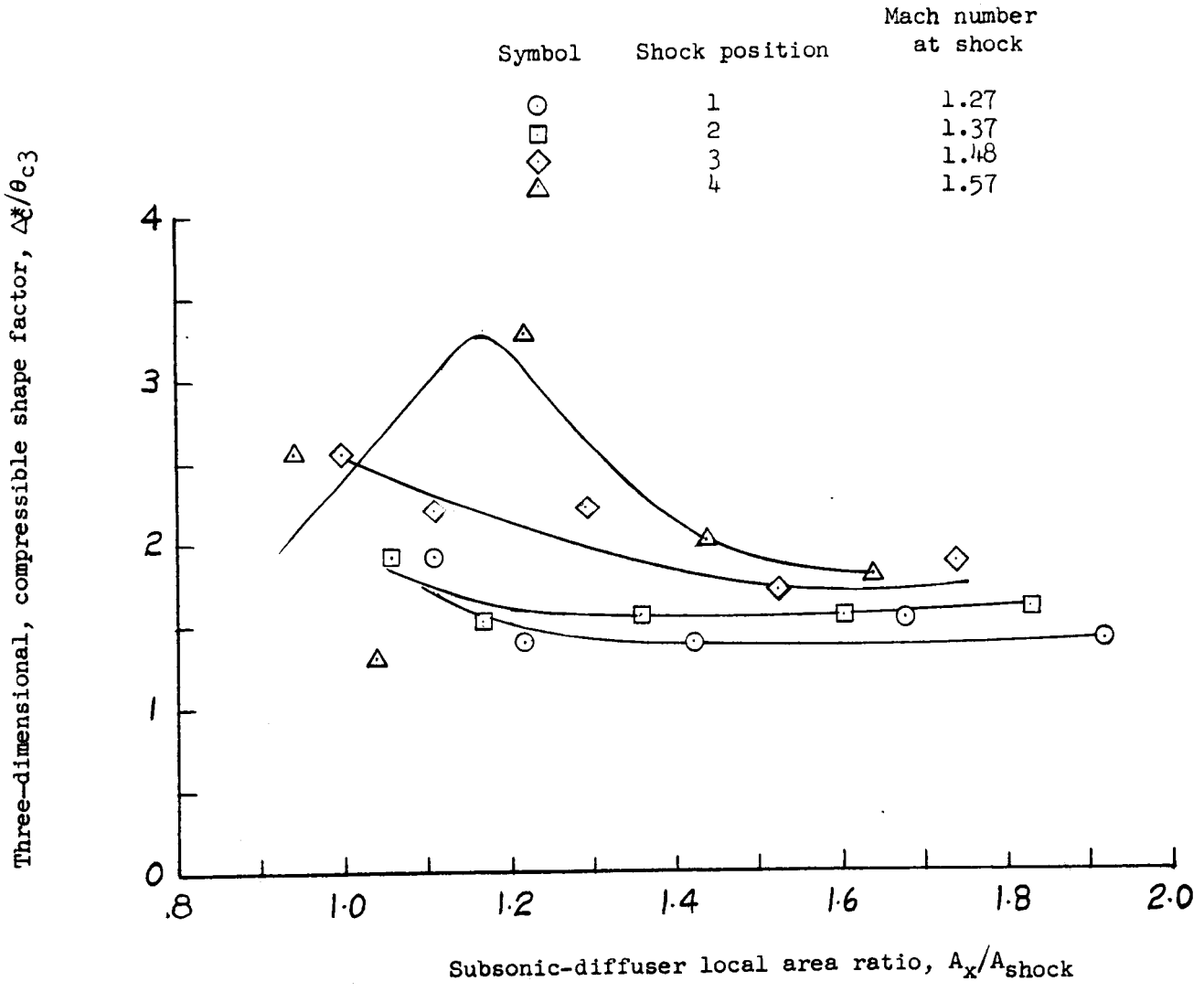

Figure 45.- Compressible three-dimensional boundary-layer shape factor as a function of survey location for various shock positions.

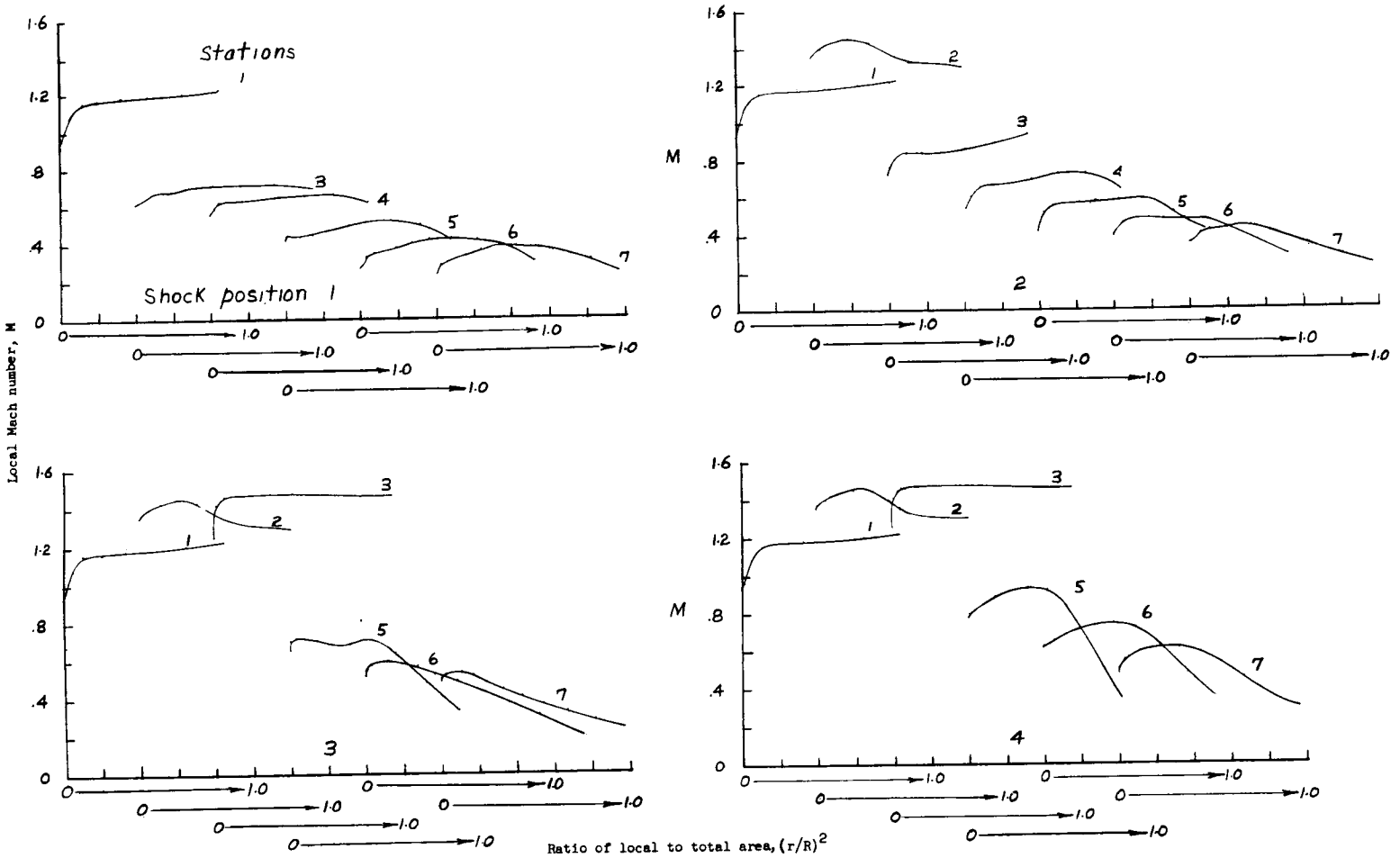

Figure 46.- Mach number distribution at several stations in the diffuser section of a convergent-divergent supersonic inlet for several different shock locations.

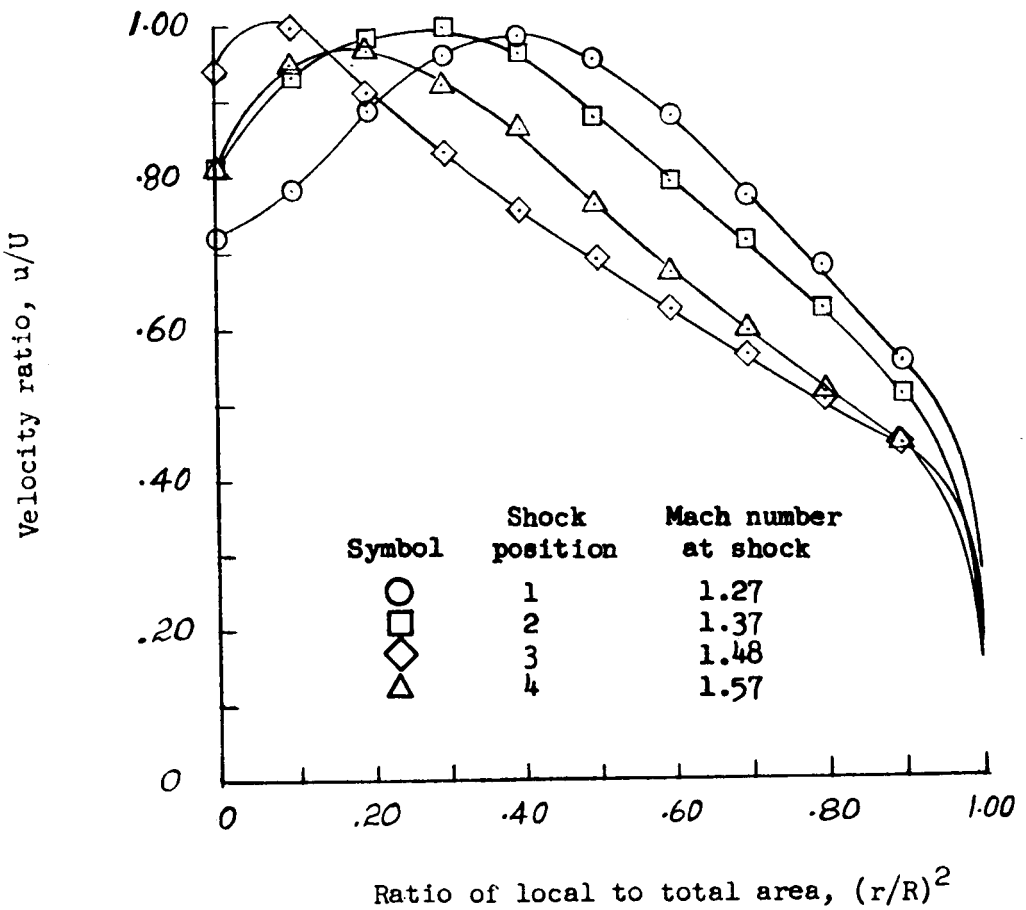

Figure 47.- Velocity distributions at station 7 in the convergent-divergent inlet.

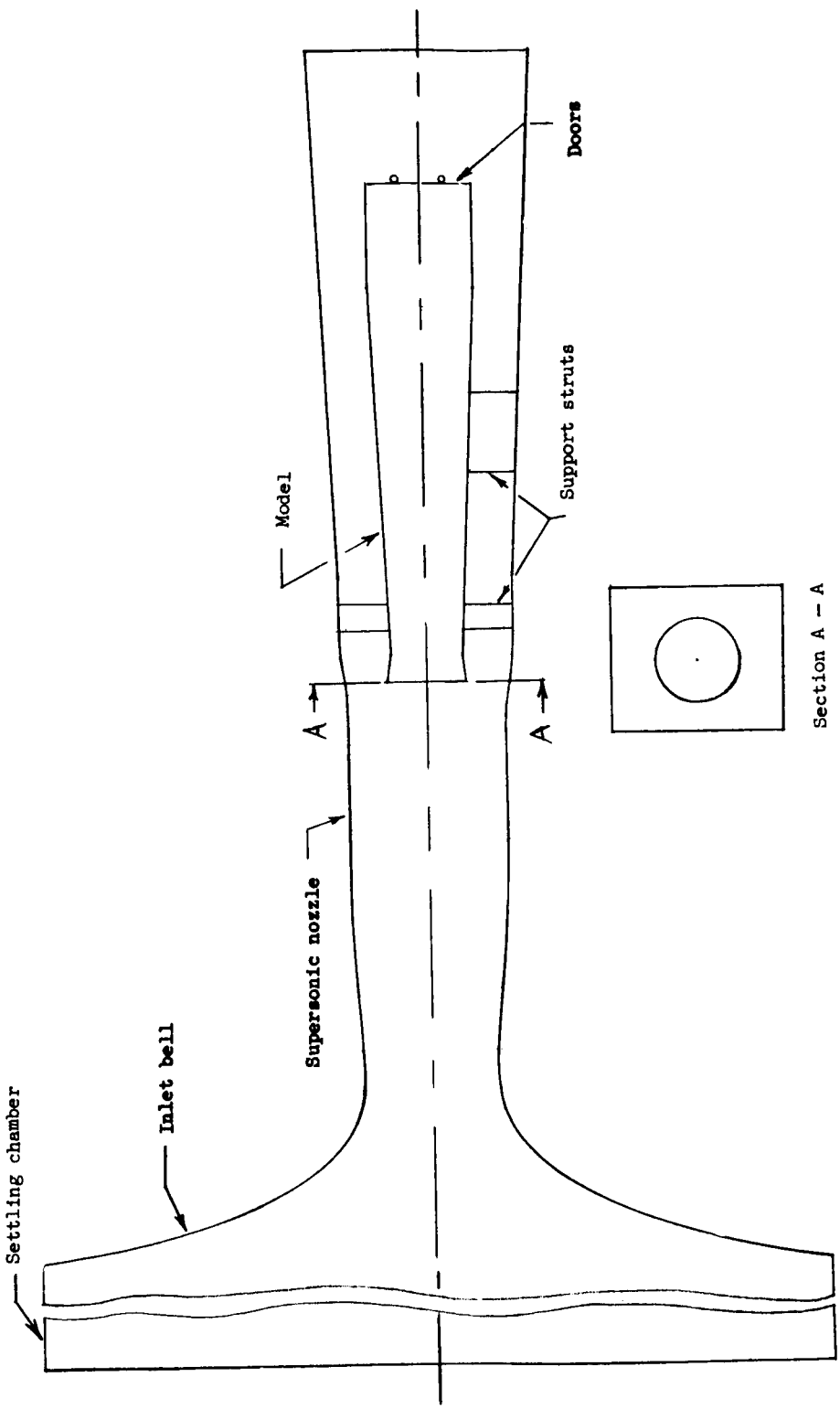

Figure 48.- Diagram of test apparatus.

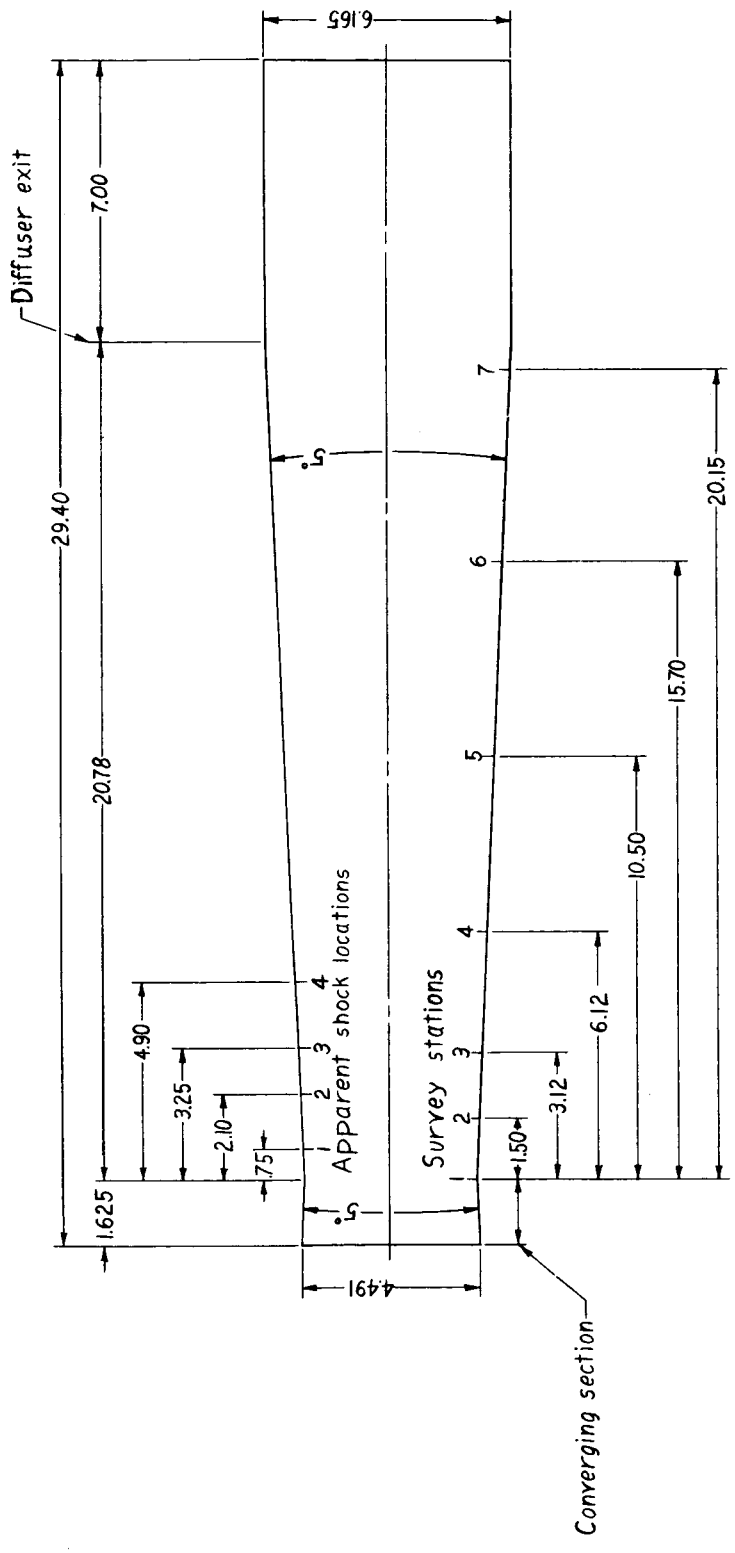

Figure 49.- Line drawing of the supersonic diffuser.

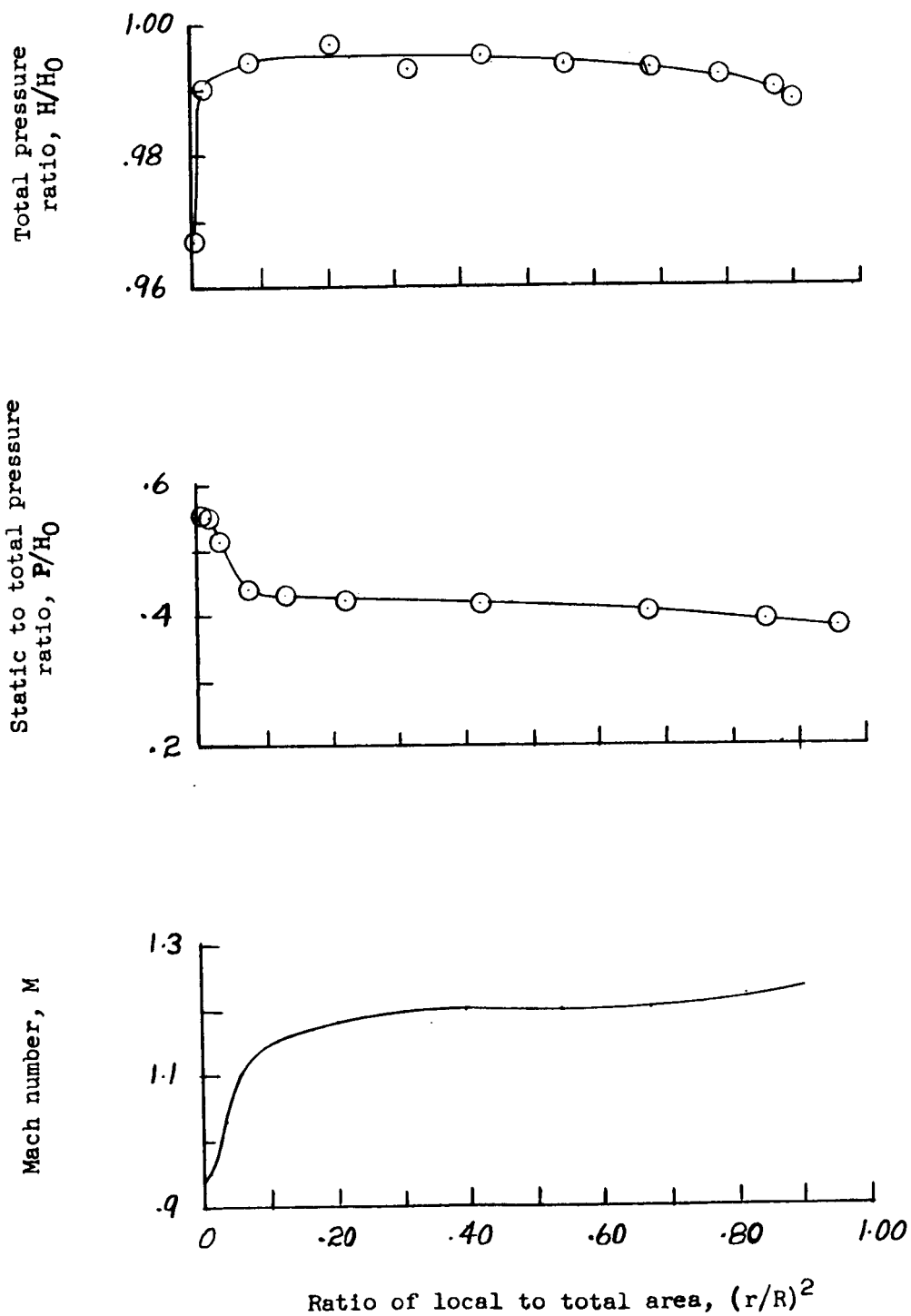

Figure 50.- Total-pressure, static-pressure, and Mach number distributions at station 1 in the convergent-divergent inlet.